IMPERIAL COLLEGE LONDON
UNIVERSITY OF LONDON

ON-LINE MEASUREMENTS OF CONTENTS INSIDE PIPES USING GUIDED ULTRASONIC WAVES

by

Jian Ma

A thesis submitted to the University of London for the degree of
Doctor of Philosophy

Department of Mechanical Engineering
Imperial College London
London SW7 2BX

October 2007

Abstract

There have been extensive demands from industries to determine information about the contents inside pipelines and it would be a great benefit if on-line measurements could be made. Guided ultrasonic wave measurements can potentially fulfill such a purpose since they are non-intrusive and can be carried out from outside of the pipe wall. This thesis investigates the principles and develops new guided wave techniques for two specific applications.

The first application relates to the fluid characterisation inside pipes. A new guided wave technique is developed to measure the acoustic properties (bulk sound velocity and shear viscosity) of fluids inside pipes. It is based on the measurements of the velocity dispersion and attenuation of guided longitudinal modes in the pipe. It allows the fluid properties to be characterised without taking samples out of the pipe and can be employed both when the pipe is completely filled or when the filling is local. In the latter case, the technique is exploited as a pipe 'dipstick' sensor dipped into the fluid to be measured. The dipstick sensor has the advantages that the velocity measurement requires a single pulse echo measurement without the need for knowing the depth of immersion of the pipe into the fluid.

The second application is for sludge and blockages detection in long-range pipelines. Existing techniques have the limitations that the sludge position needs to be known a priori and the area to be inspected needs to be accessible. Two guided wave techniques have been developed which allow the the sludge or blockages to be detected remotely without the need to access the specific location where the pipe is blocked, nor to open the pipe. The first technique measures the reflection of guided waves by sludge or blockages which can be used to accurately locate the blocked region; the second technique detects sludge by revealing the changes to the transmitted guided waves propagating in the blocked region or after it. The two techniques complement each other and their combination leads to a reliable sludge or blockage detection. Various types of realistic sludge or blockages have been considered in the study and the practical capabilities of the two techniques have been demonstrated.

Acknowledgments

I would like to sincerely thanks my supervisor Professor Mike Lowe and my co-advisors Dr. Francesco Simonetti and Professor Peter Cawley for their invaluable guidance and for offering me a chance to study in the well organised Non-destructive Testing Lab.

I would also like to thank my project collaborators, Professor Richard Challis from Nottingham University and Dr. Sam Worthington from British Nuclear Fuel Ltd (BNFL) for the discussions and insightful suggestions.

Also I acknowledge the input of my current and former colleagues in the NDT group at Imperial College, which significantly benefited the completion of this project. In particular, I am very grateful to Dr. Jimmy Fong, Dr. Mark Evans, Dr. Frederic Cegla, Mr. Prabhu Rajagopal who helped me so much when I was lost at the early stage of my Ph.D.

Furthermore, I must acknowledge the Engineering and Physical Sciences Research Council (EPSRC) and BNFL which funded this work.

I also appreciate Professor Zhemin Zhu at Nanjing University who introduced me into the field of acoustics has enlightened me with so much knowledge.

Finally, I would like to express my personal thanks to my parents and also to Xinxin for their continued encouragement and support throughout my study. Wish all my little progress will make you smile.

Contents

List of Figures

List of Tables

Chapter 1

Introduction

1.1 Motivation

There are many circumstances in the process, power and oil industries, where it is necessary to determine information about the material inside a pipeline and it would be a great benefit if a non-intrusive measurement technique could be used to make on-line measurements. There are two practical problems which particulary motivate this thesis.

The first motivation comes from a need by many industries which is to determine the material properties of fluids inside pipelines so as to help the monitoring and control of processes. For example, much effort in the pharmaceutical industry has been applied to the use of supercritical CO_2 for the formation of polymers and advanced copolymers [1, 2, 3], which has the advantage of avoiding the use of potentially toxic solvents whilst at the same time minimising toxic residues from formation processes. Supercritical water can be used to rapidly oxidise highly toxic materials in a contained vessel or pipe without recourse to incineration with the risk of toxic emissions. It is recognised that these new processes require monitoring and control. In particular it is necessary to track fluid phase behavior under conditions of high temperature and pressures, where the supercritical point may move in a complex way in response to chemical association and reaction.

Many of the properties of the fluid can be surely found by opening the pipe, using

devices which travel within the pipe, or tapping off samples. Once samples have been taken, many techniques can be used to make the measurements. Ultrasonic spectrometers using bulk ultrasonic waves have been commonly applied, for example, to monitor the physical state of colloids and emulsions [4], and to track changes such as flocculation [5] and crystallisation [6]. Ultrasound is capable of examining opaque samples where standard optical techniques fail. But the extraction of samples from the line introduces a delay to the measurements and so limits the feedback response to process changes; furthermore, the measurements are not made under the line conditions of pressure, temperature and flow which may change some properties of the fluid when it is extracted from the line.

There are a number of on-line ultrasound measurement techniques available, which will be reviewed in Sec. 3.3. However, these techniques are either intrusive to the pipeline or are limited in the range range of material they can measure such as highly attenuative fluid.

The second motivation of the thesis is to detect and even characterise sludge or blockages inside pipelines. The accumulation of sludge inside pipelines is a problem which commonly occurs in the chemical, process, oil and food industries. Ultimately blockages can result from the accumulation of sludge. The sludge and blockages can be formed by different materials depending on the types of the plants and the processing conditions. For example, in the pipelines of petroleum plants, sludge is often caused by precipitation of paraffins and asphaltenes in crude oil transportation and processing [7]. Fuel corrosion products are found by some chemical companies to be the main cause of the sludge at their plant [8].

The presence of sludge or blockages in pipelines has an impact on several of the factors that affect the plant operation. The efficiency of the plant may be reduced in terms of product flow rate, owing to the reduction in pipe diameter. The insulative effect of the sludge or blockages may reduce the rate of heat transfer from the heat exchanger to the product during heating, or vice versa during cooling. The quality of the product may also be compromised as a result of changes in the processing conditions. In addition, the product may become contaminated by pieces of the sludge that detach from the pipe. In the extreme, the plant may become unsafe to use.

Once the sludge or blockage has occurred, the operating companies have to attend to the pipeline as quickly as possible in order to restore appropriate flow conditions and prevent a threat to the environment. There are a few remedial techniques available in industry, such as external heating, coiled tubing intervention, pigging methods and using dense chemical solvents [7]. However, the cleaning and replacement of the blocked pipe often involves production down time, cleaning agents and possibly some parts of the plant being stripped, all of which result in significant loss of plant efficiency and increase the costs. Most important are the safety issues, such as the possible catastrophic failure of a gas pipeline, which is a threat to personal health.

An effective sludge and blockage detection system is very important since it can reduce production down time and costs. An accurate detection of sludge or blockages may also avoid unnecessary cleaning which may be scheduled as a regular pipeline maintenance to prevent the accumulation of sludge [9]. Also, without knowledge of the location of the sludge, whole pipelines may have to be cleaned or even replaced. Likewise, an early detection of a sludge problem in the pipeline avoids producing unqualified products that have been contaminated by the sludge. Therefore a system that can detect, locate and even monitor the accumulation of sludge build up is desired.

Current techniques to detect sludge inside pipes are limited or intrusive. For example, pipeline diameter expansion induced by internal pressurization of the pipe can be measured point by point along the pipeline and correlated to the contents in the pipe [10], but this method has the limitation that the location of the blocked region needs to be known a priori and the area to be inspected needs to be accessible. Alternatively, a technique termed acoustic pressure can be used. This technique injects an acoustic pressure wave into the gas contained in a duct or a pipe and measures the acoustic response of the duct. The presence of a blockage induces an eigenfrequency shift in the response which can be used to reconstruct an image of the blockage area [11, 12]. However, the method requires access to the inside of the pipeline which is not possible in many practical situations.

1.2 Aim of the Investigation

These two problems require techniques that can non-intrusively detect and measure materials within pipelines. This thesis investigates the feasibility of using guided ultrasonic waves which travel in the wall of the pipe for such a purpose. Guided waves can be excited from the outside of the pipe wall at one location and propagate along the length of the pipe for long distances. They are partially reflected when they encounter features in the pipe (such as welds, corrosion, cracks, etc...) that locally cause a discontinuity of the pipe wall. Technologies employing ultrasonic guided waves have been well developed for the long-range inspection of pipeline [13-18].

It would be very useful if guided waves could also be used to measure materials inside pipes. Two guided wave measurement ideas can be pursued. First, the presence of contents will change the propagation characteristics of the guided waves in the pipe, depending on the material properties of the contents. Thus, by quantitatively measuring these propagation changes, some properties of the contents can be obtained. This can be particulary useful for on-line fluid characterisation inside pipelines, since the measurements are performed at the outer surface of the pipe and are completely non-intrusive. Moreover, the guided wave measurements measure the signal propagating in the pipe wall, unlike the bulk ultrasonic wave measurements, which measure the signals traveling across the material under investigation directly. Therefore, the guided wave measurements suffer much lower attenuation due to the material damping of the content than the bulk ultrasonic wave measurements.

The second idea makes use of the fact that the localised accumulation of material inside a pipe causes a change of the acoustic impedance of the pipe which scatters the guided waves propagating in the pipe. The characteristics of both reflection and transmission of the incident guided wave depend on the nature of the guided waves and the properties of the pipe contents. Therefore, by analyzing both the reflection and the transmission, the contents can be remotely detected, and even characterized in some situations. This provides a very attractive method for detecting and characterising sludge and blockages in pipelines.

This thesis primarily aims at determining the feasibility of using guided waves to ad-

dress the two mentioned industrial problems. However, the findings will be useful to a large number of studies regarding ultrasonic wave propagation in filled waveguides. For example, research [19, 20] has been carried out to investigate the possibility of using guided ultrasonic waves to monitor the build-up of fouling films in heat exchangers and pipelines which is a widespread problem in ultra high-temperature processing plants, particularly those used for milk and milk products [21]. The fouling film has similar impacts on the operation of these plant as the sludge and blockages considered in the thesis, although it largely consists of denatured whey proteins and calcium deposits from milk and milk products. The work presented in this thesis for sludge and blockages detection using guided waves should contribute useful information to this topic.

1.3 Outline of Thesis

The thesis can generally be divided into two parts according to their applications. Chapter 2 and 3 present the work for the purpose of fluid characterisation, while the work in Chapters 4, 5 and 6 are mainly carried out for sludge and blockage detection and characterization. Specifically, subsequent to the introductory remarks in this chapter, the thesis is structured in the following way.

Chapter 2 reviews some basic concepts about bulk ultrasonic wave propagation in unbounded media and guided ultrasonic wave propagation in cylindrical pipes. In particular, the models of guided longitudinal waves propagating in pipes filled with fluids are revisited to extract the physical principles which can be exploited to develop a guided wave technique for fluid characterisation inside pipes.

Based on the principles identified in Chapter 2, a new guided wave technique to measure the longitudinal bulk velocity and shear viscosity of fluids inside a pipe is presented in Chapter 3. It is demonstrated that this guided wave technique is capable of non-intrusively measuring both low-viscosity fluid and highly viscous fluid inside the pipe. Some basic principles of ultrasound measurements and a review of existing ultrasound methods for material characterisation inside pipes are also given.

Chapter 4 studies the scattering of the fundamental guided torsional mode by a local

axisymmetrical elastic layer inside a pipe, which is a simplified model of sludge and blockages inside pipes. The study reveals the physics of the problem and leads to two measurement ideas which make use of both the reflection and transmission of the torsional mode to characterize the geometry or acoustic properties of a layer inside a pipe. The two ideas are investigated through both Finite Element simulations and experimental measurements.

Chapter 5 proceeds the work in Chapter 4 by taking into account more realistic sludge and blockage characteristics, such as their irregular profiles, bonding problems and the damping of the sludge material. The proposed reflection and transmission measurement ideas have also been implemented using commercial guided wave equipment to demonstrate the practical capabilities. An overall assessment of using guided torsional waves for practical sludge and blockage detection and characterization is made.

Some results of using guided longitudinal waves for sludge and blockage detection are presented in Chapter 6. The work is a generalization of the two measurement ideas introduced in Chapters 4 and 5 when using guided torsional waves. The measurement ideas are found to be also applicable when using the longitudinal mode for sludge and blockages detection; however, the applicability is restricted under the circumstance when fluid is present. The advantages and disadvantages of the measurements using guided longitudinal waves compared to those using torsional waves is concluded.

The main conclusions of the thesis are summarized in Chapter 7 where possible future applications are also illustrated.

Chapter 2

Guided Wave Propagation in Pipes Filled with Fluid

2.1 Background

This chapter introduces some basic concepts about bulk ultrasonic wave propagation in unbounded media and guided ultrasonic wave propagation in waveguides, such as cylindrical pipes.

In an unbounded elastic medium, bulk ultrasonic waves can propagate as homogeneous or inhomogeneous bulk longitudinal and shear waves. In a waveguide such as a pipe, partial bulk waves reverberating between the boundaries of the waveguide are superposed to form a guided wave propagating along the structure. There are a large number of guided wave modes which can propagate in pipes with different propagation characteristics. Features of guided wave modes in pipes such as their velocity dependence on frequency, called dispersion, and the distribution of the field variables over the cross section of the pipe, referred to as mode shape are introduced.

The propagation of guided wave modes in a pipe is affected by the media surrounding and inside the pipe. For the particular purpose of fluid characterisation inside pipes, this chapter summarizes the main characteristics of the guided longitudinal wave propagating in pipes filled with fluids. The main purpose is to extract some physical principles which can be exploited to develop a guided wave technique for

fluid characterisation inside pipes that will be addressed in Chapter 3.

The Chapter starts with a brief introduction of bulk ultrasonic waves propagation in an unbounded medium in Sec. 2.2. Then the propagation of guided waves in free pipes is addressed in Sec. 2.3 followed by presentations of guided longitudinal waves in pipes filled with different fluids, including inviscid fluid in Sec. 2.4 and viscous fluid in Sec. 2.5.

2.2 Wave Propagation in Infinite Media

Wave propagation in unbounded, isotropic media is well documented in many textbooks (see, for example, Refs [22], [23], [24]) and is therefore only outlined briefly in this section.

Starting in a Cartesian coordinate system the linearized equation of motion, the particle displacement $\mathbf{u}$ in a material of density ρ is related to the stress tensor σ by

$$\rho\frac{\partial^2\mathbf{u}}{\partial t^2} = \nabla \cdot \sigma, \tag{2.1}$$

∇ is the three dimensional differential operator. Hooke's law can be used to relate stresses to strains and displacements in an isotropic elastic medium as

$$\sigma = \lambda\mathbf{I}\nabla \cdot \mathbf{u} + \mu(\nabla\mathbf{u} + \mathbf{u}\nabla^{\mathbf{T}}), \tag{2.2}$$

where λ and μ are Lamé constants and $\mathbf{I}$ is the identity matrix. Combining equation 2.1 and equation 2.2 gives the Navier equation for displacement $\mathbf{u}$

$$\rho\frac{\partial^2\mathbf{u}}{\partial t^2} = (\lambda + 2\mu)\nabla(\nabla \cdot \mathbf{u}) + \mu\nabla^2\mathbf{u}. \tag{2.3}$$

By means of the Helmholtz decomposition, the displacement field can be expressed as a sum of the gradient of a compressional scalar potential ϕ, and the curl of an equivoluminal vector $\mathbf{H}$ [25]

$$\mathbf{u} = \nabla\phi + \nabla \times \mathbf{H}, \tag{2.4}$$

with

$$\nabla \cdot \mathbf{H} = 0. \tag{2.5}$$

By substituting equation 2.4 into equation 2.3, after some algebra, equation 2.3 can be split into two equations for two unknown potentials

$$\frac{\partial^2 \phi}{\partial t^2} = c_l^2 \nabla^2 \phi, \tag{2.6}$$

$$\frac{\partial^2 \mathbf{H}}{\partial t^2} = c_s^2 \nabla^2 \mathbf{H}, \tag{2.7}$$

where

$$c_l = \sqrt{\frac{\lambda + 2\mu}{\rho}}, \tag{2.8}$$

$$c_s = \sqrt{\frac{\mu}{\rho}}. \tag{2.9}$$

c_l and c_s are the velocities of dilatational (longitudinal) and rotational (shear) waves in the infinite isotropic medium. A general solution to equation 2.6 and equation 2.7 is

$$\phi = \phi_0 e^{i(\mathbf{k}_l \cdot \mathbf{z} - \omega t)}, \tag{2.10}$$

$$\mathbf{H} = \mathbf{H}_0 e^{i(\mathbf{k}_s \cdot \mathbf{z} - \omega t)}, \tag{2.11}$$

where ϕ_0 and $\mathbf{H_0}$ are arbitrary constants and $\mathbf{k_{l,s}}$ are wavenumber vectors which satisfies the secular equations

$$\mathbf{k}_{l,s} \cdot \mathbf{k}_{l,s} = \frac{\omega^2}{c_{l,s}^2}. \tag{2.12}$$

where $\omega = 2\pi f$ is the angular frequency. In general the wavenumber $\mathbf{k}$ is a complex vector

$$\mathbf{k} = k_{re}\mathbf{n} + ik_{im}\mathbf{b}, \tag{2.13}$$

where k_{re} and k_{im} represent the real and imaginary part of the wavenumber in the directions defined by unit vectors **n** and **b** respectively. The real part of the wavenumber represents the phase propagation and the imaginary part on the other hand represents a spatial attenuation. Equation 2.12 can thus be written as:

$$k_{re}^2 + 2ik_{re}k_{im}\mathbf{n} \cdot \mathbf{b} - k_{im}^2 = \frac{\omega^2}{c^2}. \tag{2.14}$$

This equation admits an infinite number of solution depending on the angle between the vectors **n** and **b**. For an elastic medium, the right hand side of this equation is pure real. It follows in this case that the real part of the wavenumber must be orthogonal to the imaginary part

$$k_{re}k_{im}\mathbf{n} \cdot \mathbf{b} = 0. \tag{2.15}$$

This results in two conditions for equation 2.14. Either $k_{im} = 0$ which describes the propagation of homogeneous plane waves, or $k_{im} \neq 0$ but $(n \cdot b) = 0$ which describes an inhomogeneous wave whose attenuation vector k_{im} is normal to the propagation direction.

The above analysis can be extended to viscoelastic materials. The approach is well described in the literature ([26], [27], [28]) and hence only the results will be mentioned here. As for elastic waves, the governing equations in the viscoelastic case can be split up into shear and longitudinal waves with their respective velocities

$$c_l = \sqrt{\frac{\lambda + 2\mu}{\rho} + i\frac{\lambda' + 2\mu'}{\rho}}, \tag{2.16}$$

$$c_s = \sqrt{\frac{\mu}{\rho} + i\frac{\mu'}{\rho}}, \tag{2.17}$$

where c_l, c_s are the complex longitudinal and shear bulk velocities respectively, ρ is the density, λ and μ are the real Lamé constants and λ' and μ' are the imaginary Lamé constants. i is defined as $\sqrt{-1}$. The Lamé constants of viscoelastic material are generally frequency dependent. This time the right hand term of equation 2.14 is complex and results in real and imaginary wavenumber vectors that are non zero and in general **n** and **b** are neither parallel nor perpendicular.

2.3 Guided Waves in Cylindrical Pipes

2.3.1 Guided waves

Guided wave propagation in cylindrical waveguide structures has been treated by many researchers ([29], [30],[31], [32]), and only a brief overview is given here. The discussion here will be focused on the case of a cylindrical pipe which is the waveguide studied in this thesis.

Since the equation 2.4 is separable in cylindrical coordinates, the solution may be divided into the product of functions of each of the spatial dimensions in cylindrical coordinates

$$\phi, \mathbf{H} = \Gamma_{\phi,\mathbf{H}}(r)\Gamma_{\phi,\mathbf{H}}(\theta)\Gamma_{\phi,\mathbf{H}}(z)e^{i}(\mathbf{k} \cdot \mathbf{r} - \omega t), \tag{2.18}$$

where $\mathbf{k}$ is the wavenumber vector, and $\Gamma_{\phi,\mathbf{H}}(r)$, $\Gamma_{\phi,\mathbf{H}}(\theta)$ and $\Gamma_{\phi,\mathbf{H}}(z)$ describe the field variation in each spatial coordinate. Assuming that the wave does not propagate in the radial direction (r) and that the displacement field varies harmonically in the axial (z) and circumferential (θ) directions, equation 2.18 can be written as

$$\phi, \mathbf{H} = \Gamma_{\phi,\mathbf{H}}(r)e^{i\nu\theta}e^{i(kz-\omega t)}, \tag{2.19}$$

where k is the component of the complex vector wavenumber in the z direction. ν is referred to as the circumferential order which must be a whole number, since only propagation in the direction of the axis of the cylinder is considered and the field variables must be continuous in the angular direction.

Substituting these expressions of the potentials into equation 2.6 and equation 2.7, $\Gamma(r)$ can be expressed in terms of Bessel functions. For example, to demonstrate the wave's behavior for an axisymmetric guided wave mode, let $\nu = 0$. $\Gamma_{\phi,\mathbf{H}}(r)$ will have the form [23]

$$\Gamma_\phi(r) = A_1 J_0(\alpha r) + A_2 Y_0(\alpha r), \tag{2.20}$$

$$\Gamma_{\mathbf{H}}(r) = B_1 J_1(\beta r) + B_2 Y_1(\beta r), \tag{2.21}$$

where

$$\alpha^2 \;\;=\;\; \frac{\omega^2}{c_l{}^2} - k^2, \tag{2.22}$$

$$\beta^2 \;\;=\;\; \frac{\omega^2}{c_s{}^2} - k^2. \tag{2.23}$$

Here J_m and Y_m are Bessel functions of the first and second kind, respectively.

Recalling from equation 2.4 and Hooke's law, the field variables such as displacements and stresses can be expressed in terms of potential functions which are functions of r satisfying the Bessel differential operator (for example, $f(r)$,$g_1(r)$ and $g_3(r)$ in reference [29]). Therefore, in general, the field variables, for example the displacements, can be written as

$$U_{r,\theta,z} \;\;=\;\; U_{r,\theta,z}(r)e^{i\nu\theta}e^{i(kz-\omega t)}. \tag{2.24}$$

$$\tag{2.25}$$

where $U_{r,\theta,z}(r)$ can be considered as radial distribution function of the displacement in r, θ and z directions, respectively.

A waveguide can consist of a number of layers itself, e.g. the pipe may be filled with liquid or solid contents (Fig. 2.1). The displacement and stress in each layer are expressed in terms of potential functions. The solutions for these potential functions are substituted into these equations. This provides, in each layer of the waveguide, six equations in terms of unknown partial wave amplitudes that correspond to the coefficients of the Bessel functions used in the solution. The amplitudes, directions and phases of the partial waves must be determined such that the boundary conditions at the boundaries of the waveguide are satisfied, where Snell's law must be obeyed [25]. A guided wave in the waveguide therefore can be thought of as a superposition of partial bulk waves which are reflected within the waveguide boundaries (see Fig. 2.1).

In order to determine the guided waves in arbitrary multilayered system, a general purpose software tool DISPERSE was developed by Lowe [33] and Pavlakovic [34,

35]. This is based on the 'global matrix method' proposed by Knopoff [36], later refined by Schmidt and Jensen [37]. The global matrix denoted [G] relates the partial wave amplitudes to the physical constraints of the multilayered waveguide and forms the equation

$$[G]\{A\} = 0, \tag{2.26}$$

where $\{A\}$ is a vector of the partial wave magnitudes. The above equation is satisfied when the determinant of the global matrix vanishes, and solutions are sought in the wavenumber-frequency space. If the material is absorbing, or the layer is immersed so that it leaks waves into the surrounding medium, then the wavenumber becomes complex whose imaginary part describes the attenuation of the guided wave. The resulting roots are connected together to form dispersion curves of different guided wave modes in the waveguide.

Three different families of modes are present in cylindrical waveguides: longitudinal, torsional, and flexural modes. Each family of modes itself comprises an infinite number of modes. The modal fields of longitudinal and torsional modes are constant around the circumference, which means that the circumferential order ν is zero, while the flexural modes are non-axisymmetric with $\nu \geq 1$.

As an example, Fig. 2.2 shows the phase velocity dispersion curves of guided wave modes in a steel pipe surrounded by vacuum, predicted with DISPERSE. The material properties for steel are given in Tab. 2.1. The phase velocity dispersion curves show velocities of the wave cycles within a signal. The mode naming convention in this thesis follows the one used by Silk and Bainton [32]. Longitudinal and torsional modes are denoted as L(0,n) and T(0,n), respectively. In this notation, the first number indicates the circumferential order, being zero for both longitudinal and torsional modes, whereas the second number is a counter in order to distinguish between the modes of the same family. Flexural modes are abbreviated according to the notation $F(\nu, n)$ and only the first order flexural modes are plotted here.

Table 2.1: Material properties of the steel pipe and the filling fluid used for DISPERSE calculations. η and ρ are the viscosity and density of the fluid respectively and ω is the circular frequency

	Longitudinal velocity(m/s)	Shear velocity(m/s)	Density(kg/m^3)
Steel	5959	3260	7392
Viscous fluid	1500	$\sqrt{\frac{2\eta\omega}{\rho}}$	1000

2.3.2   Mode shape

One effective method of examining the wave modes is to look at the mode shape at each point on the dispersion curves. The mode shape displays how the displacements, stress or energy vary through the thickness of the waveguide system. The mode shapes are calculated to be of arbitrary absolute amplitude but show the correct relative amplitude compared to another displacement or stress component.

The different mode families are best distinguished by considering the components of their displacement mode shapes:

- Longitudinal (L) modes: $U_z, U_r \neq 0$ $U_\theta = 0$
- Torsional (T) modes: $U_\theta \neq 0$ $U_z, U_r = 0$
- Flexural (F) modes: $U_z, U_r, U_\theta \neq 0$

All mode shape predictions are also calculated with DISPERSE. Fig. 2.3 shows as an example, the displacement mode shapes of the L(0,1), L(0,2), T(0,1) and F(1,3) modes respectively at 0.8 MHz in Fig. 2.2.

The displacement mode shape in Fig. 2.3a shows that at this frequency, the L(0,1) mode is characterized predominantly by the radial displacement, while the L(0,2) mode at the same frequency can be simply considered as an extensional mode as shown in Fig. 2.3b: the axial displacement is dominant compared to the radial displacement and nearly remains constant through the pipe wall. The T(0,1) mode only has the displacement in the circumferential direction as shown in Fig. 2.3c. The F(1,3) mode has displacement in all three directions (Fig. 2.3d).

2.3.3 Dispersion

The dispersion phenomenon is due to frequency-dependent velocity variations. In 1877 Lord Rayleigh [38] had already observed that the velocity of a group of waves could be different from the velocity of the individual wave. He described the concepts of phase (C_p) and group velocity (C_g). The phase velocity is the rate at which the phase of the wave propagates in space, that is the velocity at which the phase of any one frequency component of the wave will propagate. The group velocity is the velocity at which a wave packet will travel at a given frequency and is the derivative of the frequency wave-number dispersion relation. Phase and group velocities are related to each other through the following equation (see [23] and [24] for more details):

$$C_g = C_p + k\frac{\partial C_p}{\partial k} \tag{2.27}$$

where k is the wavenumber.

Another commonly used concept is the energy velocity that is the velocity at which the wave carries its potential and kinetic energy along the structure. Long range testing usually makes use of finite tone bursts or wave packets and optimally exploits waves at frequencies where there is little dispersion, thus the different frequency components within the wave packet propagate at the same velocity and so the wave packet retains its shape as it travels. Naturally it would be expected that the energy to be transported at the speed of travel of the wave packet, and typically in practice it is true to take this to be equal to the group velocity. However such a relationship does not always hold. If an attenuating wave (caused by leakage or material damping) is described, as is conventional, by a complex wave number, then the group velocity calculation yields non-physical solutions, while the energy velocity calculation is more stable and accurate [39].

Fig. 2.4a shows the group velocity dispersion curves for guided wave modes in Fig. 2.2. Fig. 2.4a shows that, except the T(0,1) mode which is completely non-dispersive, all the other guided wave modes have very different dispersion characteristics at different frequencies. To illustrate this, Fig. 2.4b and c show (calculated with DISPERSE) a 10 cycle toneburst signal of the L(0,2) mode monitored after 1

meter of its propagation with the central frequency of the signal respectively selected at the non-dispersive region (point A, 650 kHz) and dispersive region (point B, 250 kHz) on the L(0,2) mode in Fig. 2.4a. The signal becomes dispersive in Fig. 2.4c, which is exhibited by the increasing wave-packet duration and decreasing amplitude.

The effect of dispersion is undesirable for guided waves, since the energy in a dispersive wave-packet is not conserved as it propagates at different speeds depending on the frequency. The amplitude of the wave-packet reduces as the signal propagates further (see signals in Fig. 2.4b and c). This reduces the sensitivity of the measurements using guided waves.

2.4 Guided Wave Propagation in Pipes Filled with Inviscid Fluid

One purpose of this thesis is to develop a guided wave measurement technique for characterising fluid properties inside pipes, so it is important to review the model of guided wave propagation in a pipe filled with a fluid, which has been the subject of numerous studies. For example, the problem of an acoustic wave travelling in a thin-walled elastic shell with a compressible, inviscid fluid was first solved by Lin and Morgan [40]. Fuller and Fahy [41] calculated the dispersion curves for axisymmetric waves and for the first-order nonaxisymmetric modes in a pipe containing inviscid fluid. Guo presented approximate solutions to the dispersion equation for fluid-loaded shells [42] and has studied the attenuation of helical waves in a three-layered shall consisting of elastic and viscoelastic layers [43]. Sinha and co-workers [44, 45] addressed the case of axially-symmetric guided wave propagation in pipes with fluid on the inside or the outside of the pipe. Lafleur and Shields [46] discussed the influence of the pipe material on the first two longitudinal modes in a liquid-filled pipe, considering the low frequency range only. The case of a pipe filled with a viscous liquid has been theoretically analyzed by Elvira [47]. Long, et al. [48] studied the possible axisymmetric modes that propagate at low frequencies in buried water-filled pipes. Vollmann et al. [49] have theoretically studied the guided waves propagating in a cylindrical shell containing a viscoelastic medium.

2.4.1   Dispersion curves

Let us first look at the dispersion curves of guided longitudinal modes propagation in pipes filled with a inviscid fluid such as water. The material properties of the pipe and fluid are listed in Tab. 2.1, but the viscosity of the fluid (η) is assumed to be zero. Fig. 2.5 shows that the presence of the fluid significantly changes the dispersion curves of the longitudinal modes in the filled pipe. The modes of the fluid-filled pipe are labelled as L_1, L_2.... L_7. The most dramatic changes are experienced by the free pipe mode L(0,2) which is branched into several modes (L_3, L_4, L_5, L_6, L_7), which are separated by new cut-off frequencies. Also, the filling water inside the pipe introduces an extra mode referred to as '$\alpha1$' [48]. This mode was found to be a water-borne mode and therefore it can only be well excited if the excitation is made in the filling fluid [48].

2.4.2   Mode jumping

In order to have a better understanding of the dispersion characteristics of the longitudinal modes in the water-filled pipes, two families of asymptotic modes are considered: one consists of the modes in the free pipe such as L(0,1), L(0,2); the second (labelled as M_1, M_2...) includes the modes of the fluid column inside the pipe assuming a rigid boundary condition at the inside pipe wall.

The dispersion curves of the modes in the fluid column with rigid boundary condition at its outside surface are given by [50]

$$C_p = \frac{\omega}{\sqrt{\frac{\omega^2}{c_l{}^2} - \frac{m_n{}^2}{R_1{}^2}}} \tag{2.28}$$

where R_1 is the inner radius of the pipe. c_l and C_p denote the bulk longitudinal velocity in the fluid and the phase velocity of the modes in the fluid column, respectively. m_n is the nth ($n = 0, 1, 2, 3....$) root of the first J-Bessel function (e.g $m_0 = 0$, $m_1 = 3.833$, $m_2 = 7.015...$).

The cut-off frequency of the nth mode in the fluid column is then determined by:

$$f_n = \frac{c_l m_n}{2\pi R_1} \qquad (2.29)$$

Equations 2.28 and 2.29 clearly show that dispersion and cut-off frequencies of the modes in the fluid column only depend on the bulk velocity of the fluid and the radius of the fluid column.

When combining the modes in the free pipe and the fluid column as shown in Fig 2.6, the longitudinal modes in the water-filled pipe (labelled as L_1, L_2...) are found to be derived from the coupling of these two groups of asymptotic modes. The coupling causes the jumping of the longitudinal mode path between several asymptotic modes. For instance, let us consider the path of the water-filled pipe mode L_4. It originates from the fluid modes M_3, however, as frequency increase to 400 kHz, it veers towards the free pipe mode L(0,2). As frequency increases further to 560 kHz, this mode jumps to the fluid mode M_4 and follows M_4's path afterwards. Similar mode jumping phenomena has been well studied for the case of guided waves in a flat bilayer [51, 52].

2.4.3   Energy flow distribution

The energy flow of the guided wave is the rate at which it propagates energy along a particular direction. The average guided wave energy flow density over a period in the axial direction (z) is defined as the product of the velocity vector and the stress vector [53, 54]:

$$I_z \;=\; -(\sigma_{rz}[\dot{U}_z]^* + \tau_{r\theta}[\dot{U}_\theta]^* + \tau_{rr}[\dot{U}_r]^*), \qquad (2.30)$$

where the superscript asterisk means conjugate.

For the guided wave modes in the water-filled pipe, total time-averaged axial energy

flow in the pipe wall (E_p) and in the fluid column (E_f) can be obtained by integrating Eq (2.30) over the thickness of the pipe wall

$$E_p = \frac{1}{2} Re \left\{ \int_0^{2\pi} \int_{R_1}^{R_2} I_z r d\theta dr \right\}, \tag{2.31}$$

and the thickness of the fluid column

$$E_f = \frac{1}{2} Re \left\{ \int_0^{2\pi} \int_0^{R_1} I_z r d\theta dr \right\}. \tag{2.32}$$

Here, R_1 and R_2 represent the inner and outer radius of the pipe. In order to quantify the distribution of propagating energy between the pipe and the fluid, a parameter, energy flow ratio (EFR), is defined as the ratio of the energy flow in the pipe to that in the fluid

$$EFR \quad = \quad \frac{E_p}{E_l} \tag{2.33}$$

If EFR$\gg$1, the energy of the guided wave is mostly concentrated in the pipe wall, while if EFR$\ll$1 , the energy flow is mainly stored in the filling water. When EFR$\approx$1, the energy flows in the fluid and the pipe are comparable.

Fig. 2.7a shows the EFR of the selected guided wave modes shown in Fig. 2.7b. The EFR for each mode shows frequency dependence, which means the energy distribution between the pipe and the filling water changes with frequency. A general feature of the EFR curves is that the energy distribution changes accordingly as the mode jumping takes place. For each mode, energy is mainly concentrated in the pipe when the water-filled pipe modes follow the path of the free pipe modes; however, at the frequencies where the water-filled pipe modes approach the modes of the fluid column, a large amount of energy is in the fluid, which is exhibited by a small value of EFR.

2.5 Guided Wave Propagation in Pipes Filled with Viscous Fluid

2.5.1 Low-viscosity fluid

Now let us consider the case of longitudinal modes propagating in the same pipe filled with a low-viscosity fluid (its material properties are summarized in Tab. 2.1). The fluid is assumed to be Newtonian with a low viscosity ($\eta = 1 Pas$). The viscous fluid is modeled as a hypothetical solid [55] with appropriate bulk longitudinal, shear velocity and attenuation. The bulk shear velocity of the viscous fluid is different but derived from its complex shear modulus and their relationship can be retrieved as shown in [53]. Figure 2.8 shows the energy velocity dispersion curves of the longitudinal modes which can propagate in the pipe. As before, the modes of the fluid-filled pipe are labelled as L_1, L_2.... L_7. For comparison, the dispersion curves for the case when the fluid is inviscid is also plotted. The two sets of dispersion curves overlap, which means the low viscosity of the filling fluid has little influence on the dispersion curves of the longitudinal modes. Frequencies where two neighboring modes intersect each other on their energy velocity dispersion curves are also indicated which are referred to as the 'branching frequencies' [56] (marked by dashed vertical lines in Fig. 2.8).

The dispersion change of the longitudinal modes in a fluid-filled pipe is mainly determined by the longitudinal bulk velocity of the fluid and the pipe inner diameter [47, 57, 58]. Fig. 2.9a, shows the energy velocity dispersion curves of the longitudinal modes in a pipe filled with a low-viscosity liquid ($\eta = 1 Pas$), for two different longitudinal bulk velocities of the fluid. The low velocity dispersion curve below the branching points for each mode is removed, since the mode become fluid-dominant at these frequencies. Two regions on the dispersion curve of each mode are defined. The region exhibiting little dispersion and approaching the free pipe mode L(0,2) is termed the 'plateau region', while the other part will be referred to as the ' branching region'. In the branching regions, the dispersion curves are more sensitive to variation of the longitudinal bulk velocity of the fluid than in the plateau regions.

Fig. 2.10 shows the displacement mode shapes of two selected frequencies respectively at the plateau region (point A) and branching region (point B) of the L_4 mode. The mode shape at point A shows that in the plateau region of its dispersion curve, a mode is characterized by having predominantly axial displacement in the pipe wall, which means the energy is mainly concentrated in the pipe wall. The gap appearing in the axial displacement at the interface between the pipe wall and the fluid should not be interpreted as a discontinuity: this sudden change is due to the shear viscosity in the fluid which causes the appearance of a very thin boundary layer in the proximity of the pipe wall [47]. At point B, where the mode approaches its branching point, the mode shape shows that the axial displacement in the wall has decreased considerably and the mode becomes fluid dominated.

The low viscosity of the fluid has only a subtle influence on the dispersion curves of the longitudinal modes, however, it causes the attenuation of the modes [47, 57]. There are two sources of attenuation of the longitudinal modes. One is the drag exerted on the waves traveling in the wall by the shear viscosity of the fluid; the other is the leakage of longitudinal waves into the fluid and their subsequent attenuation. However, it is worth mentioning that in this geometry, there would be no leakage induced attenuation if the fluid were viscosity-free because no energy would be lost from the waveguide. Fig. 2.9b displays the attenuation of the longitudinal modes as a function of frequency for two different values of viscosity at a fixed longitudinal bulk velocity ($C_l = 1500m/s$). The attenuation of the longitudinal modes shows a good sensitivity to the viscosity at the plateau regions, where the modes show predominantly axial displacement mode shape in the pipe wall (Fig. 2.10a). Therefore, the attenuation at these frequencies is mainly due to the shear drag exerted by the viscosity of the filling fluid.

2.5.2   Highly viscous fluid

The case of the pipe containing a highly viscous fluid is also considered (its material properties are summarized in Tab. 2.1). The fluid is still assumed to be Newtonian and has a large value of viscosity $\eta = 25 Pas$. Fig. 2.11a shows the energy velocity dispersion curves of longitudinal modes for two different viscosities at a fixed longitudinal bulk velocity ($C_l = 1500m/s$) of the fluid. It shows that, besides its bulk

velocity, the high viscosity of the filling fluid also changes the dispersion curves of the longitudinal modes. The plateau regions of the separated modes in Fig. 2.9a, combine into the single L_3 mode in Fig. 2.11a, which also exhibits periodic minima almost at the branching frequencies. The sharpness of the branching regions of this mode is compromised by the increased viscosity. It is important to observe that the viscosity has little influence on the positions of the minima of the L_3 mode's energy velocity, which are only determined by the bulk velocity of the fluid.

To interpret the change of the group velocity dispersion curves due to the large viscosity of the fluid, the corresponding phase velocity dispersion curves is shown in Fig. 2.12. The two families of asymptotic modes (the free pipe modes and the modes in the fluid column with rigid boundary condition at the inside of pipe wall) are also plotted. Fig. 2.12 shows that the mode jumping between the two families of asymptotic modes does not necessarily happen when the viscosity of the filling fluid becomes large. As the viscosity of the filling fluid increases, the interaction of the two asymptotic modes becomes weak and most of the energy is confined in either the pipe or in the fluid column, and modes no longer jump. For example, the L_3 mode, whose energy travels primarily in the pipe closely follows the path of the free pipe mode L(0,2), rather than jumping down to the fluid modes as it happened when the viscosity of the filling fluid was small. On the other hand, modes such as L_4, L_5, L_6, L_7 become complete fluid-dominant modes whose energy is trapped in the fluid. These modes have little practical interest, as they are highly attenuated with distance. More discussions regarding the influence of the material damping on the mode jumping of guided wave in a flat bilayer can be found in [51, 52, 59].

Figure 2.11b shows the attenuation of the L_3 mode, which displays periodic peaks at the frequencies where its energy velocity reaches its minima. Relatively low attenuation occurs at frequencies of the plateau regions of the L_3 mode where the attenuation also has a good sensitivity to viscosity changes. Other modes have much stronger attenuation and for this reason are of no practical interest, thus for clarity they are not shown in Fig. 2.11b.

2.5.3 Density of fluid

Fig. 2.13 shows the energy velocity dispersion curves of longitudinal modes in a pipe filled with a low-viscosity fluid ($C_l = 1500 m/s$, $\eta = 1 Pas$) for two different values of fluid density. It shows that the dispersion curves of the longitudinal modes have low sensitivity to the change of the density of the filling fluid. This can be expected since the density of the fluid is much lower than that of the pipe material.

2.6 Summary

In this chapter, the theory behind the propagation of bulk ultrasonic waves in infinite media and of guided waves in cylindrical pipes has been briefly reviewed. In an unbounded elastic medium, bulk ultrasonic waves can propagate as homogeneous or inhomogeneous bulk longitudinal and shear waves. In waveguides such as pipes, partial bulk waves reverberating between the boundaries of the waveguide are superposed to form a guided wave propagating along the structure. Features of guided wave modes in pipes such as velocity dispersion and mode shape were introduced.

The model of guided longitudinal modes propagation in pipes filled with fluids has been revisited to summarize the new characteristics of the guided waves in pipes due to the presence of the filling fluid.

The longitudinal modes in pipes filled with fluid can be viewed as an interaction between the free pipe modes and the modes in the fluid column with a rigid boundary condition at the internal pipe wall. For low-viscosity fluid, the dispersion curves of the longitudinal modes in the fluid-filled pipe jump between the two families of asymptotic modes. However, as the viscosity increases the interaction becomes weak and most of the energy is confined in either the pipe or in the filling fluid, and modes no longer jump.

It is found that the presence of the fluid changes the velocity dispersion of the longitudinal modes and causes attenuation to the modes if the fluid is viscous. For low-viscosity fluid, the dispersion curves of the longitudinal modes and the corresponding branching frequencies are uniquely determined by the bulk longitudinal

velocity of the fluid, while the attenuation of the modes is sensitive to the change of viscosity of the fluid over certain frequency ranges on the dispersion curves. For the highly viscous fluid, the dispersion curves of the modes are influenced by both the bulk velocity and shear viscosity of the fluid; however, the viscosity has little influence on the branching frequencies which are almost only determined by the bulk velocity of the fluid.
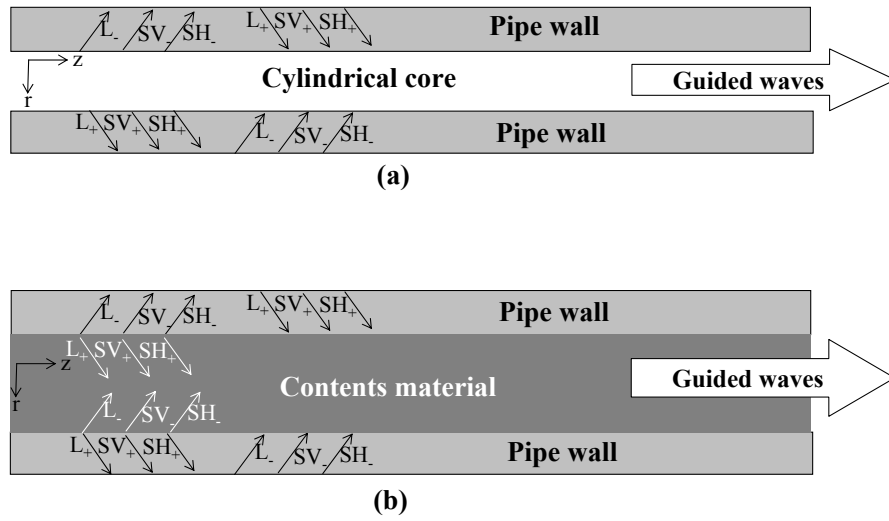
Figure 2.1: Schematics showing the superposition of partial bulk waves to form guided waves in a clean pipe (a) and (b) a pipe filled with contents. L, SH and SV stand for bulk Longitudinal waves, Shear Vertical waves and Shear Horizontal waves.
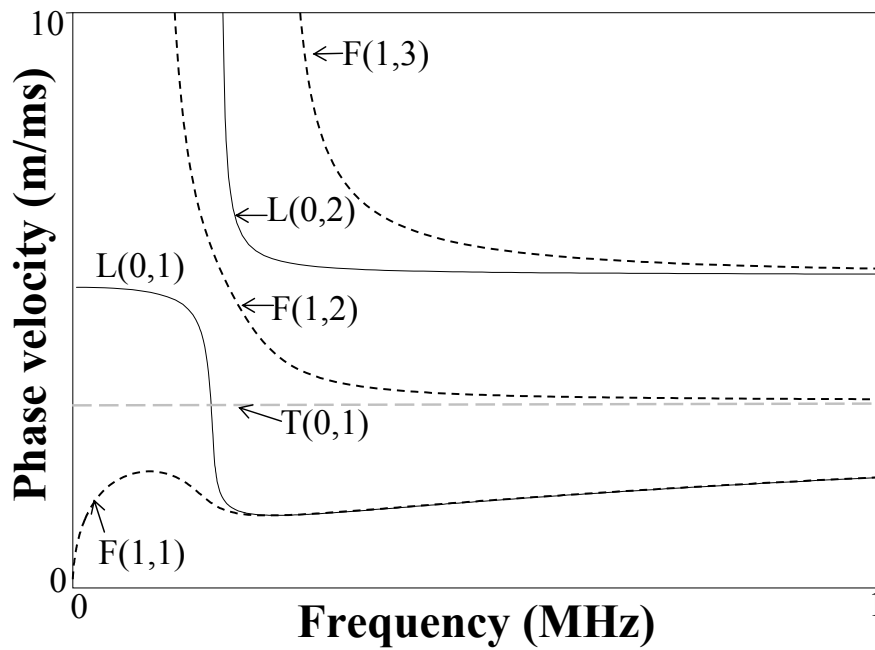
Figure 2.2: Phase velocity dispersion curves of the longitudinal (black solid curves), torsional (gray dashed line) and flexural modes (black dashed curves) in an empty steel pipe (9 mm inner diameter and 0.5 mm thickness). Material properties are given in Tab. 2.1.
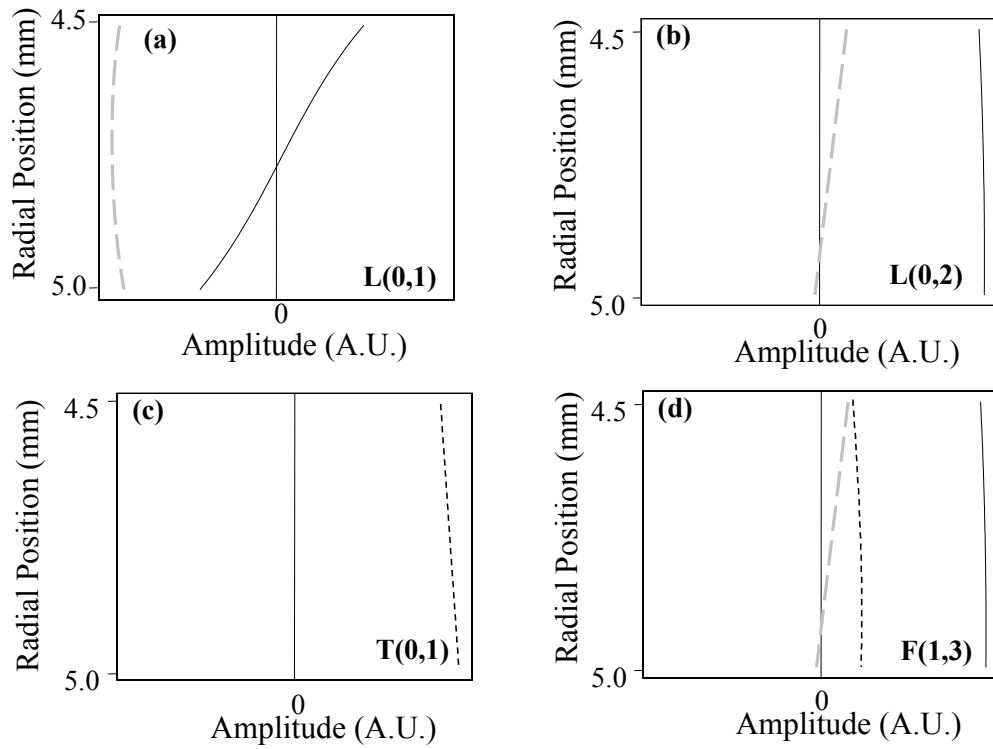
Figure 2.3: (a) Displacement mode shapes at 0.8 MHz for the L(0,1) mode (b) for the L(0,2) mode (c) for the T(0,1) mode (d) for the F(1,3) mode in Fig. 2.2. (black solid line) axial displacement; (gray dashed line) radial displacement; (black dotted line) circumferential displacement. The radial positions 4.5 and 5.0 correspond to the inside and outside surface of the pipe wall, respectively.
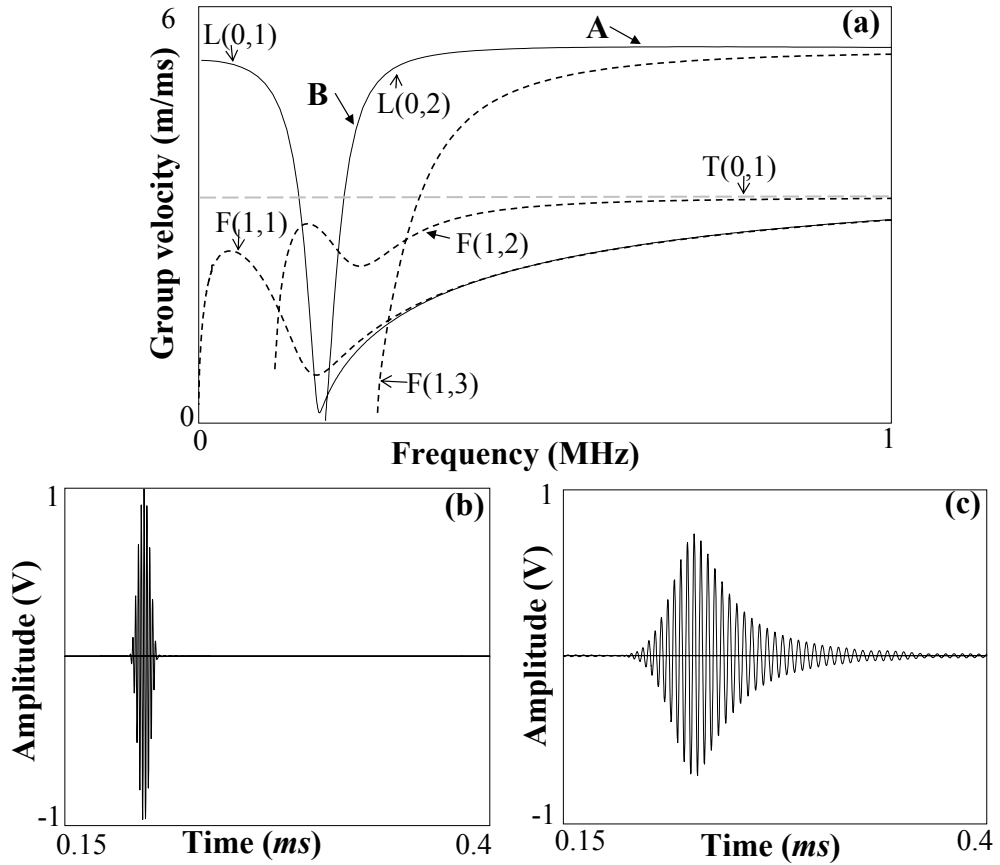
Figure 2.4: (a) Group velocity dispersion curves of the longitudinal (black solid curves), torsional (gray dashed line) and flexural modes (black dashed curves) in an empty steel pipe (9 mm inner diameter and 0.5 mm thickness). Material properties are given in Tab. 2.1; (b) The signal of the L(0,2) mode at point A in Fig. 2.4a after 1 meter of its propagation; (c) The signal of the L(0,2) mode at point B in Fig. 2.4a after 1 meter of its propagation.
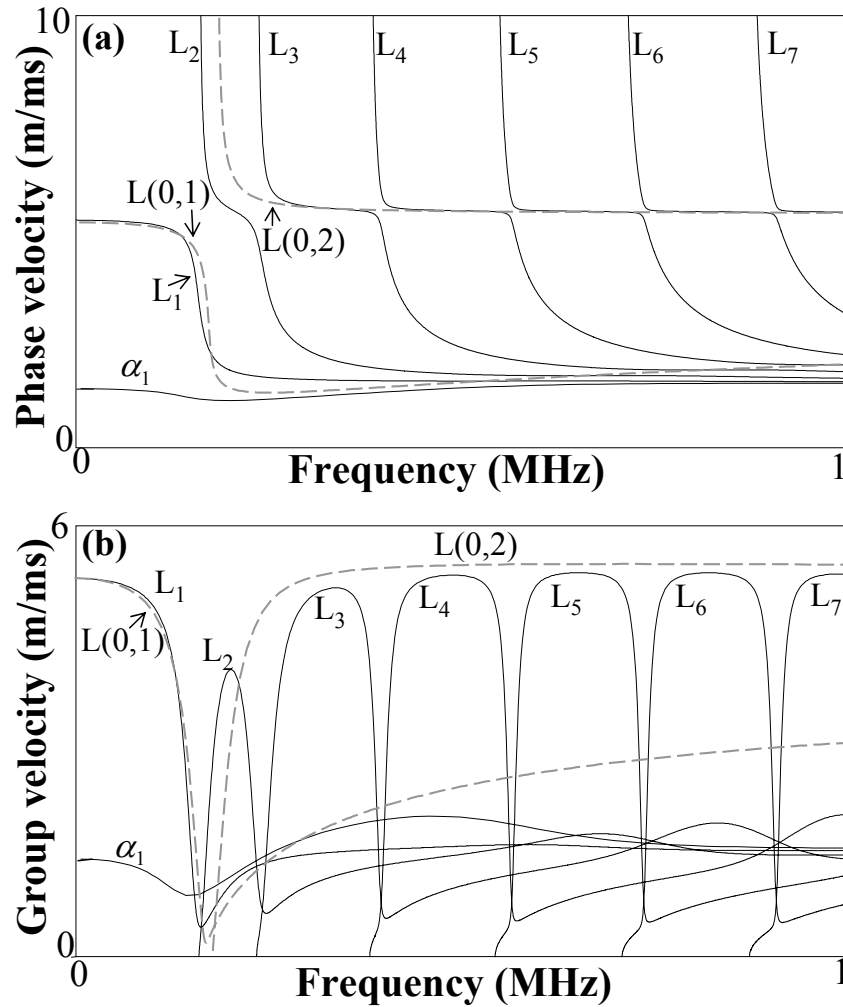
Figure 2.5: (a) Phase velocity and (b) group velocity dispersion curves of longitudinal modes in a steel pipe (9 mm inner diameter and 0.5 mm thickness) filled with water (black solid curves). For comparison, the longitudinal modes in the empty pipe are also given (gray dashed curves). Material properties are given in Tab. 2.1.
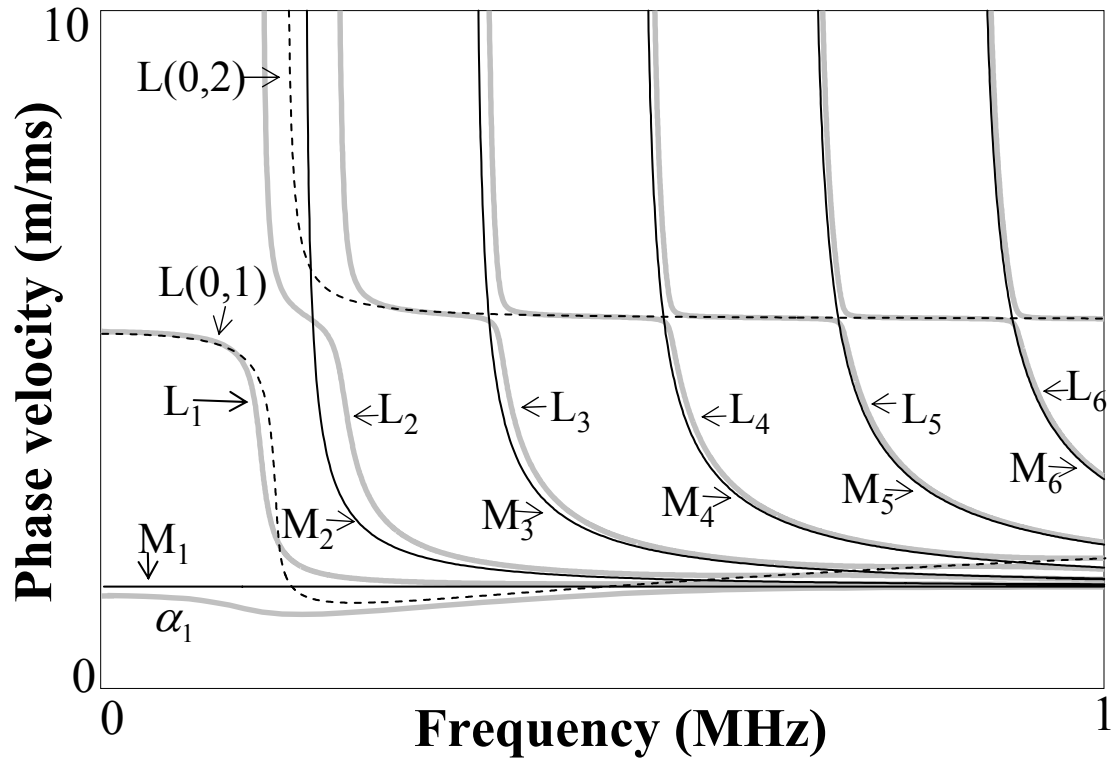
Figure 2.6: Phase velocity dispersion curves of longitudinal modes in a steel pipe (9 mm inner diameter and 0.5 mm thickness) filled with water (gray solid curves). Two family of asymptotic modes are also shown as free pipe modes (black dashed curves) and modes in the fluid column (black solid curves).
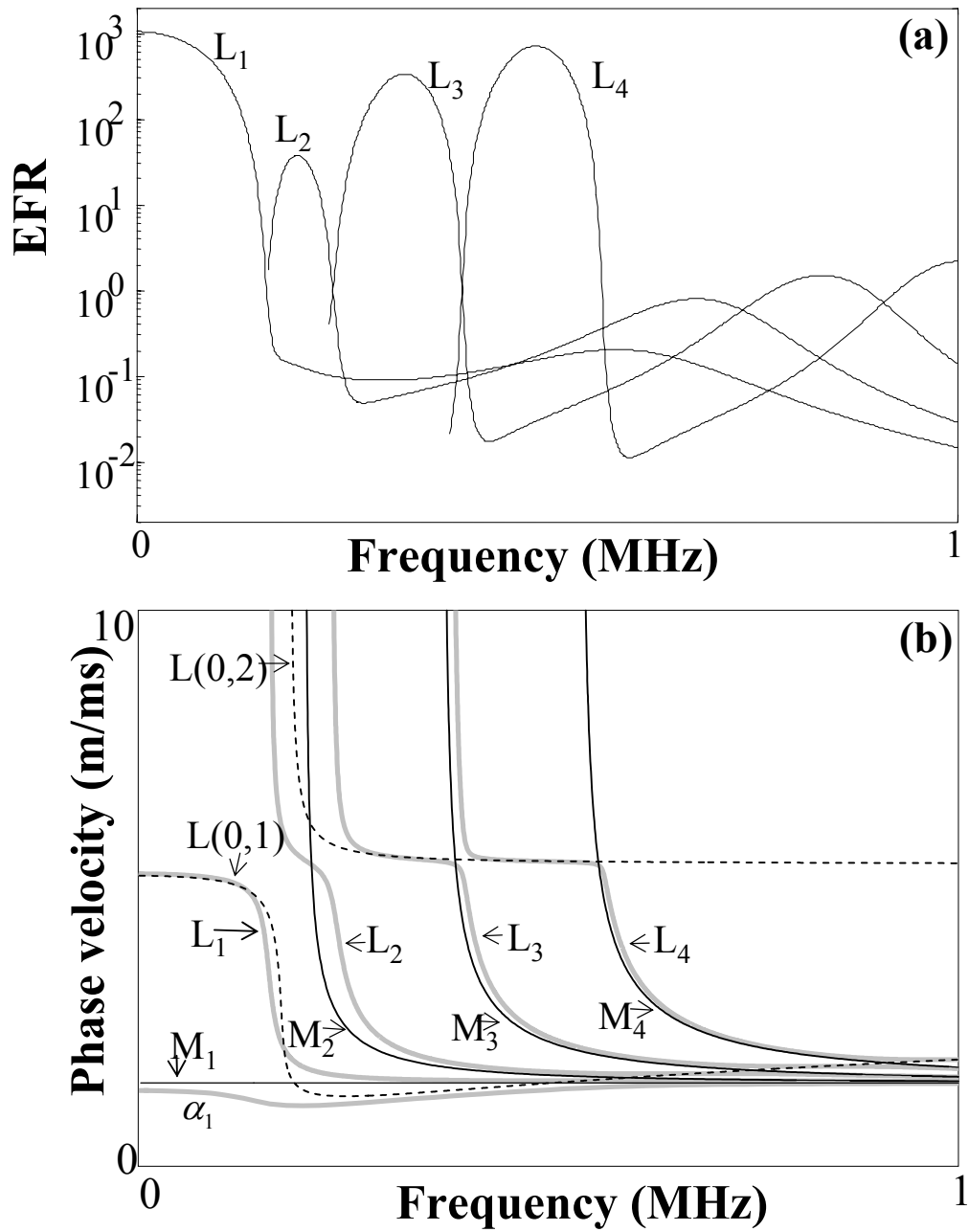
Figure 2.7: (a) Energy flow ratio (EFR) of the selected modes in the steel pipe filled with water; (b) corresponding phase velocity dispersion curves of the selected modes (gray solid curves) and two families of asymptotic modes, being free pipe modes (black dashed curves) and modes in the fluid column (black solid curves).
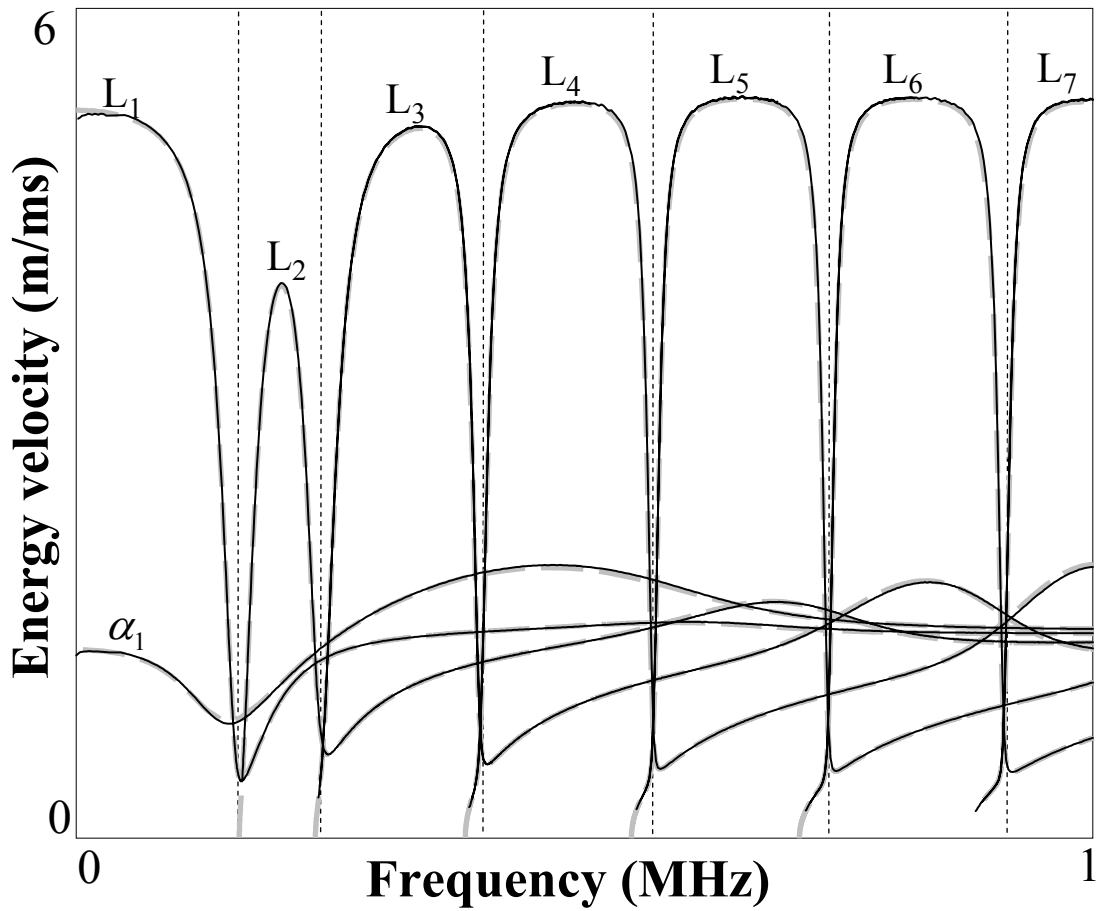
Figure 2.8: Energy velocity dispersion curves of longitudinal modes in a steel pipe (9 mm inner diameter and 0.5 mm thickness) filled with a inviscid fluid (gray dashed curves) and with a low-viscosity fluid (black solid line) (viscosity $\eta = 1 Pas$). Material properties are given in Tab. 2.1.
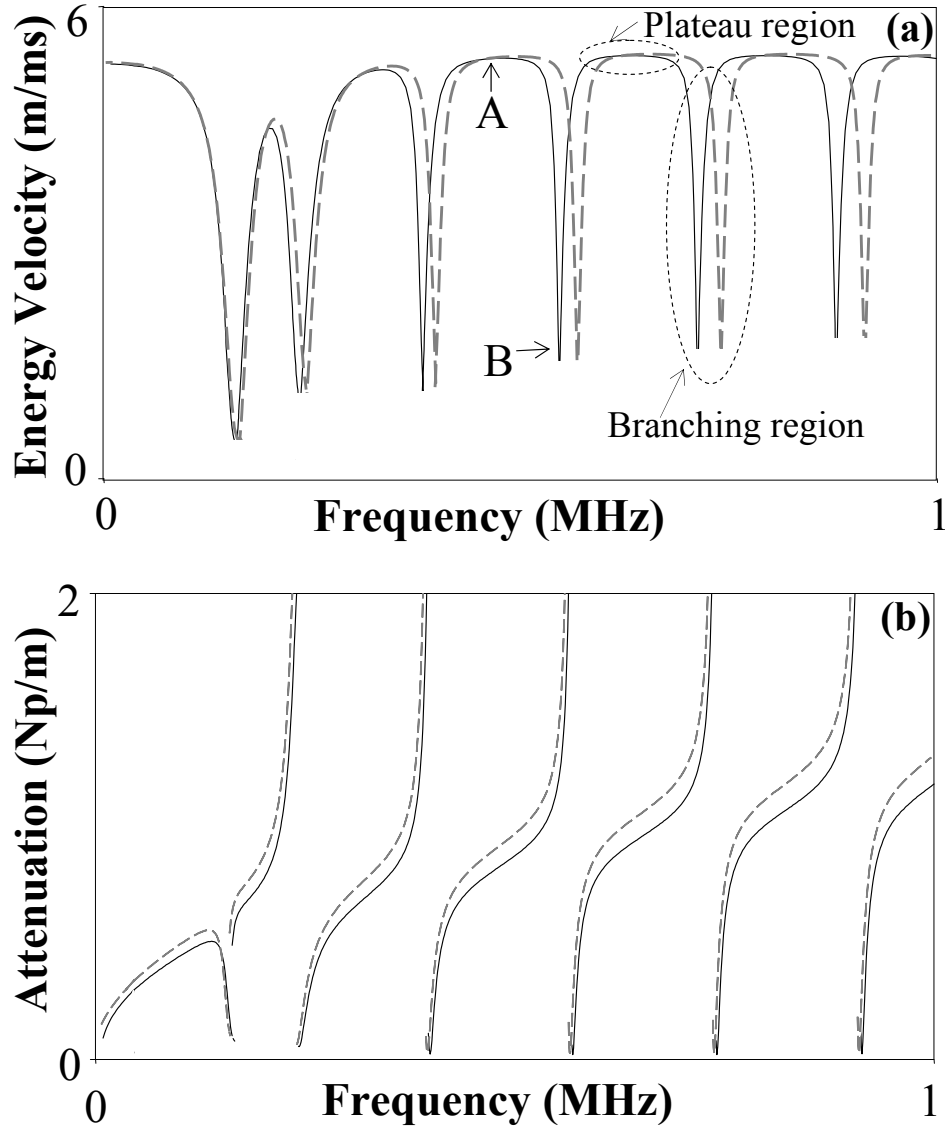
Figure 2.9: (a) Energy velocity dispersion curves (above the branching points) of longitudinal modes in a steel pipe filled with a low viscosity fluid ($\eta = 1Pas$) for different values of longitudinal bulk velocity of the fluid $C_l = 1450m/s$ (solid line); $C_l = 1500m/s$ (dashed line);(b) Attenuation of longitudinal modes (above the branching points) in a steel pipe filled with a fluid ($C_l = 1500m/s$) with different value of viscosity $\eta = 1Pas$(solid line); $\eta = 1.2Pas$(dashed line).
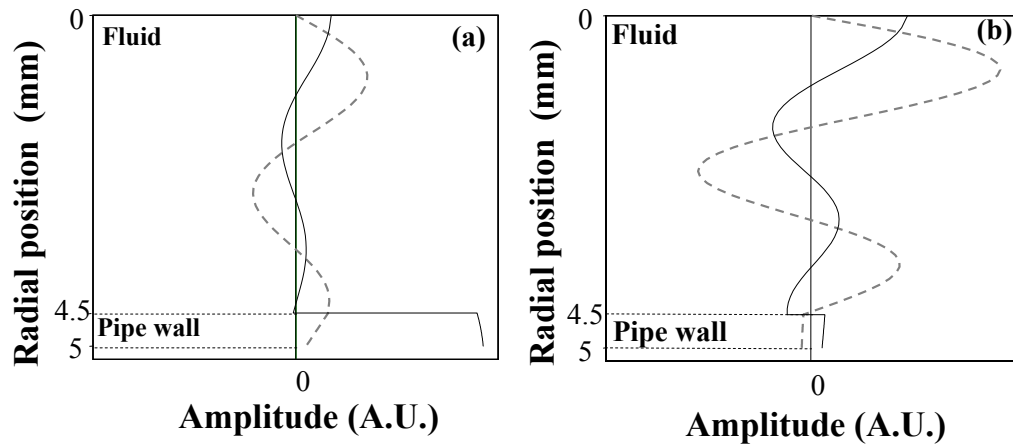
Figure 2.10: Displacement mode shapes of selected points on Fig. 2.9b. (a) Mode shape of point A. (b) Mode shape of point B. (solid line) axial displacement; (dashed line) radial displacement.
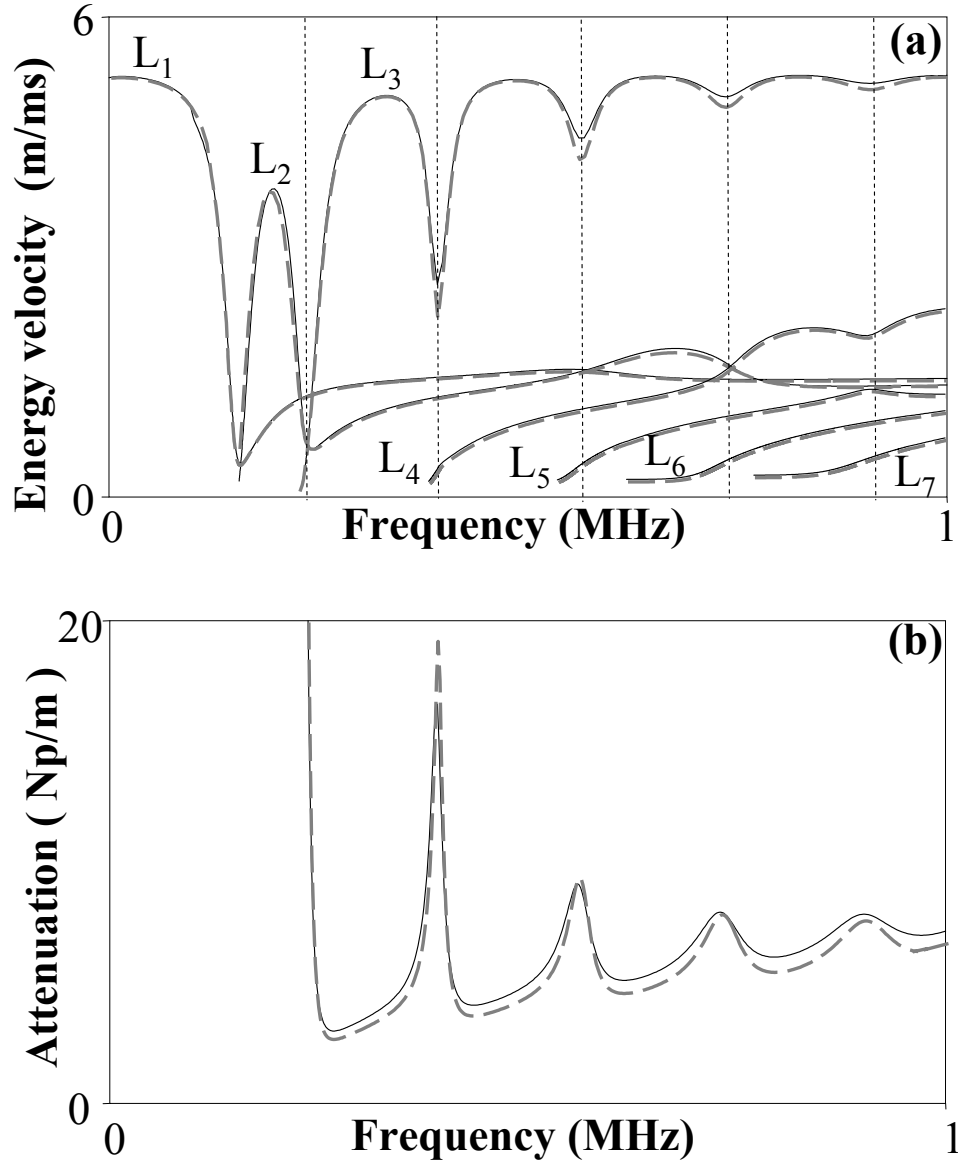
Figure 2.11: (a) Energy velocity dispersion curves of longitudinal modes in a steel pipe filled with highly viscous fluid ($C_l = 1500m/s$) with different values of viscosity. ($\eta = 25Pas$(black solid line); $\eta = 20Pas$(gray dashed line)); (b) Attenuation of the L_3 mode in Fig. 2.11a. ($\alpha = 25Pas$(black solid line); $\alpha = 20Pas$(gray dashed line))
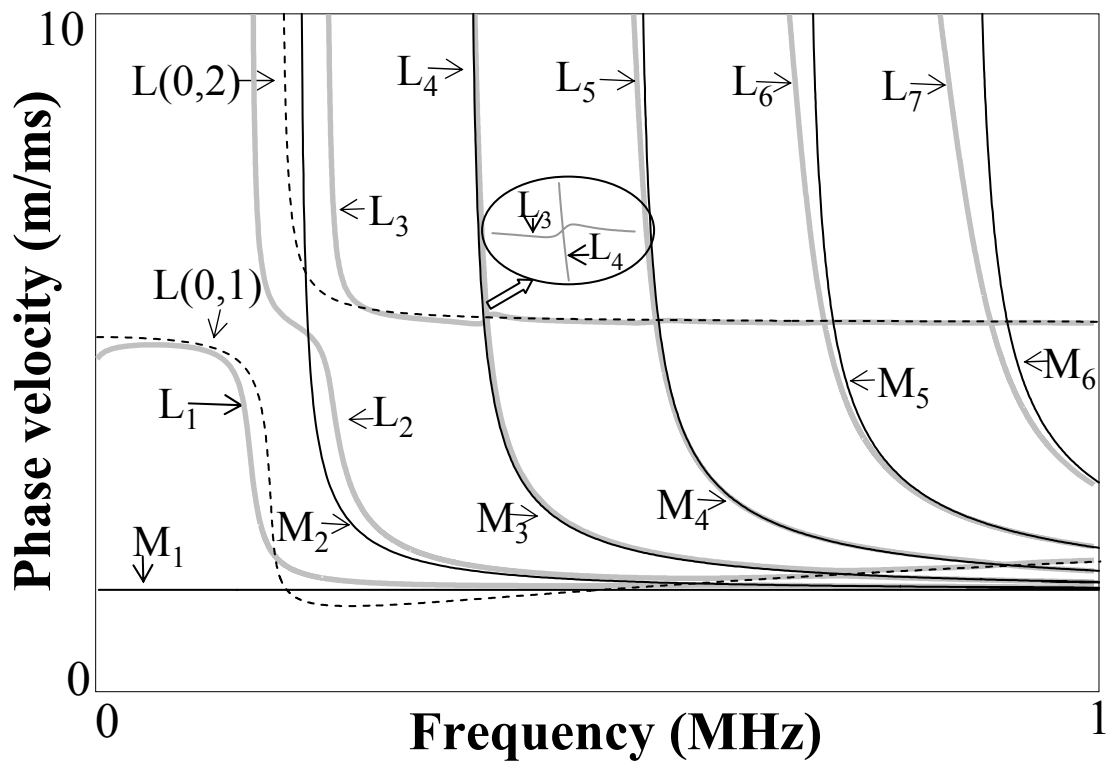
Figure 2.12: Phase velocity dispersion curves of longitudinal modes in a steel pipe filled with highly viscous fluid ($C_l = 1500m/s$, $\eta = 25Pas$) (gray solid curves). Two family of asymptotic modes are also shown as free pipe modes (black dashed curves) and modes in the fluid column (black solid curves).
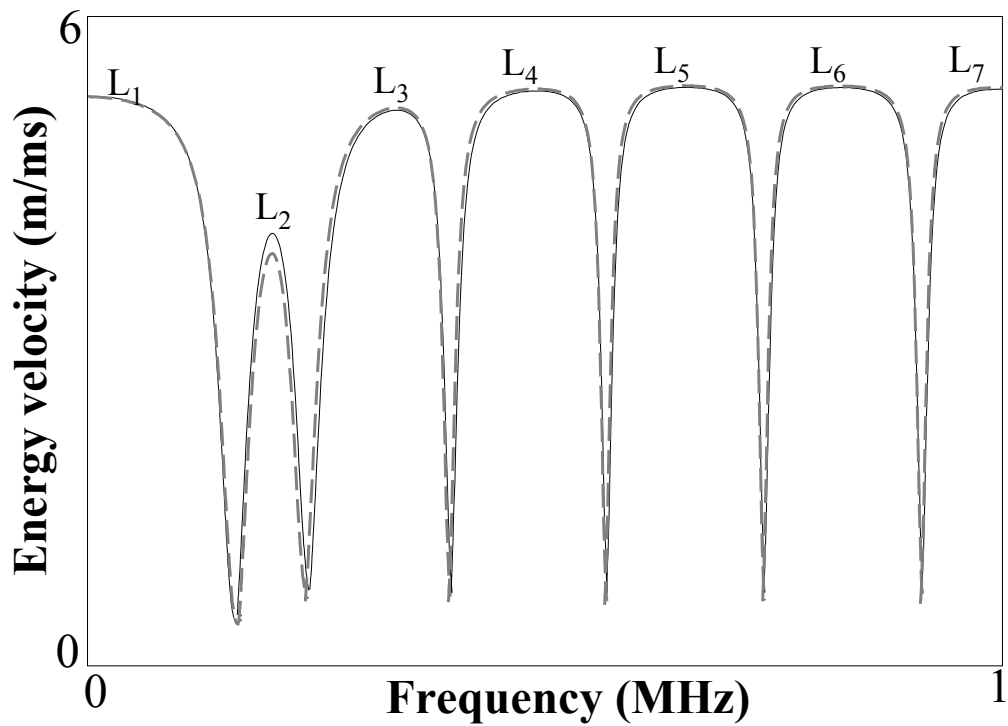
Figure 2.13: Energy velocity dispersion curves (above the branching points) of longitudinal modes in a steel pipe filled with a low viscosity fluid ($C_l = 1450m/s$, $\eta = 1Pas$) for different values of density of the fluid $\rho = 1g/cm^3$ (black solid line); $\rho = 0.7g/cm^3$ (gray dashed line).

Chapter 3

Characterisation of Fluids inside Pipes Using Guided Longitudinal Waves

3.1 Background

As shown in Chapter 2, the presence of a fluid inside a pipe brings some new features on the velocity and attenuation dispersion of guided longitudinal waves, which are not present when they propagate in a free pipe. It is therefore possible to associate these changes with some properties of the fluid. Measurements proposed by using guided waves are completely non-invasive and promise to overcome many of the limitations associated with conventional bulk wave measurement.

However, a guided wave measurement can be much more complex than a bulk wave measurement due to the complex nature of the guided wave itself due to velocity dispersion and coexistence of multiple modes. The presence of the filling fluid can significantly increase the complexity of the guided wave modes. On the other hand, the multiple guided wave modes and frequency-dependent velocities may yield more information of the material than could be found from bulk waves measurements.

In this chapter, a new technique is presented to measure the longitudinal bulk velocity and shear viscosity of a fluid inside a pipe by using the characteristics of multiple

guided wave modes propagating in the pipe. It is demonstrated that this guided wave technique is capable of non-intrusively measuring both low-viscosity fluids and highly viscous fluids inside the pipe.

The chapter begins with an introduction to some basic principles of ultrasound measurements in Sec. 3.2. A review of the existing ultrasound techniques for characterising fluids in pipes is given in Sec. 3.3. Then the experimental setup of the proposed guided wave technique is described in Sec. 3.4, followed by the explanation of the measurement methods in Sec. 3.5. Results for measurements performed with different fluids are presented in Sec. 3.6.

3.2   Basic Principles of Ultrasound Measurements

The basic idea of bulk ultrasound measurement is simple: the acoustic waves are transmitted and received after they interact with the medium under investigation. On their arrival at the receiver, the ultrasound signal carries the information about the mechanical properties of the medium in terms of speed of sound and attenuation.

The speed of sound (c) and attenuation (α) can be obtained in different ways. In principle, most methods are based on the following two equations:

$$c = \frac{\Delta x}{\Delta t}, \tag{3.1}$$

$$\alpha = \frac{1}{\Delta x} \ln(\frac{A_1}{A_2}), \tag{3.2}$$

A_1 and A_2 are the amplitude of the signals received at two position with a distance Δx and Δt is the transit time. The velocity of sound is easily and reliably measured by determination of the transit time of an ultrasound signal along a known path length. The attenuation measurement is actually an amplitude measurement which may become more complicated due to various issues such as signal interference, dispersion or diffraction in the measurement equipment.

Guided wave techniques probe the properties of a medium surrounding a waveguide by measuring the change of the guided wave characteristics due to the presence of

the medium compared to the case in which the waveguide is in vacuum or air. The velocity and attenuation of the guided wave in a waveguide can be determined in the same way as defined by equations 3.1 and 3.2. The measured change of these two parameters can be back fitted to a forward model (such as DISPERSE) to determine the bulk acoustic properties of the material. A key issue is the excitation of a suitable guided wave mode, the change of which due to surrounding material can be easily measured. Specifically, for characterising the contents of a pipe, the mode choice should be based on two main criteria.

Firstly, as shown in Chapter 2, the presence of a material inside a pipe, such as a fluid, increases the number of modes compared to the case in which the pipe is empty. For this reason, it is preferable to generate a single mode in the empty pipe, at frequencies where no other propagating modes of higher order modes exist. Thus, new modes due to the content can be easily measured and correlated to its properties.

Secondly, the modes in the clean pipe should be minimally dispersive in the selected frequency range. This will facilitate the measurement of content-induced dispersion on the guided wave modes, which can be related to the properties of the contents.

According to these two criteria, the torsional mode, T(0,1) is the best choice since it shows no dispersion and is the only torsional mode at low frequencies as shown in Fig. 2.2. The L(0,2) mode at the frequencies where it exhibits little dispersion is an alternative choice. Although, the L(0,2) mode is accompanied by the L(0,1) mode at all frequencies, it is easy to generate a pure L(0,2) mode from the end or outside surface of the pipe due to the discrepancy of the mode shapes between these two modes (see Fig. 2.3a and b).

Finally, mode choice is also influenced by the types of contents to be characterised in the pipe. The T(0,1) mode is ideal for measuring the shear properties of solid contents such as shear bulk velocity and shear bulk attenuation [60]. On the other hand, T(0,1) is a superposition of bulk shear waves in the pipe and does not couple into inviscid fluids. Therefore, the torsional mode is not suitable for measuring the modulus of fluid which is determined by its longitudinal properties. This can be achieved by using the longitudinal mode L(0,2).

3.3 Ultrasound Measurements of Contents inside Pipe

A number of ultrasound techniques have been investigated for on-line measurements of fluid properties inside pipes. For example, bulk ultrasonic waves propagating across the diameter of a pipe can be used to perform a measurement using transducers which are attached to the outside of the pipe [61]. The sound velocity in the fluid can be obtained by measuring the time-of-flight of the signals and the shear viscosity of the fluid can be determined by measuring the attenuation of the signals. As the waves travel across the diameter of the pipe, the measured results are the average properties of the fluid across the diameter of the pipe at the location of the sensors. Such an approach has also been used successfully for the measurement of flow rates based on the Doppler effect or diffraction effects [62]. Multiple ultrasound transmissions on different paths across the flow can further be applied to create tomographic images [63, 64]. However there are also a number of situations for which the propagation across the diameter will not be feasible, for example when the fluid is too attenuative for the signals to traverse a diameter of the pipe, or the pipe is only partially filled.

An alternative is to use acoustic impedance measurements which have been successfully developed as a fluid density sensor for process control by the Pacific Northwest National Laboratory, US [65, 66]. The sensor consists of a number of transducers mounted upon a plastic wedge whose base is immersed into a fluid or slurry in the pipeline. Ultrasonic beams striking the base of the wedge at several angles are reflected at the wedge fluid interface. The amount of reflection depends on the density and the sound velocity of the fluid and wedge properties. By determining the reflection coefficient at different incident angles, density and sound velocity can be determined simultaneously. However, to place the sensor in the fluid, a certain area of the pipe wall needs to be cut, which may not be possible under some circumstances, for example in reaction pipelines at high pressure or temperature, typical of many chemical processes. This shortcoming was improved later by using a flat transducer mounted directly upon the outside of the pipe wall. A ultrasound beam is normally incident on the pipe-fluid interface and multiple reflections within the

wall are used to determine the acoustic impedance of the fluid [61]. It should be noted that the impedance measurement only determines the properties of the fluid at its interface in contact with the wall or the wedge. This is in contrast to the cross section measurement which obtains the average properties of the fluid across the diameter of the pipe. It can be expected the impedance measurement will become less accurate to represent the overall properties of the fluid inside the pipe if the properties of the fluid is inhomogeneous across the diameter of the pipe.

Guided ultrasonic waves which propagate along the pipe in the length or circumferential directions have also been investigated to measure the properties of contents inside pipes. Guided waves interact with the fluid along both the circumference and the length of the pipe and therefore the measured properties of the fluid can better represent the average properties of the fluid inside the pipe over a certain distance compared to the cross section measurement and the acoustic impedance measurement which only determine the the properties of the fluid at a local position. Moreover, the guided wave measurements measure the signal propagating in the pipe wall, unlike the bulk ultrasonic wave measurements, which measure the signals traveling across the material under investigation directly. Therefore, the guided wave measurements suffer much lower attenuation due to the material damping of the content than the bulk ultrasonic wave measurements.

Aristegui et al. [57] made a series of measurements of guided wave in pipes filled and surrounded by different media, which demonstrated that it is possible to measure the change of velocity and attenuation of the guided waves due to the filling fluid. Vollmann et al. developed a technique to measure the complex dispersion curves of guided wave modes in pipes filled with different materials such as fluids and viscoelastic materials based on a so-called spectrum estimation method, which is to operate on multiple equally spaced waveforms that are sampled along the length and the circumference of the pipe [58]. The measured dispersion curves are then back fitted to a forward model to extract the modulus of the pipe content. However, this technique cannot measure the shear viscosity of the fluid. Moreover, it can be very time consuming since it requires a large number of exact, spatially sampled data. Simonetti and Cawley [60] developed a new guided wave technique to characterize the shear acoustic properties of highly attenuative viscoelastic materials in a pipe by

measuring the velocity and attenuation spectra of the fundamental torsional mode in such a waveguide. Guided waves propagating in the circumferential direction of the pipe have also been investigated for fluid characterisation, however, it is found that good sensitivity can only be achieved when the tube wall is fairly thin [67].

Although, such attempts have been made, guided waves have not been successfully exploited to measure the properties of fluid inside pipes, such as the longitudinal bulk velocity and the shear viscosity. This approach is to some extent challenging due to a number of reasons. First of all, there are multiple modes coexisting in a fluid-filled pipe and depending on the frequency range, these modes can be dispersive (branching region). As shown in Fig. 2.9a, it is the dispersive region of the modes that is sensitive to the change of the bulk velocity of the fluid. This implies that conventional group velocity measurements cannot be employed since an accurate velocity measurement can only be carried out based on a non-dispersive signal. Secondly, on the other hand, the attenuation measurement needs to be made over the frequency range where a mode has none or little dispersion (plateau region). These plateau regions of the modes need to be identified before the attenuation measurement is carried out. However, this information is not known a priori, hence it is not possible to perform the measurement in the desired regions of the dispersion curves.

3.4   Experimental Setup

This section described the experimental setup that was designed to assess the feasibility of the technique proposed in this chapter. Fig. 3.1 shows a schematic of the apparatus. The experiment was performed on a $1m$ long steel pipe (inner diameter $9mm$, wall thickness $0.5mm$) partially immersed into a tank containing the fluid to be characterized. The tank was placed beneath the pipe on a table of adjustable height so as to change the immersed length of the pipe. The material properties of the pipe were determined by guided wave velocity measurement and are listed in Tab. 2.1. Part of the steel pipe was inserted into an aluminum sleeve supported by a teflon ring at one end, in order to keep the pipe outside surface dry.

As explained in Sec. 3.2, the longitudinal mode L(0,2) is the best choice to measure the fluids inside pipes. A longitudinal piezoelectric (PZT) ring element ($9mm$ ID, $11mm$ OD, and $0.5mm$ thickness) was glued at one end of the steel pipe to excite a longitudinal vibration. The displacement field produced by the ring was to a large extent axisymmetric, therefore, it excited the longitudinal mode (symmetrical mode) primarily with little flexural modes (asymmetrical modes) being excited. The excitation was carried out in the frequency range above the cut-off frequency of the L(0,2) mode. Due to the good matching of its mode shape displacement to the excitation field (see Fig. 2.3a and b), the L(0,2) mode was predominantly excited compared to the L(0,1) mode. The signal was sent by a waveform generator (Macro Design Ltd) and recorded by a LeCroy 9400A oscilloscope, the data was then transferred to a PC for processing.

The PZT ring element was excited with a Hanning windowed tone burst. The excited L(0,2) mode travelled along the free pipe until the point where the pipe started being immersed into the fluid (stage 1 in Fig. 3.2). Because the acoustic impedance of the fluid is much smaller than that of steel, no reflected signal was observed from the free surface of the fluid. On the other hand, the L(0,2) mode was mode-converted into the fluid-filled pipe modes (stage 2 in Fig. 3.2) which were subsequently reflected from the immersed end of the pipe (stage 3 in Fig. 3.2). The fluid filled pipe modes were converted back into the L(0,2) mode at the free surface of fluid, which was received by the same PZT ring in pulse echo mode (stage 4 in Fig. 3.2). The received L(0,2) mode is modulated due to the fluid-filled pipe modes (L_1, L_2....) and also experiences attenuation due to the viscosity of the fluid. So by analyzing the spectrum of the signal received by the ring, it is possible to reveal properties of the fluid-filled pipe modes, which then can be used to characterize the fluid as explained in the next section.

The experimental setup to a reasonable extent matches the case of on-line measurement of a pipeline completely filled with fluid. However, the on-line measurement may require the excitation of longitudinal modes to be made at the outside surface of the pipe, since access to the ends is always difficult. The excitation and detection of longitudinal modes in such a configuration has been successfully achieved by using a transducer ring clamped on the outside of the pipe [68, 13].

3.5   Measurement Methods

This section describes a two step technique to measure the longitudinal velocity and the viscosity of a fluid within a pipe.

3.5.1   Measurement of longitudinal bulk velocity

The measurement of the longitudinal bulk velocity of the fluid is based on the measurement of the energy velocity dispersion of the longitudinal mode which, as shown in the previous section, is very sensitive to the fluid bulk velocity in the branching regions. The measurement employs a broadband pulse signal in a pulse echo mode to excite the L(0,2) mode in the free pipe, which is then converted into multiple longitudinal modes propagating in the fluid-filled pipe. Two signal processing methods can be used to analyze the reflected signal, namely the amplitude spectrum and the reassigned spectrogram, respectively.

An assumption can be made that at each frequency, the L(0,2) mode converts into a single fluid-filled pipe mode. This assumption is appropriate since the modes with larger displacements in the pipe wall are excited much more strongly than the fluid dominated modes. If also neglecting the damping in the steel pipe, the end reflection signal received by the ring can be expressed as:

$$U(\omega) = U_0(\omega)T_{pf}(\omega)T_{fp}(\omega)R_f(\omega)e^{-2d\alpha}e^{i2k_f d}e^{i2k_p l}, \tag{3.3}$$

where, $U_0(\omega)$ is the excitation amplitude of the signal, $T_{pf}(\omega)$ is the transmission coefficient of the signal from the free pipe into the fluid-filled pipe whereas the $T_{fp}(\omega)$ is the transmission coefficient of the signal from the fluid-filled pipe to the free pipe. $R_f(\omega)$ is the reflection coefficient from the end of the pipe. k_p and k_f are the wave number of the mode propagating in the free pipe region and fluid-filled region respectively. α represents the guided wave attenuation in the fluid-filled pipe region. l and d denote the length of free pipe and fluid-filled pipe respectively. The equation shows that the received L(0,2) mode has been modulated after the signal has traveled through the fluid-filled region. When the signal propagates in the free

pipe region, the factor $e^{i2k_p l}$ makes the frequencies of the signal arrive at almost the same time, since the L(0,2) mode has little dispersion after its cut-off. However, when the signal travels in the fluid-filled pipe, the factor $e^{i2k_f d}$ causes the frequencies of the signal to arrive at different times as determined by the dispersion curves of the fluid-filled pipe modes. In the time domain, this is exhibited by a long duration of the signal [56]. The frequencies at the plateau region of a mode arrive early, while those at the branching region arrive later due their reduced velocity. In particular, the branching frequencies arrive last, since the energy velocity of the fluid-filled pipe modes reach local minima at these frequencies.

When a Fourier Transform is made on the windowed signal, the amplitude spectrum displays periodic dips which are not shown in the amplitude spectrum of the free pipe signal. These periodic dips were found to occur just at the branching frequencies. This is shown in Fig. 3.3 which refers to the case of a water-filled pipe. The dips are due to several reasons. First, the window on the signal has a finite span over a period of time, which is not enough to include the branching frequencies arriving much later than the front part of the signal. Kwun et al [56] have already shown in a similar experiment that in a large steel pipe (168.3mm OD, 7.1mm wall) fully filled with water, the signal contains leading and trailing portions which are well separated from each other. The amplitude spectrum of the leading portion showed similar missing components at branching frequencies, while the amplitude spectrum of the trailing portion showed mainly periodic peaks at those missing branching frequencies. Secondly, at the branching frequencies, a considerable amount of energy is contained in the fluid, so more energy is transmitted into the water tank from the immersed end of the pipe.

The longitudinal bulk velocity of the fluid can be obtained by best fitting the branching frequencies calculated using DISPERSE (dashed curve in Fig. 3.3) to the dips on the amplitude spectrum (shown in Fig. 3.3), with respect to the longitudinal velocity of the fluid. A particular advantage of this measurement is that it can be carried out at a remote position without the need to know the length of the fluid-filled region.

The second method to measure the longitudinal velocity of the fluid is based on the reconstruction of the dispersion curves of the received signal which has been modulated by the fluid-filled pipe modes (the factor $e^{i2k_f d}$ in (3.3)). However, the coexis-

tence of multiple signals and their dispersive nature make the signal too complicated to be interpreted directly. Recently, time-frequency representations (TFR) such as the spectrogram, the scalogram, and the Wigner-Ville method have shown promise for the interpretation of guided wave signals containing multiple modes [69]. These representations analyze one single time-domain signal by quantitatively resolving changes in the frequency content, as a function of time. By using the spectrogram of the short-time Fourier transform (STFT), Kwun et al. have experimentally measured the dispersion change of the longitudinal modes of a pipe due to the presence of water [56]. The time-frequency resolution of a spectrogram depends only on the window size and type and is independent of frequency. A wide window gives better frequency resolution, but worsens the time resolution, whereas a narrow window improves time resolution but worsens frequency resolution. Thus, it was also observed by the authors that the STFT spectrogram representation suffered from this uncertainty principle, making it impossible to simultaneously have perfect resolution in both time and frequency [56].

It is possible to improve the time-frequency resolution of a spectrogram with the reassignment method, a technique developed by Auger and Flandrin [70] that provides a computationally efficient way to compute the modified moving window method for the spectrogram. The basic principle lies that the value that normal spectrogram takes at a given point (t, f) of the time-frequency plane cannot be considered as pointwise but rather results from the summation of weighted values at the neighboring points $(t - t', f - f')$. The aim of the reassignment method is to improve the sharpness of the localization of the signal component by reallocating its energy distribution in the time-frequency plane. The reassignment method moves each value of the normal spectrogram computed at any point (t, f) in the time-frequency plane to another point $(\hat{t}, \hat{f})$ which is the center of gravity of the signal energy distribution around (t, f). Therefore, the time-frequency resolution of a normal spectrogram is improved by concentrating its energy at a center of gravity. More details of this technique can be found in Ref. [70, 71, 72].

Researchers at Georgia Institute of Technology have shown that the Reassigned Spectrogram (the reassigned energy density spectrum of the STFT) is capable of distinguishing multiple Lamb wave modes from only a single signal, and giving

excellent representation of its dispersion curves [69, 73]. The work by this group has used the reassigned spectrogram to represent the dispersion curves of Lamb waves in free plates and plates with cracks [69, 73, 74].

In this chapter, the reassigned spectrogram is applied to reveal the dispersion curves of the fluid-filled pipe modes from the signal reflected from the end of the pipe. Then, to transform the signal into the time-frequency domain, instead of considering the amplitude spectrum method, the short time Fourier Transform (STFT) is used through a reassigned procedure, which effectively refines the time-frequency resolution [69, 73]. The longitudinal bulk velocity of the fluid can be obtained by best fitting the analytical dispersion curves (calculated with DISPERSE) to the measured ones, with respect to the longitudinal bulk velocity of the filling fluid. DISPERSE provides the energy velocity of each mode, which can then be converted into the arrival time for a certain propagation distance. The arrival time of each frequency was corrected to account for the time required for the L(0,2) mode to travel from the transducer to the fluid free surface.

3.5.2 Measurement of viscosity

The shear viscosity of the fluid can be measured from the attenuation of the longitudinal modes. An accurate attenuation measurement of guided waves can only be made by carefully choosing the frequency range where a mode has none or little dispersion and does not interfere with other modes. Thus, the attenuation can be measured in the plateau region of the dispersion curve of each mode, which also shows good sensitivity (Fig. 2.9b). Instead of using a broadband excitation as in the velocity measurements, a tone burst signal with a number of cycles had to be used to narrow the excitation band into the plateau region of each mode, which can be identified from the reassigned spectrogram analysis. In principle it is sufficient to evaluate the viscosity at one single frequency. However, in order to increase the accuracy by averaging, measurements were taken at several frequencies. This resulted in a discrete attenuation spectrum.

To apply the technique in on-line measurements, one would need to use two receivers at different positions along the pipe, whereas in this case, it can be realized by

conveniently changing the immersion depth of the pipe. The attenuation of a guided wave mode can be calculated using the following equation:

$$\alpha = \frac{1}{2(x_1 - x_2)} \ln(\frac{U_2(\omega)}{U_1(\omega)}), \tag{3.4}$$

where $x_1 < x_2$ are two different axial positions along the pipe, and U_1 and U_2 are the signal amplitudes at the respective positions. The change of immersion depth was chosen such that the signal was attenuated around 50% to reduce variance error [75].

3.6 Results

3.6.1 Distilled water

This experiment was made to measure the longitudinal bulk velocity of distilled water which is an extremely low-viscosity fluid. The temperature was recorded to be $25^{o}C$. The longitudinal bulk velocity of the distilled water was extracted based on the signal reflected from the end of the pipe immersed for $160mm$. First, the amplitude spectrum analysis of the signal was performed. The longitudinal bulk velocity of the fluid was obtained by best fitting the branching frequencies calculated using DISPERSE (dashed curve in Fig. 3.3) to the dips on the amplitude spectrum (shown in Fig. 3.3), with respect to the longitudinal velocity of the water. Thus, it was possible to extract the longitudinal velocity of the distilled water as $1500 \pm 10m/s$. The other spikes and dips at high frequencies were due to electrical noise and possibly the interference from other unwanted flexural modes generated by a non perfect axisymmetric excitation. The uncertainty of the measurement may come from the slight position shift of dips on the amplitude spectrum due to the interference of noise.

The reassigned spectrogram analysis was also made on the same signal, which is shown in Fig 3.4. The dispersion curves of the water filled pipe are clearly represented by the reassigned spectrogram. Both the plateau region and branching region of each mode can be easily defined. The best fitting of analytical dispersion curves (by DISPERSE using different values of the longitudinal bulk velocity of the

water) to the measured one over a broad frequency range gave the same mean value of longitudinal bulk velocity of distilled water i.e. $1500 \pm 10m/s$. The uncertainty of the measurement mainly comes from the resolution limit of the dispersion curves represented by the reassigned spectrogram.

To validate the results, a bulk ultrasonic wave measurement of the longitudinal velocity in the water was carried out. This yielded a value of $1498m/s$. The measured results also agree well with the literature data of $1495m/s$ at the recorded temperature [76].

Because the viscosity of water is very small (approximately $10^{-3}Pas$ at $25^{o}C$), it is not possible to measure it at the relatively low frequencies used in this experiment.

3.6.2 Glycerol

Measurements were also carried out on the pipe filled with glycerol. The density of the glycerol sample was measured to be $1258kg/m^3$. The temperature was recorded to be $25^{o}C$, at which the viscosity of glycerol is usually below $1.2Pas$. Its contribution to the energy velocity changes of the longitudinal modes may be neglected, so the longitudinal velocity of glycerol can be determined directly from the dispersion changes of the longitudinal modes and the corresponding branching frequencies.

The pipe was immersed into the glycerol for $400mm$, and the end reflection signal was measured. The longitudinal velocity determined by the amplitude spectrum method shown in Fig. 3.5 is $1905\pm5m/s$. The reassigned spectrogram analysis was also made to represent the dispersion curves shown in Fig. 3.6, in which the best fitting with analytical curves (dashed line) gave the value of $1918\pm5m/s$. Both measured values compare well with a bulk wave measurement, which yielded a value of $1915m/s$. The reassigned spectrogram analysis is somehow more accurate than the amplitude spectrum, since it extracts results by best fitting through a broad frequency range, avoiding error due to noise, which may slightly change the dip positions on the amplitude spectrum. The literature data for the longitudinal velocity of glycerol at $25^{o}C$ are inconsistent and can be found to vary from $1920m/s$ [77] to $1904m/s$ [78]. However, these values still agree well with the measurements in the order of 0.8%

Table 3.1: Comparison of measured longitudinal bulk velocity and viscosity with literature data and other independent measurements. $C_{l(AS)}$ and $C_{l(RS)}$ are the longitudinal bulk velocity measured by amplitude spectrum and reassigned spectrogram respectively.

	Measurements			Validations.	
	$C_{l(AS)}$ (m/s)	$C_{l(RS)}$ (m/s)	η (Pas)	C_l (m/s)	η (Pas)
Distilled water	1500	1500		1498/1495	
Glycerol	1905	1918	0.94	1915/1920/1904	0.97
VP8400	1525		18.8	1510	19.1/19

(see Tab. 3.1). The difference can be due to the difference of the water content of the glycerol sample used.

The viscosity of the glycerol was obtained by measuring the attenuation of the second and the third modes on the plateau regions of their dispersion curves, which could be identified from the represented dispersion curves (Fig. 3.6). The attenuation was calculated according to Eq. 3.4 and the immersion depth change was $380mm$. The mean viscosity evaluated from the measured attenuation is $0.94 \pm 0.04Pas$. The uncertainty mainly comes from the slight dispersion on the plateau regions chosen for the attenuation measurement. The viscosity of glycerol strongly depends on temperature and water content of the sample. A change in temperature of 1^oC can change the viscosity by $0.1Pas$ and a change in water content of 1% can shift the viscosity by $0.2Pas$. Thus, a simultaneous measurement of the viscosity of glycerol is required to validate our measurement. This involved the measurement of the $SH0$ shear horizontal wave mode attenuation when a plate is immersed in glycerol. This mode is the equivalent plate mode of the torsional T(0,1) mode in a wire that was used by Vogt et al to measure the viscosity of fluids [79]. Using this approach the viscosity of the glycerol was determined to be $0.97 \pm 0.02Pas$, which agrees in the order of 3% with the measurement using the longitudinal modes and the range of their standard error overlapped (see Tab. 3.1).

3.6.3 Highly viscous fluid

Further measurements were performed on the pipe filled with highly viscous fluid. A commercial viscosity standard Cannon VP8400 (C.I. Company,VP8400 Viscosity Standard, State College, PA), which is a mineral oil was used for this experiment. The viscosity standard can be used to calibrate viscometers and estimate the accuracy of the guided wave measurement. The density of VP8400 at the temperature of measurement (25.5^oC) was $885.2kg/m^3$. An example procedure will be demonstrated in which the velocity and viscosity measurements addressed above are combined to extract the properties of highly viscous fluids.

First, the amplitude spectrum analysis was made on the reflected signal from the end of the pipe immersed into VP8400 for $215mm$, which still exhibited periodic dips as shown in Fig. 3.8. As it was shown in Fig. 2.11a the large viscosity of the fluid also changes the dispersion curves of the longitudinal modes, however, it has little influence on the branching frequencies. So it is first assumed that the fluid is a perfect fluid without viscosity, and best fit is made use of the branching frequencies calculated by DISPERSE (dashed black curves) to these dips with respect to the longitudinal bulk velocity of the fluid (shown in Fig. 3.8). This yielded the initial mean value of $1530 \pm 5m/s$ for the longitudinal bulk velocity of VP8400.

The reassigned spectrogram analysis was then performed on the same signal and the results are shown in Fig. 3.9. It proved that for highly viscous fluid, the reassigned spectrogram is only capable to represent the plateau regions on the dispersion curves of some modes. The lack of definition at the branching regions of the dispersion curves is due to two factors. First, the longitudinal modes have high attenuation at branching regions, since most of their energy is trapped in the fluid. Even at the plateau region, the modes have considerable attenuation. Therefore, the signal to noise ratio is lower, which reduces the sharpness of the dispersion curves represented by the reassigned spectrogram as shown in Fig. 3.9. Secondly, the high viscosity makes the branching regions become less sharp than those for the low-viscosity fluid case. This has been shown in Fig. 2.11a. So in order to represent a sharp branching region in the time-frequency domain, the mode needs to propagate longer distance in the fluid-filled pipe, which in turn will have more energy attenuated. Therefore, the revealed spectrum of dispersion curves is insufficient for an accurate best fitting.

With the value of longitudinal bulk velocity obtained with the amplitude spectrum method, the viscosity measurement can be made on the frequency ranges with little dispersion revealed by the reassigned spectrogram. The results are shown in Fig. 3.10 and the viscosity was determined to be $18.8 \pm 1.1 Pas$. This agrees very well with the viscosity value $19.1 Pas$ for the standard given at the recorded temperature. The simultaneous measurement using the SH0 mode in a plate yielded the viscosity to be $19 \pm 0.5 Pas$.

To confirm the assumption that the viscosity has little influence on the branching frequencies, the best fitting of the dips of the amplitude spectrum to the branching frequencies (calculated by DISPERSE) with respect to the longitudinal bulk velocity of VP8400 (dashed gray curve in Fig. 3.8) was repeated. This time, the obtained viscosity of $18.8 Pas$ was used in the calculation for the best fit. This procedure gave the value of $1525 \pm 5 m/s$ for the longitudinal bulk velocity, which was very close to the initial value ($1530 \pm 5 m/s$) and the difference is in the same order of measurement uncertainty. The quasi-Scholte guided wave mode in a plate was used to measure the longitudinal velocity of the VP8400 which gave a value of $1510 m/s$ [80]. This agreed with the value obtained by amplitude spectrum in the order of 1%. The difference is mainly due to the increased influence from the noise, which slightly shifts the dip positions on the amplitude spectrum. The calculated dispersion curves (dashed white curves) using the measured fluid properties ($C_l = 1525 m/s$, $\eta = 18.8 Pas$) also agreed well with the represented one by reassigned spectrogram on the plateau region of the dispersion curves, which are shown in Fig. 3.9.

3.7 Summary

A new method has been presented in this chapter to measure the acoustic properties of a fluid inside a pipe by using guided longitudinal waves. It allows the fluid properties to be non-intrusively characterized without taking samples out of the pipe. The method can be employed both when the pipe is completely filled or when the filling is partial; in the latter case, the velocity measurement requires a single pulse echo measurement without the need for knowing the length of the fluid column inside the pipe, and it can be carried out at a remote position away from the fluid

free surface.

It has been shown that the longitudinal bulk velocity of the filling fluid with low viscosity can be extracted from the reconstructed dispersion curves of the longitudinal modes propagating in the fluid-filled pipe or from their branching frequencies. Once the dispersion curves of the modes are obtained, the viscosity can be determined from the attenuation of the modes measured in the suitable frequency ranges identified from the reconstructed dispersion curves, where the modes have little dispersion. For pipes filled with highly viscous fluids, the dispersion curves of the longitudinal modes are affected simultaneously by the longitudinal bulk velocity and viscosity of the fluid. The longitudinal bulk velocity can be obtained from the measured branching frequencies which are almost independent of the viscosity of the fluid. The viscosity can be extracted in the same way as for the case of low viscosity fluids.

Experiments have been carried out to test the method on both low viscous (distilled water and glycerol) and highly viscous fluids (viscosity standard VP8400). The measured values have been validated by other independent measurements and available literature data. For low-viscosity fluid, the measurements using longitudinal modes in pipes and the validation methods or literature data agreed well to within 0.8% for the longitudinal bulk velocity and the viscosity agreed to well within 4%. The accuracy of velocity measurement was reduced slightly (within 1%) by the increase of viscosity of the filling fluid, while the viscosity measurement became more accurate (within 1%).
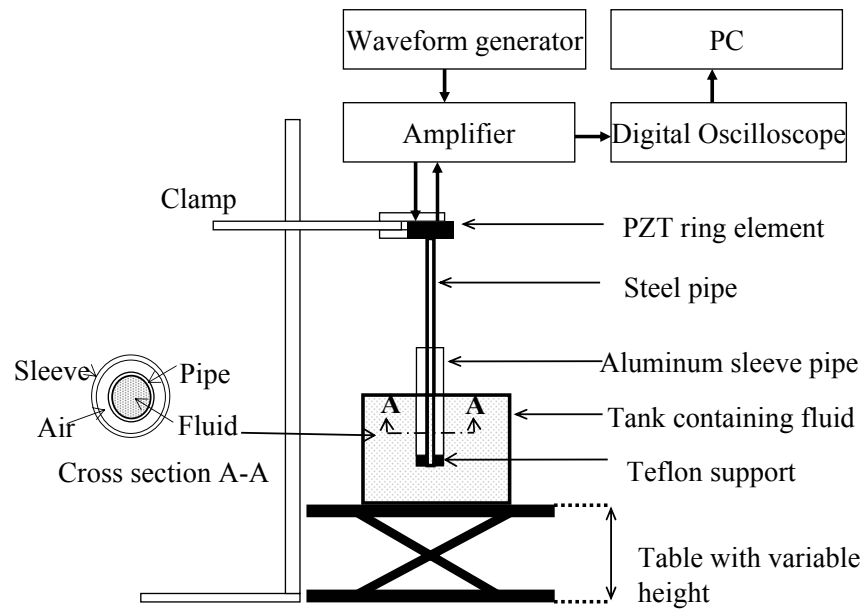
Figure 3.1: Schematic of the experimental setup.
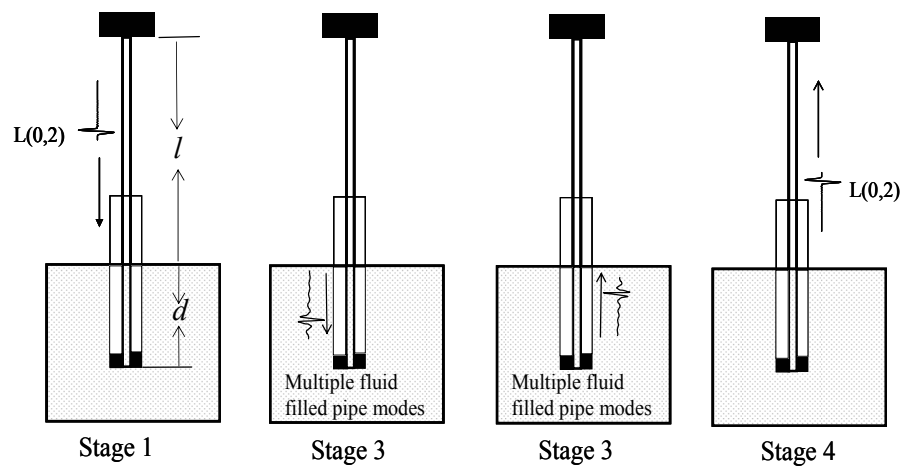
Figure 3.2: The sequence of propagation of longitudinal modes in a pipe partially immersed into a fluid.
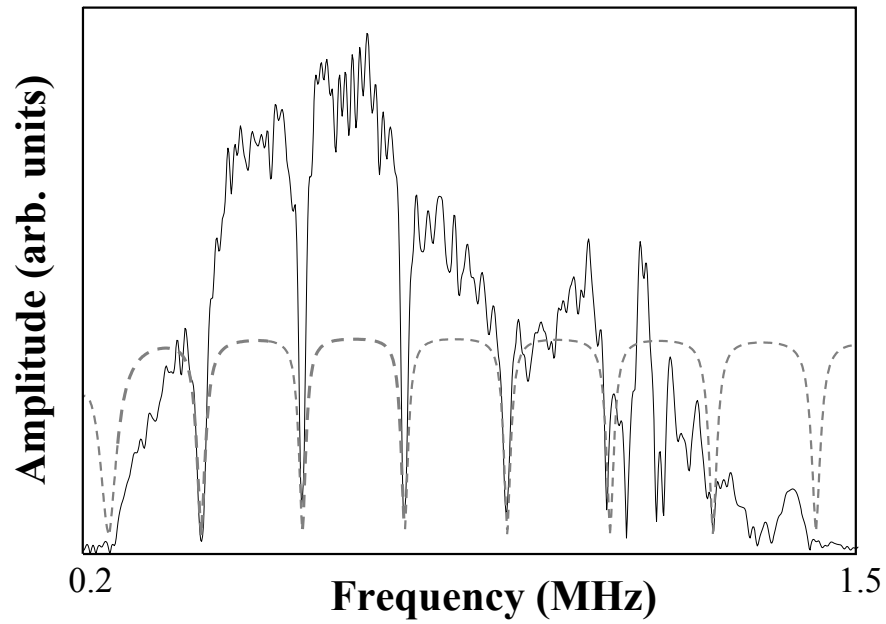
Figure 3.3: Amplitude spectrum of end reflection signal from a steel pipe immersed into water (black line) and the branching frequency best fit calculated by DISPERSE (dashed gray line).
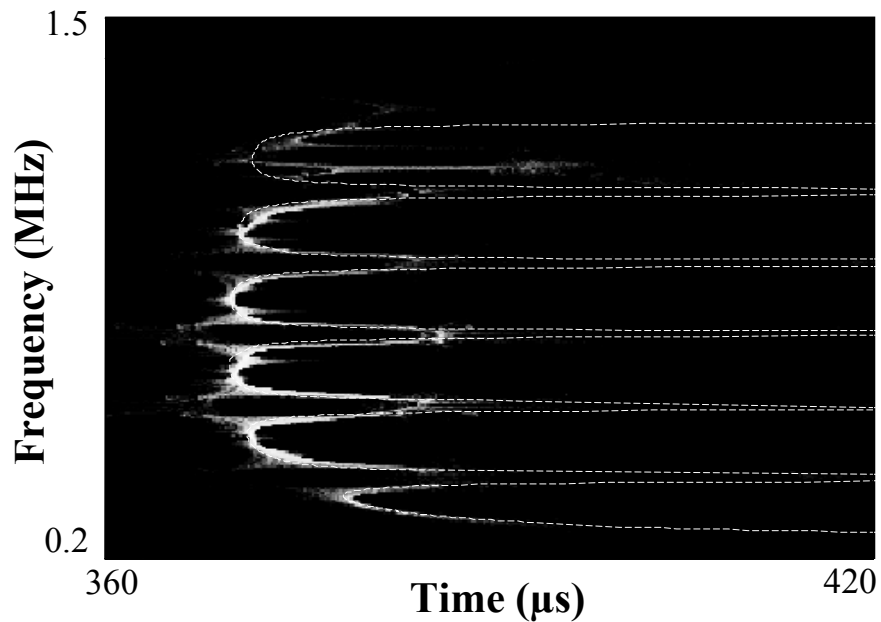
Figure 3.4: Reassigned spectrogram analysis of end reflection signal from a steel pipe immersed into water and best fit curves (white dashed curves) calculated with DISPERSE.
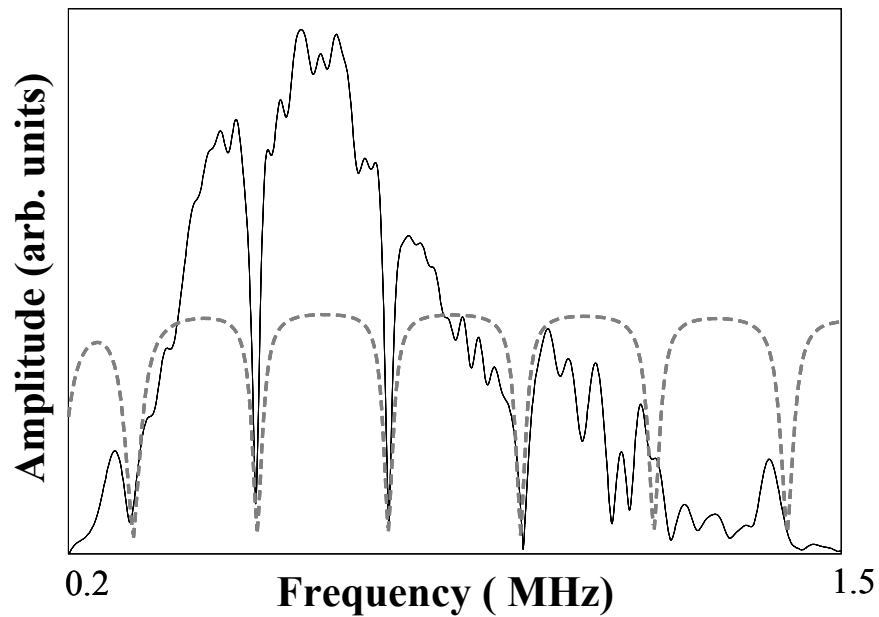
Figure 3.5: Amplitude spectrum of end reflection signal from a steel pipe immersed into glycerol (black line) and the branching frequency best fit calculated with DISPERSE (dashed gray line).
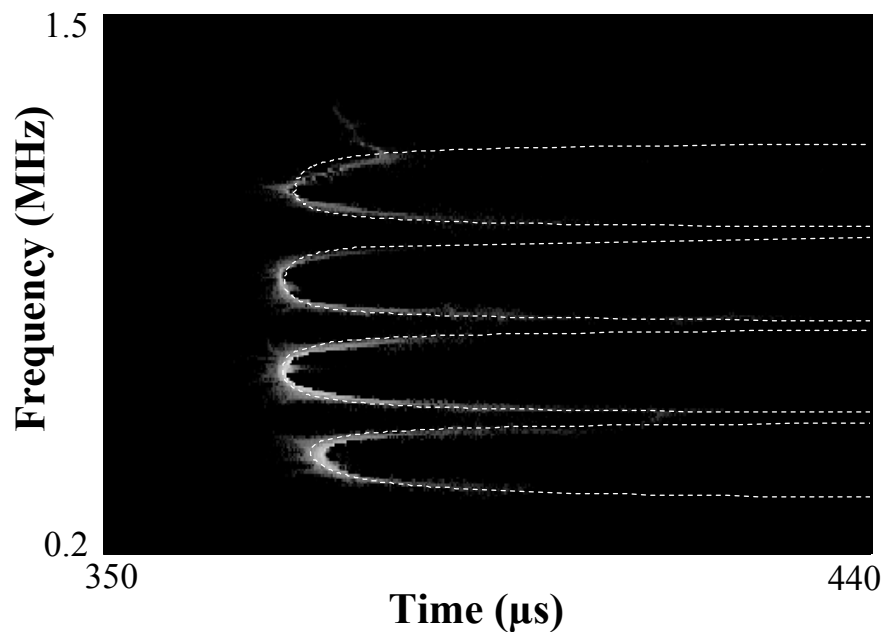
Figure 3.6: Reassigned spectrogram analysis of end reflection signal from a steel pipe immersed into glycerol and best fit curves (white dashed curves) calculated with DISPERSE.
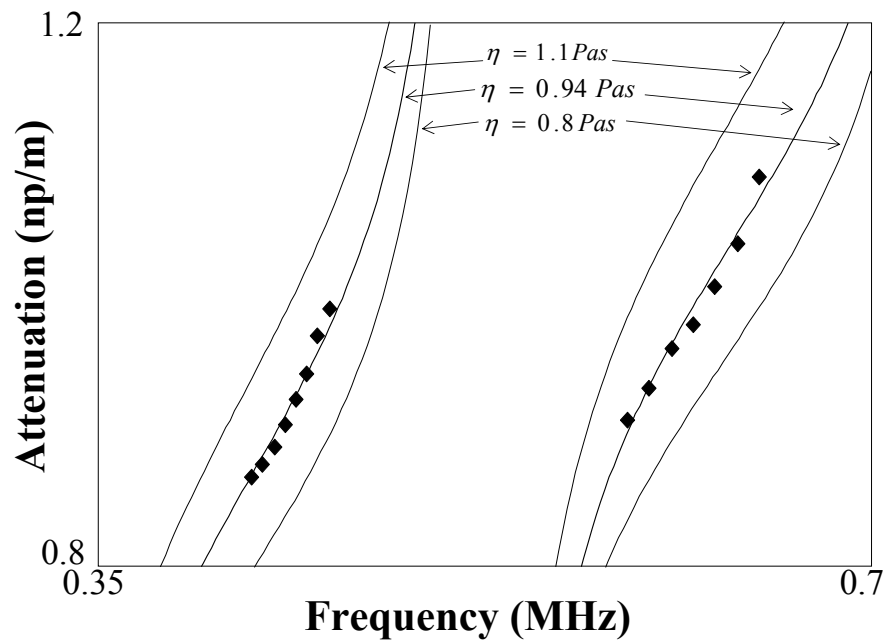
Figure 3.7: Measured (black square) and theoretically predicted (black line) attenuation of longitudinal modes in a steel pipe immersed into glycerol (predictions by DISPERSE).
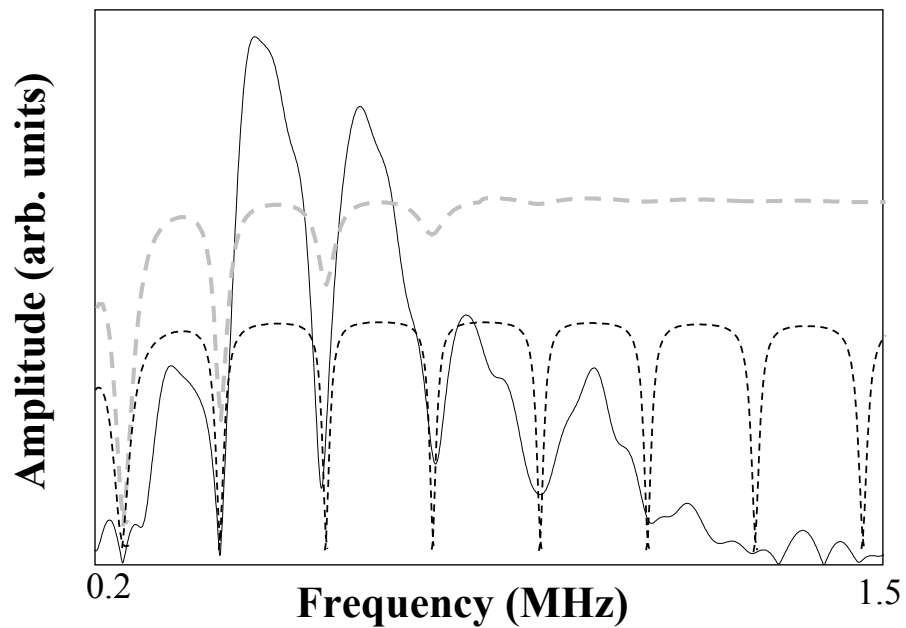
Figure 3.8: Amplitude spectrum of end reflection signal from a steel pipe immersed into a commercial Cannon VP8400 viscosity standard (black line) and the branching frequency best fit calculated by DISPERSE assuming that the fluid has no viscosity (dashed black line). The branching frequency best fit calculated with DISPERSE using the measured viscosity $\eta = 18.8 Pas$ for the fluid (dashed gray line).
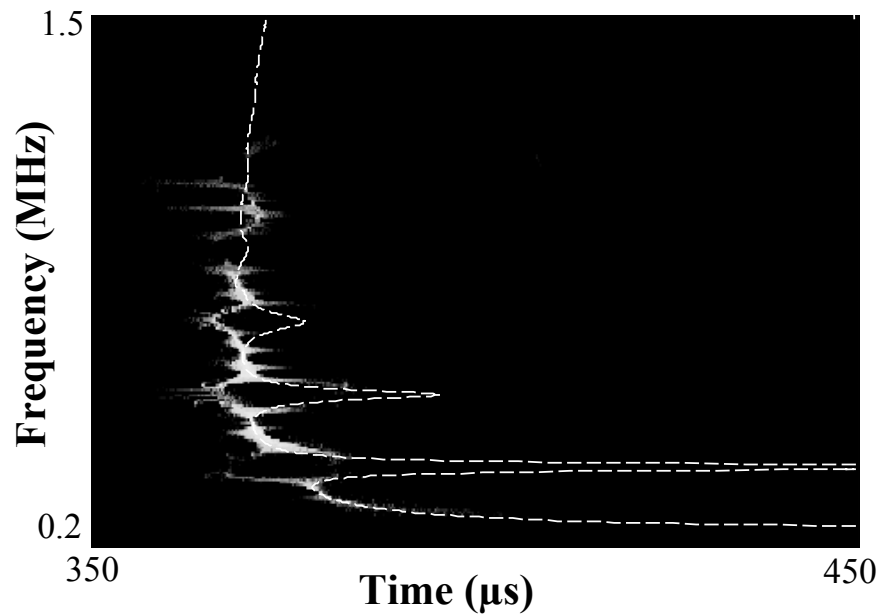
Figure 3.9: Reassigned spectrogram analysis of end reflection signal from a steel pipe immersed into a commercial Cannon VP8400 viscosity standard and the analytical curves (white dashed curves) calculated with DISPERSE using the measured values of longitudinal bulk velocity ($C_l = 1525m/s$) and viscosity ($\eta = 18.8Pas$)for the fluid.
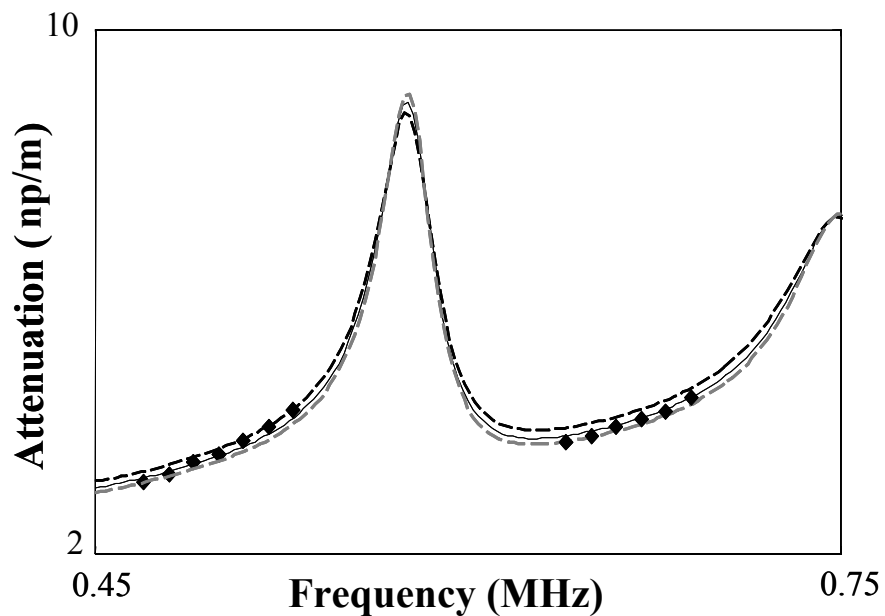
Figure 3.10: Measured (black square) and theoretically predicted (by DISPERSE using the initially measured longitudinal bulk velocity $C_l = 1530m/s$ for the fluid) attenuation of longitudinal modes in a steel pipe immersed into a commercial Cannon VP8400 viscosity standard. ($\eta = 18Pas$ (dashed gray line); $\eta = 18.8Pas$ (black line); $\eta = 20Pa.s$ (dashed black line))

Chapter 4

Scattering of the Fundamental Torsional Mode by an Axisymmetric Layer inside a Pipe

4.1 Background

Chapters 2 and 3 presented the guided wave measurement of fluid contents inside pipes. On the other hand, detecting and characterizing solid contents inside pipes is also required by many industries. For example, it is important for the process industry to monitor the accumulation of sludge in pipes in order to prevent the formation of blockages. In this context, it would be valuable to be able to quantify the material and geometry properties of sludge non-invasively.

As stated in the introduction, guided ultrasonic waves propagating along the pipe wall can provide an attractive method for such an application, because of their capability of inspecting a long length of pipe from a single point [13, 14]. Furthermore, the excitation of the guided wave can be achieved externally, ideally without emptying the pipe, so that the measurement can be made non-intrusively. The basic idea is that the presence of sludge would scatter the guided waves and change their propagation characteristics, so that measurements of these changes by processing reflected or transmitted signals could be used to detect and maybe characterize the

sludge.

However, the problem can become very complicated due to the irregular shape and properties of the sludge layers that can be encountered in practice. In order to understand the fundamental physics and assess the feasibility and potential of such an approach, a simplified model of sludge and blockages should be studied first. The model studied here consists of a pipe locally coated inside with an axisymmetric layer with uniform thickness (Fig. 4.1). It also assumed that the layer is perfectly bonded with the pipe wall and has no internal material damping. The region where the pipe is coated with the layer was referred to as a 'bilayered pipe' [81].

As identified in Chapter 3, the fundamental torsional mode T(0,1) is most suitable to measure solid contents inside pipes. This mode is considered as the best choice for this application; the limitations of using longitudinal modes are discussed in Chapter 6.

The investigation starts with an introduction of the propagation of torsional waves in bilayered pipes, followed by a detailed analysis of their energy flow distribution (Sec. 4.2). The physical insight gained from this analysis enables the design of the two guided wave measurement concepts to characterize the coating layer inside the pipe. These are demonstrated first by finite element modelling in Sec. 4.3 and later confirmed by experimental measurements in Sec. 4.4.

4.2   Torsional Waves in the Bilayered Pipe

In order to understand the nature of the scattered field of the T(0,1) mode from the discontinuity where the free pipe meets the bilayered pipe, the characteristics of the torsional waves propagating in the bilayered pipe need to be studied.

Let us consider a hollow, elastic and isotropic cylinder coated with an axisymmetric elastic layer inside. The cylindrical coordinates (r, θ, z) are appropriate here to represent the geometry of the system (r, θ, z denote the radial, angular and axial position respectively).

The Fourier transformed wave equation describing the propagation of distortional

waves in a homogeneous medium is given in equation 2.7. The generic solution to equation 2.7 will be of the form

$$\mathbf{H} = [AJ_0(k_r r) + BY_0(k_r r)]e^{ikz}, \tag{4.1}$$

where $\mathbf{H}$ is the vector potential which is parallel to z. A and B are arbitrary constants, k_r and k are the projections of the wave vector along the r and z directions, and J_0 and Y_0 are the Bessel function of the first and second kind. The displacement field can be obtained by applying the curl operator to $\mathbf{H}$, thus

$$U_\theta = [CJ_1(k_r r) + DY_1(k_r r)]e^{ikz}, \tag{4.2}$$

where $C = -Ak_r$ and $D = -Bk_r$, the displacement field being tangential. The phase velocity of a guided mode is defined as $C_p = \frac{\omega}{k}$. The non zero components of the stress tensor are therefore

$$\tau_{r\theta} = \mu(\frac{\partial U_\theta}{\partial r} - \frac{U_\theta}{r}), \tag{4.3}$$

$$\tau_{z\theta} = \mu(\frac{\partial U_\theta}{\partial z}), \tag{4.4}$$

The displacement field associated with a torsional mode propagating in a bilayered pipe can be expressed according to equation 4.2 where the constants C and D are different in the pipe wall and the internal layer, leading to four unknown constants. As we introduced in Chapter 2, the unknown can be determined by using the global matrix method when imposing suitable boundary conditions. In particular, we assume a good bond state between the pipe and the coating layer, which means the continuity of the displacement and the stress component $\tau_{r\theta}$ at the interface. Also the zero traction condition is imposed on both the free surfaces of the pipe and the internal layer [33]. Moreover, if the pipe is completely filled , the constant D has to vanish in order to remove the singularity of Y_1 at $r = 0$.

The solution can be obtained by using DISPERSE, which solves the exact secular equation obtained with the global matrix approach numerically. The group velocity

Table 4.1: Material properties of the aluminium pipe and epoxy layer used for DISPERSE calculation and FE modelling.

	Longitudinal velocity(m/s)	Shear velocity(m/s)	Density(kg/m^3)
Aluminium	6320	3130	2700
Epoxy	2610	1100	1170

dispersion curves are shown in Fig. 4.2(a). The material and dimensions of the pipe and the coating layer are summarized in Table 4.1. The modes of the bilayered pipe are labelled as T_1, T_2, T_3. For comparison, the torsional mode in the free pipe labelled as T(0,1) is also given. This shows that in the same frequency range there are many more modes occurring in the bilayered pipe compared to the single T(0,1) mode in the free pipe. Note that although only one torsional mode can propagate in the free pipe in the frequency range considered in Fig. 4.2(a), higher order modes will occur at higher frequencies. With the occurrence of the new modes, new cutoff frequencies labeled as F_2, F_3 are generated accordingly. Also, the modes of the bilayered pipe are very dispersive, unlike the T(0,1) mode of the free pipe which always keeps a constant velocity value for all frequencies.

Theoretical investigations of guided wave propagation in layered structures have been carried out for a long time [51, 52, 55, 82, 83, 84]. Of particular significance here, is a theoretical study on the propagation of shear horizontal (SH) waves in a plate coated with a viscoelastic layer, which is a counterpart to our model, but flat rather than cylindrical [51]. In the bilayered plate case, the bilayer modes originate from the interaction between the modes of the free plate and those of the coating layer, if it were rigidly clamped at the bilayer interface. The cutoff frequencies of the SH modes of the bilayer were found to correspond to the cutoff frequencies of the clamped-free coating layer, which only depend on the thickness and bulk shear velocity of the coating layer [51]. They are in direct proportion to the bulk shear velocity and inverse proportion to the thickness of the layer and can be approximated as

$$F_n \simeq \frac{c_s}{4d}(2N - 1), \tag{4.5}$$

where $N \in \{1, 2, 3...\}$, c_s and d are the bulk shear velocity and thickness of the coating layer, respectively. As a result, if the cutoff frequencies can be measured and the velocity of the coating is known, the thickness of the layer can be obtained by inverting equation 4.5.

This principle is also valid here for the case of torsional modes in the bilayered pipe. However, equation 4.5 is no longer an exact expression of the cutoff frequencies in cylindrical structures, but it still indicates a qualitative relationship between the cutoff frequencies and the internal layer. Here, one needs to solve the secular equation numerically as explained later.

As shown in previous chapters, the energy flow distribution is useful to help to understand the energy distribution of guided waves in multiple layer waveguides. Specifically for torsional modes in the bilayered pipe, the energy flow density in the axial direction (z) at any radial position r can be expressed as [54]

$$I_z(r) = \frac{\omega^2 \mu |U_\theta(r)|^2}{2C_p}, \tag{4.6}$$

Total time-averaged axial energy flow in the pipe wall (E_p) and in the coating layer (E_l) can be obtained by integrating equation (4.6) over the pipe wall thickness

$$E_p = \frac{\pi \omega^2}{C_p} \int_{R_1}^{R_2} \mu_1 |U_{\theta 1}|^2 r \, dr, \tag{4.7}$$

and the coating thickness

$$E_l = \frac{\pi \omega^2}{C_p} \int_{R_0}^{R_1} \mu_2 |U_{\theta 2}|^2 r \, dr. \tag{4.8}$$

Here, R_1 and R_2 represent the inner and outer radius of the pipe and R_0 is the inner radius of the coating layer. The subscripts 1 and 2 refer to the pipe and the layer

respectively. The energy flow ratio (EFR) is similarly defined as the ratio of the energy flow in the pipe to that in the layer

$$EFR \quad = \quad \frac{E_p}{E_l} = \frac{\int_{R_1}^{R_2} \mu_1 |U_{\theta 1}|^2 r \, dr}{\int_{R_0}^{R_1} \mu_2 |U_{\theta 2}|^2 r \, dr} \tag{4.9}$$

The EFR spectra calculated for the modes shown in Fig. 4.2a are given in Fig. 4.2b, their significance being addressed in the next section.

4.3   Scattering of the T(0,1) Mode at the Discontinuity

Consider a torsional wave T(0,1) which is incident from the free end of a pipe (Fig. 4.1). At the point where a coating layer starts inside the pipe, the incident T(0,1) mode is partly reflected back into the free pipe (reflected signal), and also partly transmitted into the multiple torsional modes in the bilayered pipe (local signal) and then further converted back into the T(0,1) mode after the bilayered pipe (transmitted signal). It also needs to be mentioned that, since the layer is axially symmetric, no mode conversion into longitudinal or flexural modes occurs. Since all the reflected, local and the transmitted signals are caused by the presence of the layer, their characteristics should depend on the layer properties and the nature of the guided wave behavior.

4.3.1   Reflected signal

As introduced in Sec. 3.2, in the case of a plane wave incident at the interface between two different media, we would analyze the reflection and transmission by studying the change of impedance between the two media. The situation here for guided waves is more complex, but it is the extent to which the modes in the free pipe match those in the bilayered pipe, which determines the strength of the reflection, according to the modal analysis theory [54]. In particular, if the energy flow associated with the mode shape of T(0,1) in the free pipe matches well that of a bilayered mode within the pipe wall, the mode is transmitted with little energy being reflected. On the

other hand, if the matching is poor, a strong reflection occurs. The extent of the mode matching can be assessed by studying the EFR spectrum.

Let us consider the T(0,1) mode incident at the cutoff frequency of T_2 (Fig. 4.2). The EFR of T_2 is always larger than that of T_1 (as it can be deduced from Fig. 4.3 a,b, which show the normalized energy flow distribution through the thickness of the bilayered pipe), which means that T_2 tends to carry more energy in the pipe wall than T_1. Therefore, it is expected that T(0,1) in the free pipe will transmit more energy into T_2 rather than T_1. However, it can be observed that as the frequency increases, the EFR of T_2 increases up to a maximum value labelled C in Fig. 4.2b, where the amount of energy traveling in the pipe wall is maximum (see Fig. 4.3c). As a result, as the frequency increases from the cutoff frequency of T_2 to C, T(0,1) tends to transmit more energy into T_2; conversely the reflected energy tends to decrease by the energy conservation law. If the frequency increases further, the EFR of T_2 starts decreasing together with the transmitted energy from T(0,1), since the matching of the energy flow mode shape deteriorates. When the frequency reaches the cutoff of T_3 a transition occurs and the energy of T(0,1) starts to be mostly transmitted into T_3, since it will have a larger EFR than T_1 and T_2 afterwards. The same phenomenon will repeat periodically as the frequency increases. It can be concluded that the frequencies where a maximum EFR occurs will approximate the minimum of the reflection coefficient, whereas the maximum of the reflection coefficient should occur at the frequencies close to the cutoff frequencies of the bilayered pipe modes.

To validate these predictions, a Finite Element (FE) simulation was performed to study the scattering of torsional waves in such a structure, using the FE software FINEL, developed at Imperial College [85]. The details of the models are outlined in the Appendix A.1. The material properties used for the FE modelling are the same as those used for the previous calculation and are listed in Table 4.1.

As illustrated in Fig. 4.1, the monitoring point of the reflected signal is set at one point in the free pipe region indicated as the reflection measurement. The time domain signal from the FE simulation at this monitoring point is shown in Fig. 4.4a. The time trace shows the incident wave on its way to the bilayered pipe region, and the reflection from the entry point of the epoxy layer. The reflection coefficient spectrum, calculated by dividing the magnitude of the Fourier transform of the

reflected signal by that of the incident signal, is plotted in Fig. 4.4b, which exhibits periodic peaks and troughs. The roughness of the curves is due to the window effect on the time domain signal. The cutoff frequencies of the bilayered pipe modes (T_2, T_3) are marked as F_2, F_3 in the frequency axis for comparison. It can be seen that the peaks of the reflection coefficient spectrum occur almost exactly at the cutoff frequencies of the bilayered modes, which confirms our analysis above. Since these cutoff frequencies are, for an assigned pipe, uniquely determined by the epoxy layer thickness and bulk shear velocity, the shear acoustic properties or thickness of the coating layer can be characterized by measuring the peak positions of the reflection coefficient spectrum.

4.3.2   Local and transmitted signals

The incident T(0,1) mode also transmits into the multiple dispersive torsional modes in the bilayered pipe region, which are contained in signal received at the local measurement point in Fig. 4.1. These modes are converted back to the transmitted T(0,1) propagating past the bilayered region which can be expressed as:

$$U(\omega) = U_0(\omega)e^{ik_c(L-l)} \sum_{J=1}^{N(\omega)} T_J^{cb}(\omega)T_J^{bc}(\omega)e^{ik_J^b l}, \tag{4.10}$$

where, U_0 is the amplitude of the excitation signal, ω is the angular frequency and $N(\omega)$ is the number of torsional modes in the bilayered pipe at the frequency ω. $k_c = \frac{\omega}{C_c}$, $k_J^b = \frac{\omega}{C_J^b(\omega)}$. C_c, $C_J^b(\omega)$ are the phase velocity of the modes propagating in the clean pipe, and in the bilayered pipe respectively. $T_J^{cb}(\omega)$ is the transmission coefficient from the incident T(0,1) mode into the Jth bilayered pipe mode, whereas $T_J^{bc}(\omega)$ is the transmission coefficient from the Jth bilayered pipe mode to the transmitted T(0,1) mode. L denotes the total length between the transmitter and the receiver and l is the length of the bilayered pipe. Note that equation 4.10 is an approximate expression because it does not account for multiple reflections of modes within the bilayered pipe region.

The equation shows that the transmitted T(0,1) carries information about the dispersion characteristics of the torsional modes in the bilayered pipe which is given by the factor $e^{ik_j^b l}$. Both the transmission measurement and the local measurement essentially make use of this layer-induced dispersion, however, the transmission measurement has the advantage compared to the local measurement of being a remote measurement method.

It has have shown in Chapter 3 that the reassigned spectrogram is capable of quantitatively representing the dispersion curves of multiple longitudinal modes in a fluid-filled pipe. In this chapter, the same technique is applied to analyze the transmitted signal (Fig. 4.5a) simulated by FE modelling. As before, a wide band excitation is required and only one time-domain signal is needed for processing.

The contour plot of the square root of the reassigned spectrogram of the transmitted signal is given in Fig. 4.5b. It reveals for each mode and at each frequency, the arrival time of the transmitted signal which is determined by its group velocity. The reassigned spectrogram provides a very clear representation of the individual modes of the bilayered pipe. The accuracy of the reconstructed dispersion curves can be assessed by comparison with the analytical results from DISPERSE (dashed curves), which shows excellent agreement. For reference, the reassigned spectrogram analysis was also performed on the incident T(0,1) mode in the clean pipe region and is shown in Fig. 4.5c. Obviously, the dispersive nature of the transmitted signal can be a clear indicator of the presence of the layer. The extraction of the thickness of the layer can be achieved through a best-fitting procedure, provided that the shear bulk velocity of the layer and the length of the layer are known.

4.4   Experiments

Experiments have been also carried out to validate the analysis and FE calculations. The general setup for the experiments is shown in Fig. 4.6. Two samples of aluminium pipes (16.5-mm inner diameter and 1.4-mm wall thickness) with partial coating inside were manufactured. The first was a 1.25m long pipe, 0.55m of which was coated inside with a 6-mm thickness epoxy resin layer to represent the model

Table 4.2: Material properties of the aluminium pipe and epoxy layer used for FE calculations to compare with the remote measurement results. The bulk shear velocity of epoxy was determined by an independent measurement.

	Longitudinal velocity(m/s)	Shear velocity(m/s)	Density(kg/m^3)
Aluminium	6320	3130	2700
Epoxy	2610	1000	1170

studied in this paper. Due to application difficulty, the epoxy layer built inside the pipe was not perfectly symmetrical all along its length. The second sample consisted of the same pipe, but the epoxy resin completely filled the pipe for 0.3m from one end. This sample aimed to simulate the case of ultimate blockage inside the pipe. The epoxy was cured inside the pipe so as to meet the theoretical assumption of good bond condition between the layer and the pipe. The epoxy resin employed is a commercial adhesive, Araldite 2020, whose acoustic properties were determined using conventional ultrasonic time of flight method [86] and are listed in Table 4.2.

The torsional mode T(0,1) was excited by four pieces of shear-vibration piezoelectric (PZT) elements. These four piezoelectric elements were mounted axisymmetrically on the external surface of the pipe to generate the torsional vibration as shown in Fig. 4.6. The piezoelectric elements were excited by a Hanning windowed toneburst generated by a custom-made waveform generator and amplifier. T(0,1) is the only axisymmetric propagating mode in the free pipe with significant circumferential displacement below the cutoff frequency of T(0,2), which will occur at 1.16 MHz for the tested pipe. Therefore, only T(0,1) will be generated below 1.16 MHz, provided the excitation is perfectly axially symmetric. A single element attached to the pipe surface would excite both torsional modes (axisymmetrical modes) and flexural modes (non-axisymmetrical modes). However, if a series of elements are attached axisymmetrically around the pipe to form a ring, it should be possible to suppress the flexural modes to a certain extent [68]. The use of four balanced transducers is sufficient to suppress the excitation of only two asymmetric flexural modes F(1,1) and F(1,2) below 110 kHz. The torsional vibration was detected by a laser interferometer (sensor head: Polytec OFV 512, controller: Polytec OFV 3001) operating in differential mode. The tangential displacement was measured by

focusing the two beams at 30° with respect to the radial direction and by orienting the beams in the plane perpendicular to the axis of the pipe.

Different procedures for the excitation and reception of torsional modes were used according to the signals to be measured. To measure the reflected signal, a five cycle excitation signal in a Hanning window was used to narrow the frequency band into the range in which the current setup could guarantee only the T(0,1) mode being excited without flexural modes. The receiver was set at a position halfway between the free end of the pipe and the start point of the bilayered pipe, so both the incident and the reflected signals would be received. To further remove the influence of the flexural mode, measurements were carried out at four equally spaced points around the circumference of the pipe, but at the same axial location. By adding the four sampled waveforms, we can obtain both the incident and reflected signal only containing a single T(0,1) mode, since the flexural modes which have a sinusoidal displacement distributed along the pipe circumference are cancelled by circumferential averaging. A typical time-domain signal from the reflection measurement is shown in Fig. 4.7a.

Due to the configuration of the setup and the geometry of the samples, no transmitted signal propagating past the bilayered pipe region was present. To measure the local signal, a two cycle excitation signal with central frequency 150 kHz in a Hanning window was used, which covers a wide frequency band from 40 kHz up to 300 kHz. Therefore, multiple axially symmetric modes in the bilayered pipe are excited. Since four PZT elements are not enough to suppress flexural modes of order higher than two, the excitation of T(0,1) is accompanied by weakly excited higher order flexural modes. The local signal was received by the laser at a position in the bilayered region. Only one signal waveform is needed for the signal processing. The results of the local measurement will be to a great extent similar to that of the transmission measurement.

4.4.1 Reflected signal: experimental results

The reflection coefficient is calculated by dividing the frequency spectrum of the measured reflected signal by that of the incident signal. The reflection coefficient

amplitude spectrum obtained from the pipe partially coated on the inside surface with a 6-mm thickness epoxy layer is plotted in Fig. 4.7b. The measured curve is obtained as a superposition of measurements performed at different central frequencies, ranging from 50 kHz to 110 kHz. For comparison, the results of an FE calculation performed with the material properties given in Table 4.2 are also shown. We can see that the measured reflection coefficient spectrum displays the characteristic peak and trough, which follow the trend of the FE calculation well. The most important feature of the reflection coefficient spectrum is that the first measured peak occurs at the position of the FE prediction (86kHz), which is very close to the predicted cutoff frequency (83 kHz) of the T_2 mode of the corresponding bilayered pipe.

However, it is clear that the magnitude of the measured reflection coefficient spectrum is not as sharp as that of the FE prediction, especially at the frequencies around the peak position. The disagreement is largely due to the material damping of the epoxy. So far the FE modelling considered the epoxy to be an elastic material; however, the epoxy is known to behave more like a viscoelastic material. Since the reflection peak is due to the presence of standing waves in the coating layer, material absorption weakens the resonance phenomenon, so resulting in a lower reflection coefficient.

Fig. 4.8 shows the reflection coefficient spectrum obtained for the pipe sample, completely filled with epoxy over part of its length. The measured reflection spectrum shows very similar characteristics to those shown in Fig. 4.7, but the position of the first peak position shifts to a slightly lower frequency (80.5 kHz) due to the increase of thickness of the filling epoxy. For this configuration, Prof. M. Castaings at the University of Bordeaux I has provided FE simulations which incorporate the material damping of epoxy assuming a damping coefficient of 0.13 Neper/wavelength given in the literature [87]. The details of this FE technique can be found in [88]. For reference, the FE modelling without considering the material damping of the epoxy is also provided. These results confirm that material damping reduces the magnitude of the reflection coefficient at the cutoff frequencies, and the agreement between the FE prediction and the experimental results is very good.

4.4.2 Local signal: experimental results

The local signal was measured in the bilayered region of the pipe and only one time domain signal was needed. The reassigned spectrogram was applied to the measured local signals to represent the group velocity dispersion curves of the torsional modes in the bilayered pipe. The signal was first measured on the sample of pipe locally coated with 6-mm thickness layer, at a bilayer pipe position 0.15m away from where the coating layer starts in the pipe (Fig. 4.9a). The contour plot of the reassigned spectrogram analysis is shown in Fig. 4.9b, where the dashed curves represent the analytical curves calculated with DISPERSE using the material properties obtained from the reflection measurement of the same sample (listed in Table 4.2). While the T_2 and the T_4 modes agree well with the analytical curves, the dispersion curve of the T_3 mode is influenced by some additional modes, which were not present in the FE simulations (Fig. 4.5). These additional modes are flexural bilayered pipe modes (asymmetrical modes) caused by the asymmetrical thickness of the coating layer inside the pipe. Since the dispersion curves of some flexural modes are close to that of the T_3 mode (these are not shown for clarity in Fig. 4.5), they cannot be well separated in either the time domain or the frequency domain, in which case the reassigned spectrogram is incapable of distinguishing them [69]. Also, the mode structure of the T_1 mode is destroyed by the asymmetrical layer, and little energy is transmitted into this mode.

The local signal was also measured on the sample of pipe locally filled with epoxy, at a position 0.09m away from where the epoxy filling starts (Fig. 4.10a). The result of the reassigned spectrogram analysis is shown in Fig. 4.10b. In this case the layer is perfectly symmetrical, so the dispersion curves of the first four torsional modes of the bilayered pipe and their cutoff frequencies can easily be identified and no flexural modes are present. The white dashed curves are the analytical curves calculated from DISPERSE. The mode arriving later is the reflection of the local signal from the end of the bilayered pipe.

It should be observed from the measured dispersion curves that the cutoff regions of the modes cannot be represented as well as in the case of the FE prediction shown in Fig. 4.5b. The lack of definition is due to the large attenuation of torsional modes at their cutoff frequencies caused by the material damping of the epoxy filling

[52]. Moreover, no dispersion curves can be extracted above 220 kHz, since material damping increases with frequency. However, the measured dispersion curves are sufficient to be used to extract the properties of the layer. An effective method is to best fit the analytical dispersion curves (by DISPERSE) to the measured ones, with respect to the thickness or the bulk shear velocity of the coating layer (dashed curves). The measured dispersions of high order modes are highly sensitive to the change of these two parameters of the coating. To show this, we estimated the thickness of the filling epoxy through the best fit procedure, using the bulk shear velocity of epoxy obtained from the remote measurement (listed in Table 4.2). The radial thickness of the epoxy filling obtained in this way is 8.2 ± 0.1 mm. This is within 2% of the pipe inner radius (8.25 mm).

4.5 Conclusion

This chapter has studied the scattering of the fundamental torsional mode T(0,1) by a local axisymmetric coating layer inside a pipe. The presence of the layer inside the pipe increases the number of torsional modes that can propagate in a clean pipe. When the T(0,1) mode is incident at the local bilayered pipe region, due to the mismatch of its mode shape with that of the modes in the bilayered pipe region, the T(0,1) mode is scattered: part of it is reflected back and part is transmitted into the multiple torsional modes in the bilayered pipe and then converted back into the T(0,1) mode after the bilayered pipe region.

Such phenomena can be used to develop two methods to detect and characterize the properties of a layer inside a pipe.

The first method makes use of the reflected T(0,1) mode which can effectively locate the layer inside the pipe. The amplitude spectrum of the reflection coefficient of the T(0,1) is found to exhibit periodic peaks, which just occur at the cutoff frequencies of the modes in the bilayered pipe. The phenomenon is due to the fact that at the cutoff frequencies, the energy of torsional modes in the bilayered pipe region tends to flow in the coating primarily, while little remains in the pipe wall. This causes a large mismatch between the modes of the free pipe and those of the bilayered pipe

region, so resulting in a strong reflection. Since the cutoff frequencies depend on the thickness and bulk shear velocity of the layer, the peak positions of the reflection coefficient spectrum can be used to determine the thickness of the coating layer, if its bulk shear velocity is known, and vice versa.

A second method measures the local signals travelling in the bilayered pipe region or the transmitted T(0,1) mode propagating past the bilayered pipe region. The reassigned spectrogram has been employed to quantitatively reveal the dispersive nature of modes contained in the signals. This can be a clear indicator of the presence of the layer since no dispersion occurs in a clean pipe. The extraction of the thickness of the layer can be achieved by best fitting the reconstructed dispersion curves by reassigned spectrogram to the analytical prediction, provided that the shear bulk velocity of the layer and the length of the layer are known. The measurement is very efficient, since only a single time domain signal is needed.

The two methods are clearly viable for the idealised bilayered pipe case, but it remains to be seen whether they will work on realistic cases in which the sludge and blockages have irregular shapes and properties. This will be investigated in the next chapter.

Reflection measurement   **Local Measurement**   **Transmission measurement**

Incident T(0,1) mode

Reflected T(0,1) mode

Epoxy layer

Multiple bilayered
pipe modes

Transmitted T(0,1) mode

Bilayered pipe region
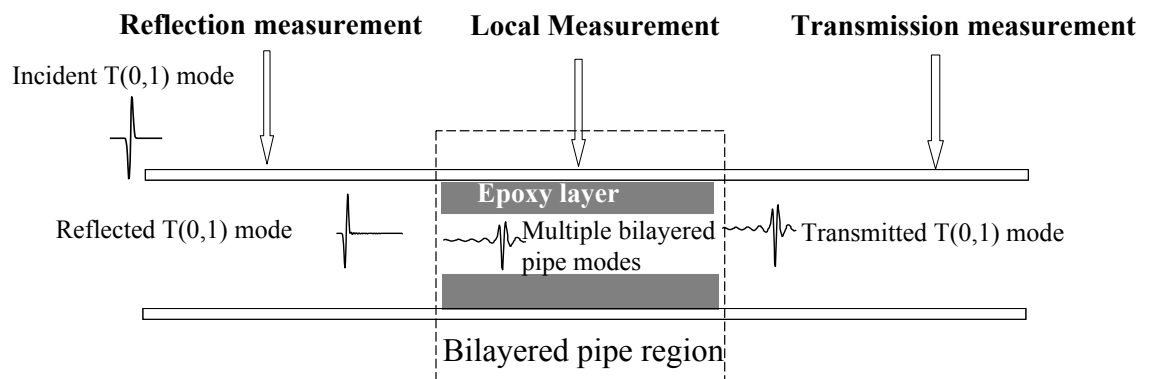
Figure 4.1: Schematic of the model investigated in this chapter.
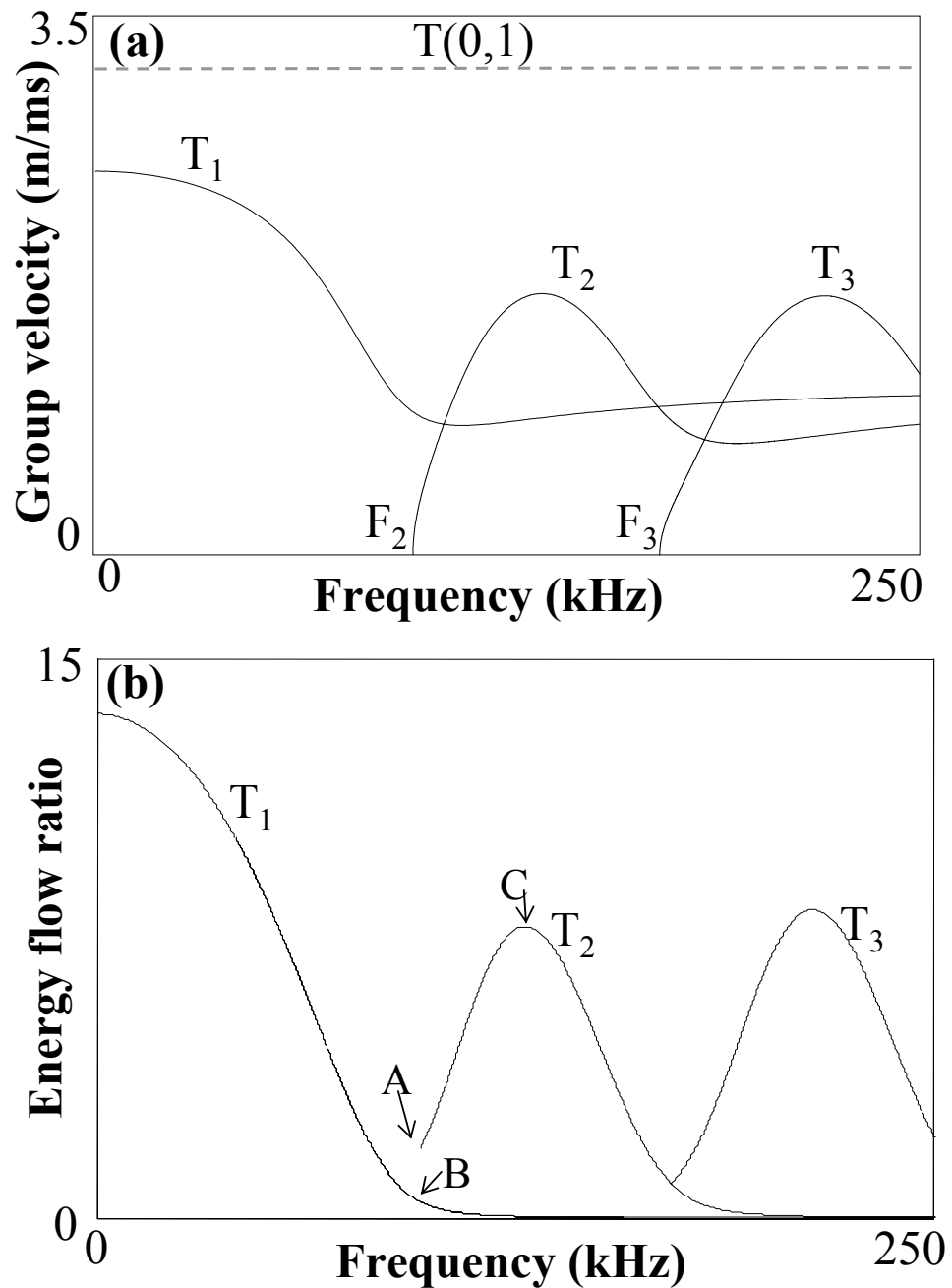
Figure 4.2: (a) Group velocity dispersion curves of torsional modes in an aluminum pipe (Inner diameter 16mm and thickness 1.4mm) coated with a 6-mm thickness epoxy layer inside. Material properties are given in Table 4.1. For comparison, the torsional mode in a pipe without coating is also shown, by the dashed line. (b) Energy flow ratio.
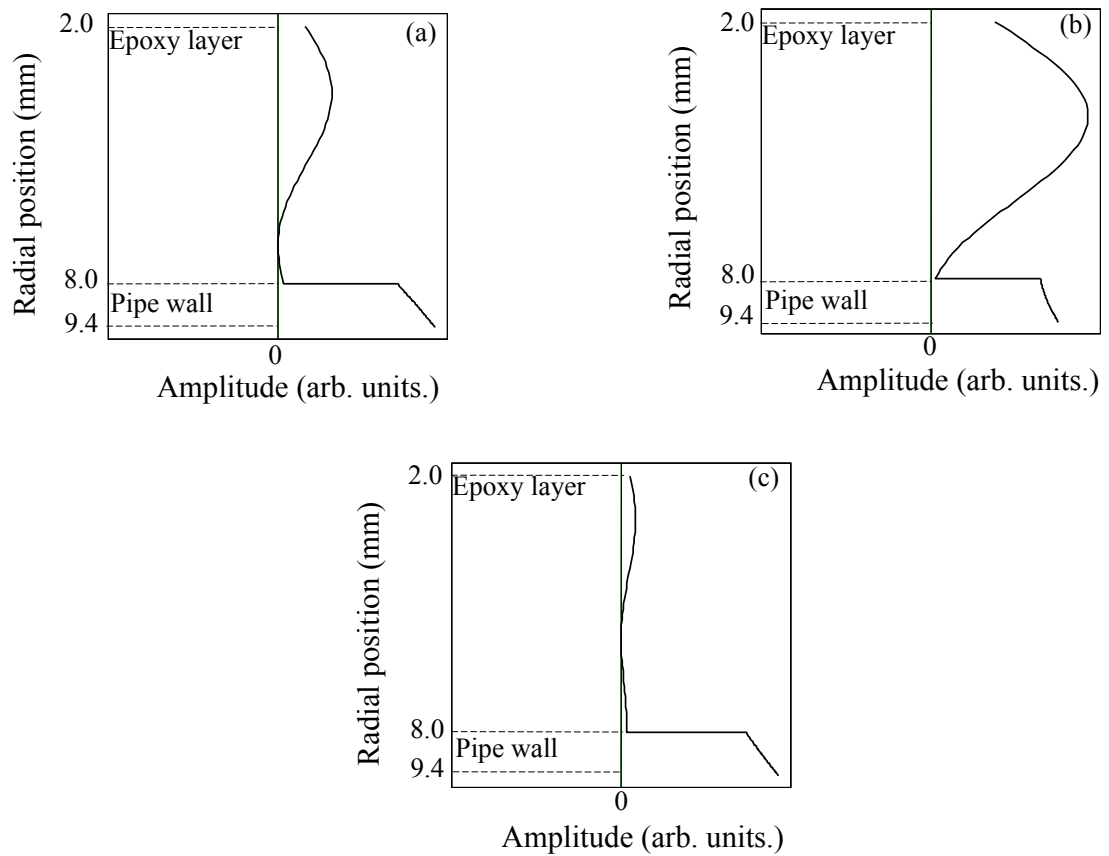
Figure 4.3: Energy flow density mode shapes for bilayered pipe, at points labelled in Fig. 4.2b. (a) Mode shape of point A on the T_2 mode. (b) Mode shape of point B on the T_1 mode. (c) Mode shape of point C on the T_2 mode.
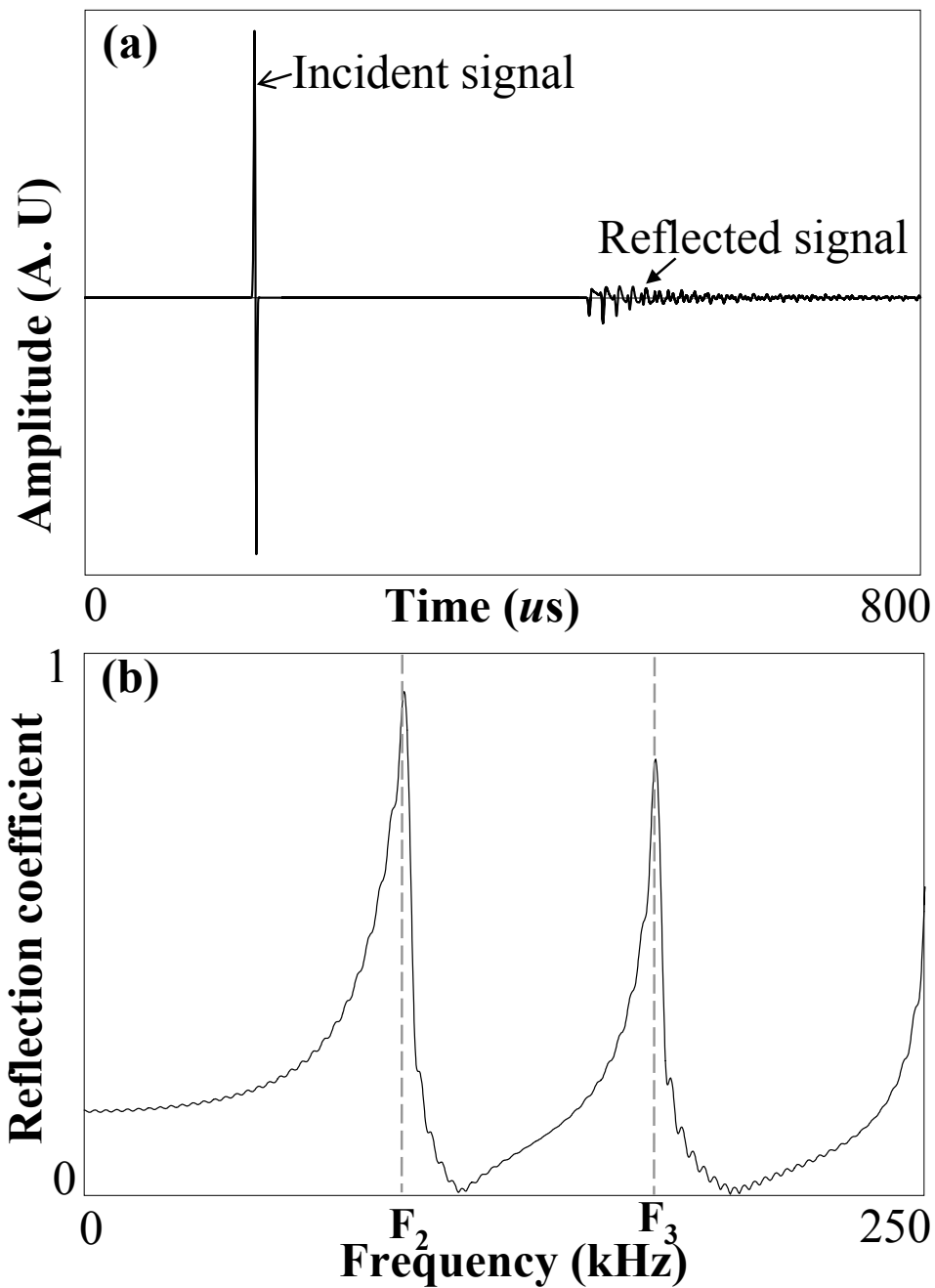
Figure 4.4: (a) Time trace, simulated by FE modelling, of the scattering of T(0,1) in an aluminium pipe partially coated with a 6-mm thickness epoxy layer inside, showing the incident and reflected signals received at the Reflection measurement point in Fig. 4.1; (b) Corresponding reflection coefficient amplitude spectrum. F_2, F_3 are cut-off frequencies of the bilayered pipe.
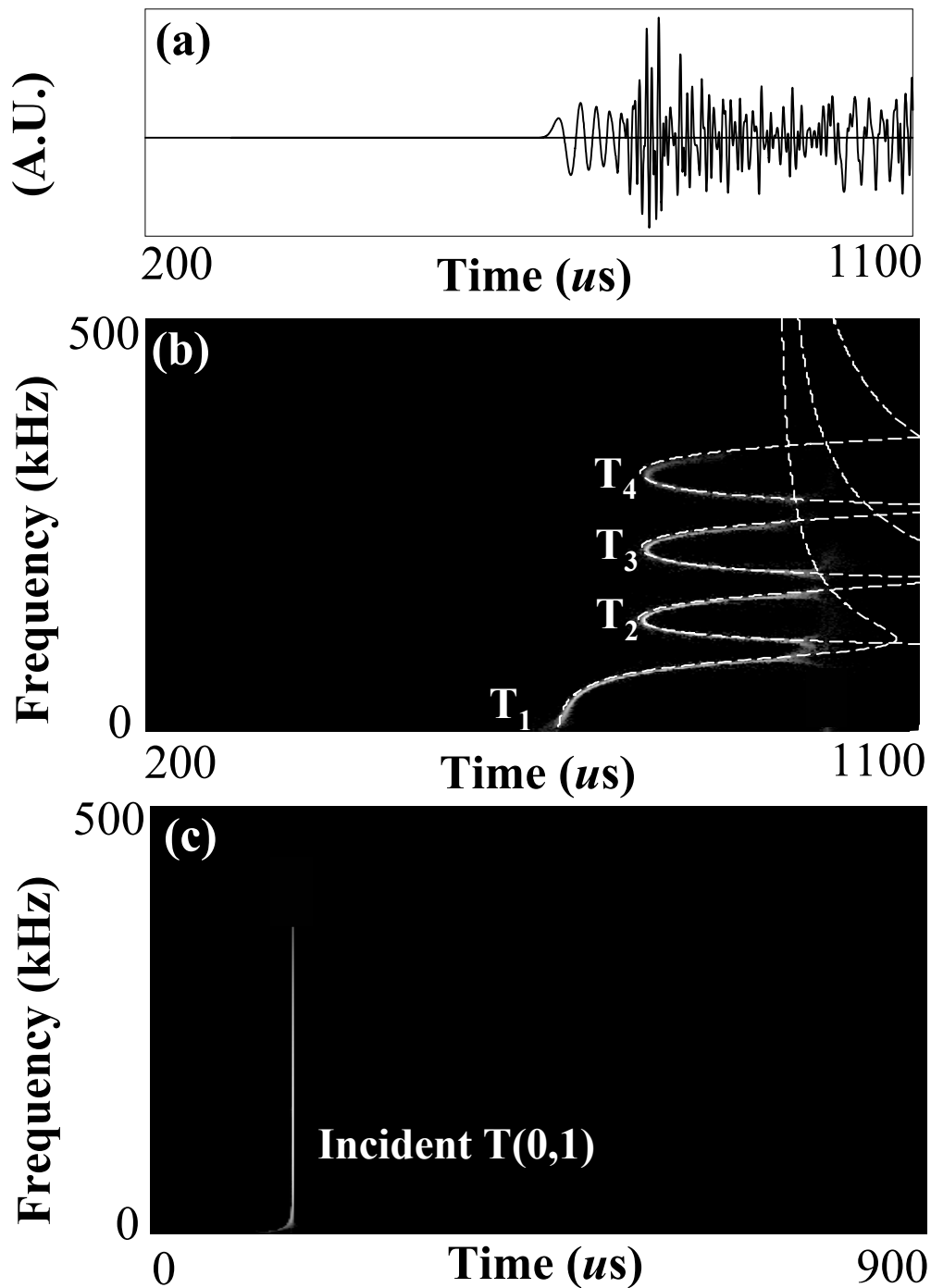
Figure 4.5: (a) Time trace, simulated by FE modelling, of the transmitted signal propagating past the bilayered part of a pipe; (b) Reassigned spectrogram analysis of the transmitted signal and the corresponding analytical calculation (white dashed curves) by DISPERSE; (c) Reassigned spectrogram analysis of the incident signal of the T(0,1) mode in the clean pipe (FE signal).

Differential optical sensor head

Displacement and velocity decoder

Receive point of reflected signal

Receive point of transmitted signal

PC

Digital Oscilloscope

Epoxy layer

Waveform generator

Free Pipe

Torsional excitation

PZT element
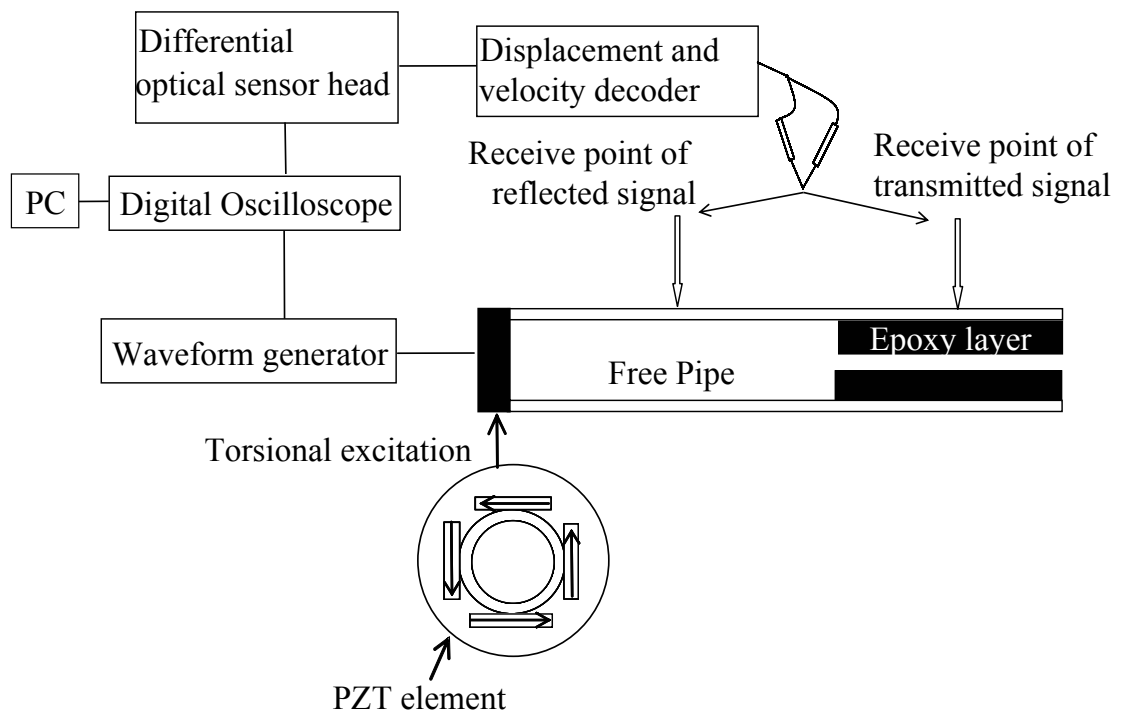
Figure 4.6: Schematic of the experimental setup.
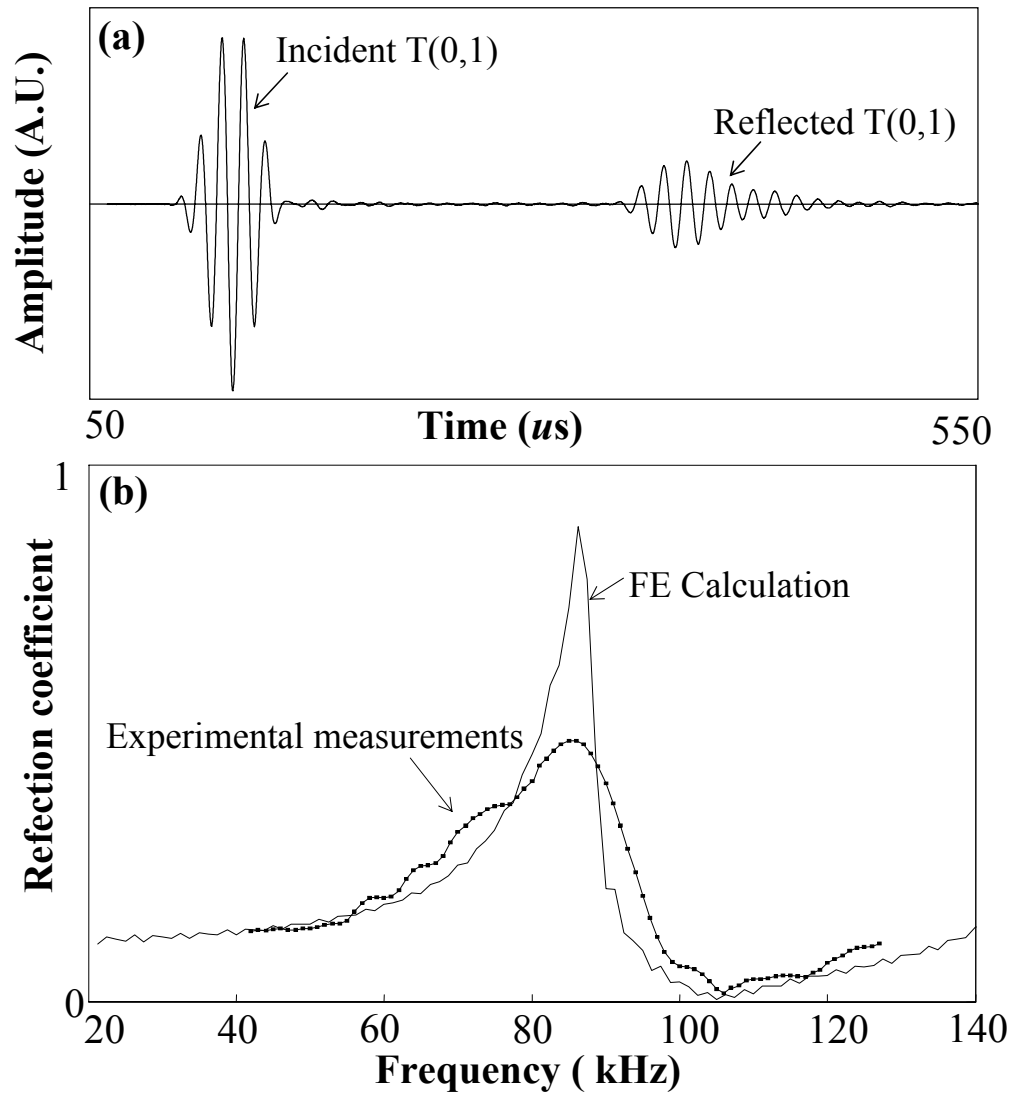
Figure 4.7: (a) A typical time-domain signal of the reflection measurement, showing the incident signal and the reflected signal by the layer; (b)Reflection coefficient amplitude of the T(0,1) mode from the aluminium pipe coated inside with a 6-mm thickness epoxy layer, obtained by experimental measurement (line with black squares) and FE calculation (black solid line).
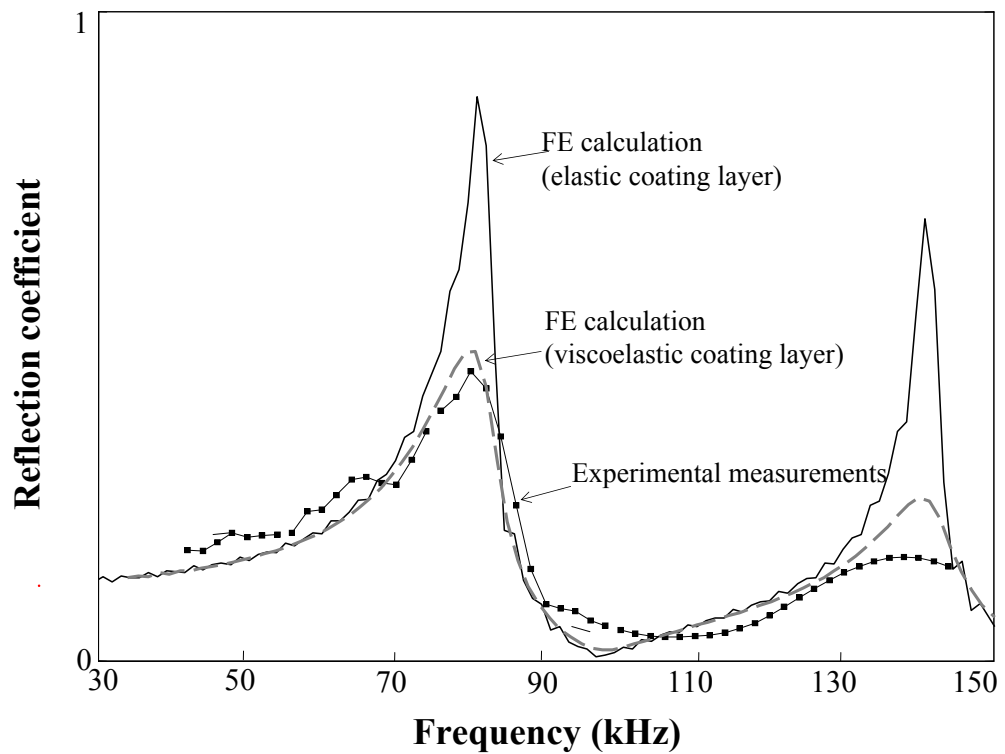
Figure 4.8: Reflection coefficient amplitude of the T(0,1) mode from the aluminum pipe completely filled with epoxy over part of its length, obtained by experimental measurement (line with black squares), FE calculation assuming an elastic coating (black solid line) and FE calculation assuming a viscoelastic coating (gray dashed line).
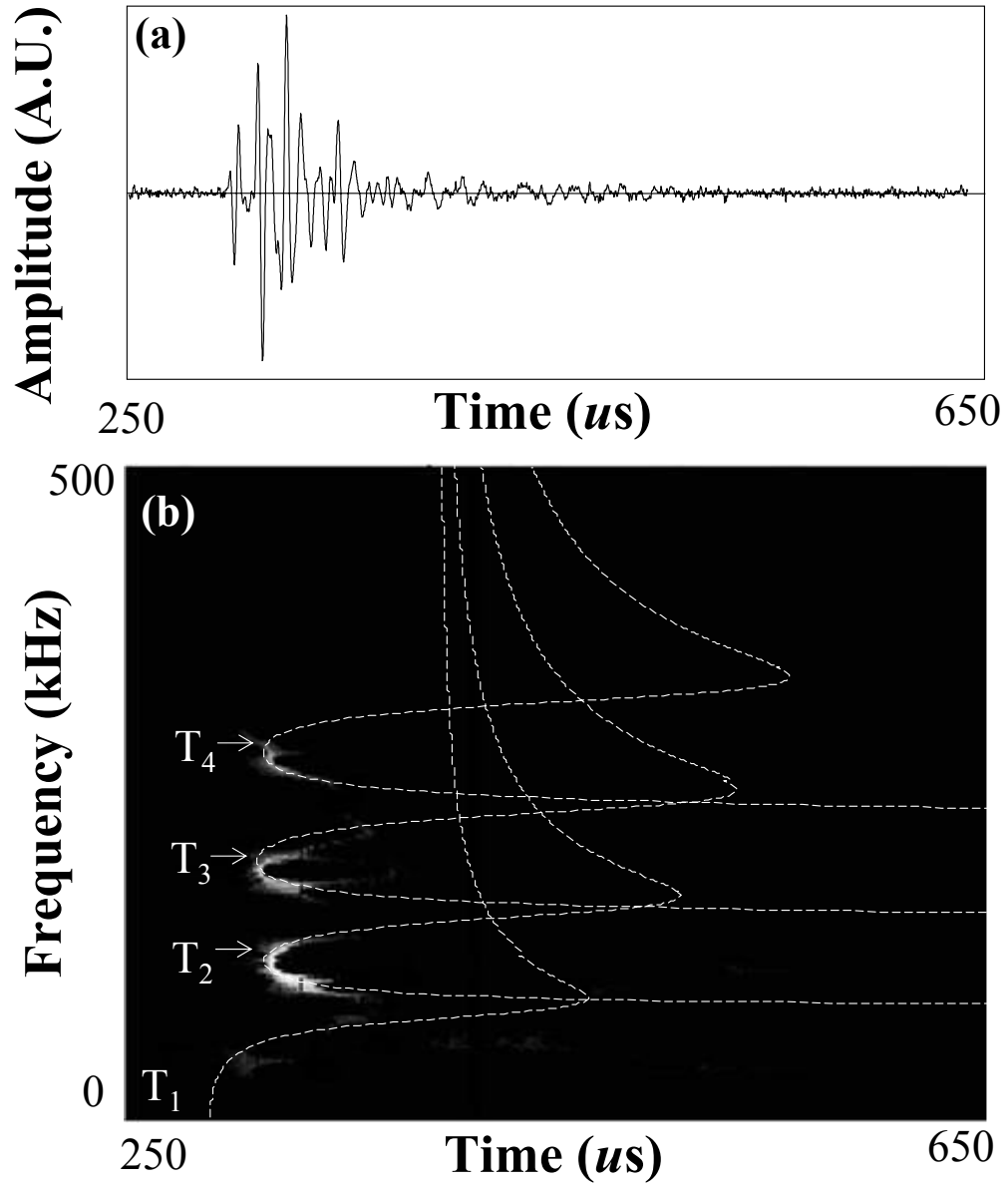
Figure 4.9: (a) Time-domain signal measured in the bilayered part of the aluminium pipe locally coated inside with a 6-mm thickness epoxy layer; (b) Reassigned spectrogram analysis of the measured local signal shown in Fig. 4.9a and analytical calculation (white dashed lines) by DISPERSE.
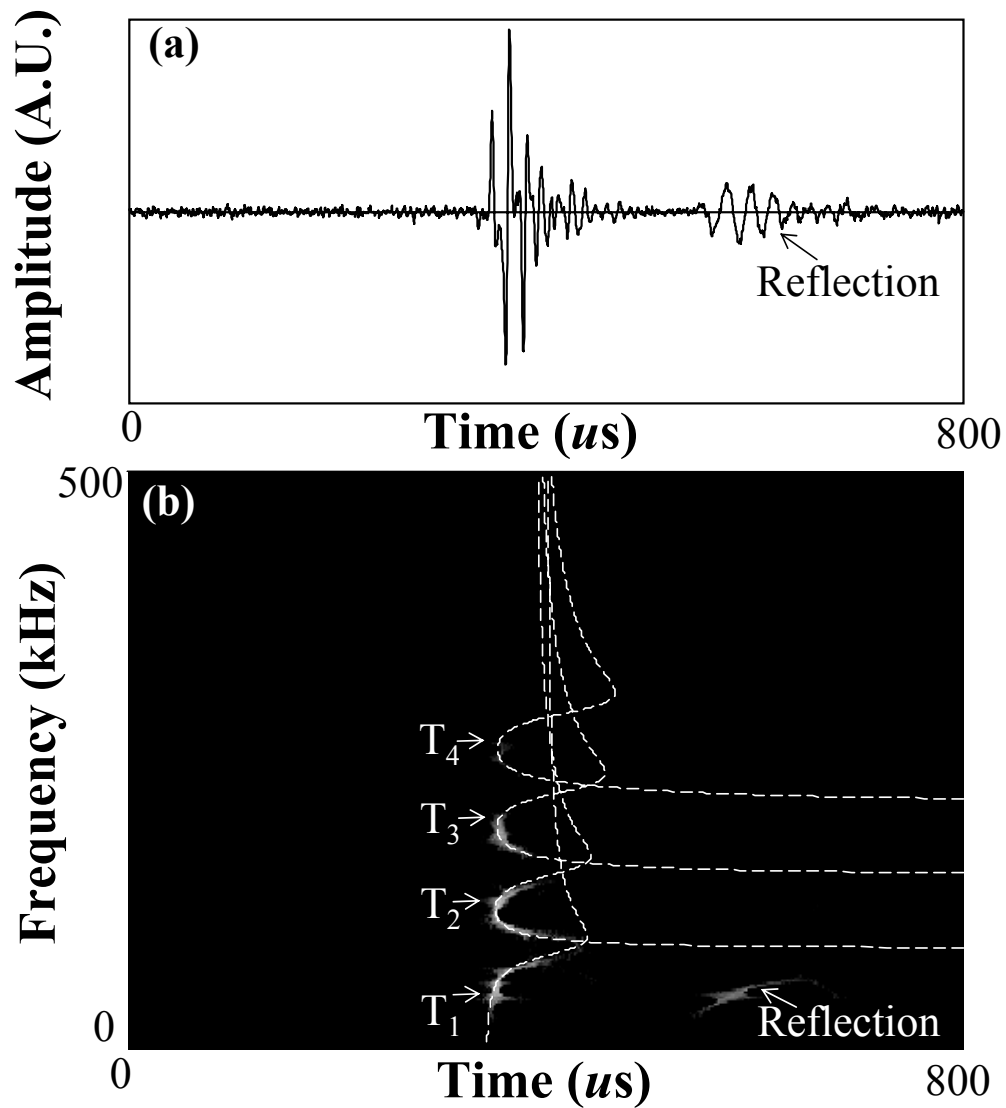
Figure 4.10: (a) Time-domain signal measured in the filled part of the aluminium pipe locally filled with epoxy; (b) Reassigned spectrogram analysis of the measured local signal and best fit curves (white dashed lines) calculated by DISPERSE for the aluminum pipe locally filled with epoxy.

Chapter 5

Feasibility Study of Sludge and Blockage Detection inside Pipes Using Guided Torsional Waves

5.1   Background

The results from Chapter 4, based on the idealised model, have shown the potential of using the fundamental torsional mode T(0,1) to detect and characterise a layer inside a pipe; however, the applicability of the two proposed techniques for the detection of realistic sludge and blockage needs further investigation. This is obviously due to various practical issues associated with realistic sludge that were not considered in the idealised model. These issues can significantly complicate the problem and affect the proposed techniques in different ways. This chapter proceeds the work by taking into account these more practical issues, including irregular axial and circumferential profiles of the sludge layer, imperfect bonding state between the sludge and the pipe and the material damping of the sludge. The purpose is to investigate how the reflection and transmission techniques are affected by each of these issues so as to find out the most critical factors and therefore assess the potential of using guided ultrasonic waves to detect and characterize sludge and blockages in practice.

Besides this specific inspection application, the models studied in this chapter are also linked to models of guided wave propagation in filled waveguides. As reviewed in previous chapters, a number of models have been conducted to study the effect of liquid or solid content on the propagation of guided waves [44, 45, 49, 58, 57, 60]. Most of these works assume that the contents are axisymmetric and also have regular properties along the axial direction. The models considered in this chapter will show the effect of irregular properties and asymmetric geometry of the contents on the propagation of the guided waves.

The chapter starts with the model studies of the effects of the irregular properties of sludge on the two techniques developed in the last chapter (Sec. 5.2). Then results from a number of experimental measurements are presented in Sec 5.3, including model experiments for validating the principles and realistic experiments for testing the practical capabilities. Limitations of the guided wave techniques for sludge detection and characterization are discussed in Sec. 5.4 and an overall assessment is given in Sec. 5.5.

5.2 Model Study

The effects of sludge irregularity on the reflection and transmission measurements are first investigated by FE modeling. A 2D model with the FE software FINEL [85] was used to study the case in which the sludge layer has an irregular axial profile, but an axisymmetric circumferential profile. The details of the models are outlined in Appendix A.1. The dimensions and the material properties of the pipe and the layer used in the 2D model are the same as those used in the idealised model and are listed in Table 4.1.

5.2.1 Imperfect bonding state

It is very likely that the bonding between the sludge layer and the pipe is imperfect. The effect of the bonding state can be studied by using a spring layer model which has been commonly used to represent imperfect bonding conditions [89]. A fictitious layer with compressional stiffness K_L and shear stiffness K_T is inserted between the

pipe and the sludge as shown in Fig. 5.1. Only the shear stiffness K_T will affect the torsional modes since they only have tangential displacements. The thin fictitious layer used in the FE simulation is 0.1mm thick and the other parts of the model are the same as in the idealised case. The decreasing of bonding is simulated by reducing the shear stiffness of the spring layer. More details of the model can be found in Appendix A.1.

The dispersion curves of the torsional modes in the bilayered pipe with imperfect bonding state can be numerically calculated with DISPERSE by treating the interface as a special layer with the properties stated above. Fig. 5.2 shows the group velocity dispersion curves of the first two bilayered pipe modes for three different value of the spring layer stiffness. For comparison the case of perfect bonding ($K_T \in \infty$) is also given. It can be observed that as the stiffness of the bonding decreases, the cutoffs of the higher order bilayered pipe modes move towards lower frequencies. A similar trend was found by Lanza di Scalea and Rizzo [90] and Cheng et al. [91] when comparing the dispersion curves of Lamb waves in two bonded plates with different degrees of bonding state.

As a result, the peak positions on the reflection coefficient spectrum magnitude (calculated from the FE simulated signals monitored at the reflection measurement point in Fig. 5.1) shift to lower frequencies with the decreasing of the bond state, which is shown in Fig. 5.3a. This implies that in practice, due to the uncertain bonding state, in order to detect the layer, either a broadband frequency excitation or a frequency sweep is required to guarantee obtaining a strong reflection from the layer. However, although this approach could lead to the detection of the sludge, it is not possible to characterize it by measuring peak positions of the reflection coefficient spectrum since the degree of bonding is normally uncertain in practice.

The reassigned spectrogram analysis of the transmitted T(0,1) mode (FE simulated signal monitored at the transmission measurement point in Fig. 5.1) from an imperfectly bonded bilayered pipe (case 2: $K_T = 0.71 GPa/mm$) is shown in Fig. 5.3b. It shows that the layer-induced dispersion of the transmitted signal can still be clearly revealed if the bonding condition is imperfect. The revealed spectrum is compared with the numerical calculation by DISPERSE showing excellent agreement. In terms of characterization, it becomes difficult to extract the properties of the layer (thick-

ness or shear acoustic velocity) from the dispersion of the transmitted signal, since
the degree of bonding also plays a crucial role in the dispersion of the transmitted
signal.

5.2.2 Varying thickness

In practice, a sludge layer may accumulate gradually along the pipe, which means
its thickness varies along its length. Here we discuss the case in which the layer has
a very gentle thickness change at both ends as illustrated in Fig. 5.4a. The part
where the layer has varying thickness is termed the 'tapered bilayered pipe'; while
the part where the layer has uniform thickness will be referred to as the 'uniform
bilayered pipe'. In this model, we assume a perfect bonding state consistently along
the layer. The details of this model can be found in Appendix A.1.

The time trace signal (Fig. 5.5a) from the FE model monitored at the reflection
measurement point in Fig. 5.4a shows the incident wave (70kHz central frequency
with 5 cycles) on its way to the layered pipe region, and a little reflection from the
layer due to the gentle change of its thickness. With the same excitation, about 30%
reflection can be achieved when the thickness change is abrupt as in the idealised
model (Fig. 4.4b). This implies that the smooth thickness change of the sludge layer
will considerably reduce the strength of the reflection from the layer.

On the other hand, there is more energy of the incident signal transmitted through
the tapered bilayered pipe. The reassigned spectrogram of the transmitted signal
from the FE model monitored at the transmission measurement point in Fig. 5.4a is
given in Fig. 5.5b. It shows that the gentle thickness change of the layer delays the
frequencies which are above the first cutoff frequency of the torsional mode in the
uniform bilayered pipe (indicated by F_2 in Fig. 4.2a). The layer-induced dispersion
of the transmitted signal can be revealed at the frequencies below F_2.

The torsional modes in the tapered bilayered pipe adapt to the thickness varia-
tion of the layer: their phase velocity and wavenumber change continuously during
propagation, depending on the local thickness. However, as the thickness change of
the layer is very gentle along its length, we can approximately consider the tapered

bilayered pipe region to be equally divided into a large number of 'local uniform bilayered pipes' whose thickness can be considered uniform over a length of l_t (shown in Fig. 5.4a). Due to the thickness variation of the layer, these local uniform bilayered pipes have different dispersion curves and accordingly, the cutoff frequencies of the modes also change according to the thickness of the layer: the thinner the layer is, the higher the cutoff frequencies tend to be. This is illustrated in Fig. 5.6: the cutoff frequency of the second mode in the tapered bilayered pipe is plotted as a function of the thickness of the layer. Since the thickness of the layer changes continuously from zero to the thickness of the uniform part of the layer, the cutoff frequency of the second mode T_2 in the tapered bilayered pipe decreases monotonically from the cutoff frequency of the clean pipe mode T(0,2) to F_2 which corresponds to the cutoff for the uniform bilayered pipe.

When the T(0,1) mode containing broadband frequencies is incident on the tapered bilayered pipe region, the frequencies below F_2 can freely pass the tapered bilayered pipe without encountering any cutoff frequency. However, the frequencies above F_2 will inevitably match a cutoff frequency of a certain local tapered bilayered pipe, from where they will be greatly delayed after propagating for a distance of l_t due to the low propagation velocity at the cutoff. Therefore, the dispersion induced by the uniform bilayered pipe on the transmitted signal can only be preserved in the frequency range below the F_2.

We should also note that when the thickness change of the layer becomes sharp, the length l_t during which the thickness of the layer can be assumed uniform will tend to be infinitesimal. In this case, all the frequencies can freely pass the tapered bilayered pipe region since l_t is too short to delay the frequencies even if they match the cutoff frequencies of the tapered bilayered pipe. So the transmitted signal will be similar to that in the idealised model.

5.2.3 Varying thickness and varying bonding state

Besides the thickness change, the sludge may simultaneously have a non-uniform bonding state along its axial profile. We proceed next to model a case in which the sludge layer has the same thickness variation as in the previous case. Moreover, the

bonding state varies along the tapered bilayered pipe region as shown in Fig. 5.4b. This is a very likely scenario in practice due to the non-uniform bonding condition. A spring layer was used to simulate the imperfect bonding and the stiffness of the spring layer in the front part (state 1) of the layered pipe is half of the latter part (state 2). This case was made to study the effect of abrupt bonding change along the sludge layer. More details of the model can be found in Appendix A.1.

The FE simulated signals monitored at the reflection measurement point (in Fig. 5.4b) are shown in Fig. 5.7a. It shows the incident wave on its way to the layered pipe region, and a little reflection from the start of the tapered bilayered pipe due to the gentle thickness change of the layer. However, a much stronger reflection occurs from the point where there is an abrupt bonding change, although the change of thickness of the layer at this point is very gentle. This implies that an abrupt change in bonding state will result in strong reflections regardless of the gentle thickness change of the layer. Essentially, bonding state, thickness and even material properties of the sludge will change the mode shape of the torsional mode, any such change being the cause of reflection. Therefore, we can expect that the reflection may occur anywhere along the layer where the layer has an abrupt change of its properties. The more abrupt these change are, the stronger the reflections will be.

The reassigned spectrogram analysis of the transmitted signal from the FE model monitored at the transmission measurement point (Fig. 5.4b) is shown in Fig. 5.7b. Similar to the previous case, the layer-induced dispersion of the transmission signal can be revealed below the first cutoff frequency of the torsional mode in the uniform bilayered pipe region.

5.2.4 Non-symmetric circumferential profile

For the next stage of the FE work, a 3D FE model was developed to study the effects of the circumferential extent of the layer on both techniques. The pipe studied in this model is different from the 2D model. A 3 inch aluminium pipe (89mm OD and 2.5mm wall thickness) coated with a 10-mm thickness epoxy layer was modelled. The corresponding dispersion curves of the torsional mode in such a pipe is shown in Fig. 5.8a. The model uses the same material properties as the 2D modelling that are

listed in Table 4.1. The pipe is 2.5m in length, 0.5m of which is coated with a layer inside. The layer was modelled to have a constant axial profile (perfect bonding and uniform thickness), but a non-symmetric circumferential profile as shown in Fig. 5.9a. Four cases were modelled for different circumferential extents of the layer. The model was carried out using the FE software ABAQUS [92] and the details of the 3D model are described in Appendix A.2.

The signals are first monitored at the reflection measurement point in Fig. 5.9a to receive the incident and reflected T(0,1) mode. The effect of circumferential extent of the layer on the reflection coefficient amplitude spectrum is shown in Fig. 5.8b. To validate the 3D FE model, the result obtained for the 100% circumferential extent case were compared to those calculated from the 2D model in FINEL, showing excellent agreement. Fig. 5.8b clearly indicates that the reduction of the circumferential extent of the layer decreases the strength of the reflection throughout the frequency range. However, the frequencies at which strongest reflections occur are not affected by the circumferential extent of the layer.

The transmitted T(0,1) mode was monitored at the transmission measurement point in Fig. 5.9a. The reassigned spectrogram analyses of the transmitted T(0,1) mode from the pipe partially coated with the layer of different circumferential extents, are shown in Fig. 5.10. The signals coming later are the transmitted signal reflected from the end of the pipe. When the layer is axisymmetric (100% circumferential extent), the layer-induced dispersion of the transmitted signal can be clearly revealed and shows excellent agreement with the analytical calculation by DISPERSE; however, as the layer becomes non-axisymmetric, the layer-induced dispersion of the transmitted signal becomes irregular and complex. As the circumferential extent of the layer reduces, the dispersion of the transmitted T(0,1) mode evolves from the dispersion curve of the torsional bilayered pipe modes (100% circumferential extent) to the dispersion curve of the incident T(0,1) mode (non-dispersive). The complexity of the dispersion of the transmitted T(0,1) mode is still a good indicator of the presence of the sludge compared to the non-dispersive T(0,1) mode in the clean pipe; however, the complexity of the dispersion makes it difficult to characterize the layer quantitatively from the measurements.

The 3D FE model was also extended to study a case when the layer has differ-

ent thickness around the circumference as illustrated in Fig. 5.9b. The layer was modelled to have a 10-mm thickness part and a 5-mm thickness part, each occupying 50% circumferential extent. The circumferential profile of the layer is constant along its length. All the other parameters of the pipe and the layer are the same as the last model. The reflection coefficient spectrum calculated from the signals monitored at the reflection measurement point is shown in Fig. 5.11a. For comparison, the reflection coefficient spectra calculated from the two fully bilayered pipe model (100% circumferential extent) with respectively 10-mm layer thickness and 5-mm layer thickness are also presented. Fig. 5.11a shows that the peaks on the reflection coefficient spectrum occur at the frequencies where the peaks of the thin and thick layers would occur if they were present in the pipe separately with full circumferential extent. This will increase the possibility of detection.

The transmitted T(0,1) mode was monitored at the transmission measurement point in Fig. 5.9b with its reassigned spectrogram analyses being shown in Fig. 5.11b. It is clear that the thickness variation of the layer around the circumference increases the complexity of the dispersion of the transmitted T(0,1) mode.

5.3 Experiments

Model experiments and realistic experiments have also been conducted. The model experiments were conducted to validate the principles predicted by the FE models. The setup of the model experiments are the same as described in Chapter 4 (Fig. 4.6). The model experiments were conducted on two small aluminium pipes (16.5-mm inner diameter and 1.4-mm wall thickness) coated with layers made of different materials. Due to manufacturing difficulty, the layers were built at one end of the pipe rather than in the middle of the pipe.

The same setup for the model experiments was used as the one introduced in Chapter 4 (Fig. 4.6). The reflection measurement and local measurements also followed the same procedures. The slight difference is that the setup uses more pieces of PZT elements (six pieces) mounted on the external surface of the pipe for excitation and samples more waveforms for circumferential averaging. This was done to further

eliminate the flexural modes at higher frequencies.

5.3.1   Model experiment

The reflection measurement was performed on the aluminum pipe containing an epoxy circular tube of 16.5-mm external diameter and 4.5-mm inner diameter. The tube was press-fitted inside the pipe to represent the imperfectly bonded layer. The pipe was 1.3m in length while the epoxy tube was 0.3m long and placed at one end of the pipe.

The measured reflection coefficient amplitude spectrum from this sample is shown in Fig. 5.12. For comparison, we also show the results from a sample of pipe with a perfectly bonded epoxy layer which was presented in Chapter 4. This was made by casting the epoxy layer (6mm uniform thickness) inside the pipe. The press-fit epoxy layer gives reduced contact to the pipe wall compared to the cast epoxy, which is to represent a poorer bonding condition. The epoxy resin employed for both cases is a commercial adhesive, Araldite 2020, whose acoustic properties are listed in Table 4.2.

The FE predictions for both cases are plotted in Fig. 5.12. As shown before, the measured peak position of the reflection coefficient amplitude spectrum matches very well with the predicted one in the case of perfect bonding. The agreement for the imperfect bonding case was achieved by choosing a suitable contact stiffness value in the FE model. The discrepancy between the modelling and the experiments on the magnitude of the reflection coefficient spectrum has been known as being caused by the material damping of the epoxy, which was not considered in the FE modelling. Most importantly, both measurements and simulations confirm that the imperfect bonding condition between the layer and the pipe shifts the peaks of the reflection coefficient amplitude spectrum to lower frequencies.

The local signal was measured on the part of the pipe coated with the imperfectly bonded layer, at a position 0.05m away from where the layer starts in the pipe. The reassigned spectrogram analysis of the measured local signal is shown in Fig. 5.13a. For comparison, the reassigned spectrogram analysis of the incident signal T(0,1)

measured in the clean pipe region is also given in Fig. 5.13b. It is clear from Fig. 5.13a that the layer-induced dispersion of the local signal can still be measured when the bonding of the layer is imperfect. The first two cut-off regions can be identified where the frequencies are delayed due to the low propagation velocity at the cut-off frequencies of the bilayered pipe modes.

Measurements were then performed on another sample of pipe coated with an irregularly shaped layer made of simulants of a potential real sludge material shown in Fig. 5.14. A mixture of Magnesium Hydroxide, Magnesium Oxide and water was proposed by an industrial partner (Nexia Solutions Ltd) as a useful sludge simulant. The simulant was transferred into the 1.6-m long pipe to form a 0.4m long sludge layer. The time trace in Fig. 5.15a is the reflection measurement made at clean pipe region, 0.8m away from the start of the layer (the reflection measurement point in Fig. 5.14). It shows the incident signal (30 kHz central frequency with 10 cycles) followed by a lower amplitude signal (reflection 1) which is the reflection from the entry point of the sludge. A much stronger signal (reflection 2) arriving later is reflected from the middle of the blocked pipe according to its arrival time. Although the sludge layer has an irregular shape due to the manufacturing difficulty, we believe that the variation of the thickness of the layer is free from any abrupt change. Thus, we speculate that this stronger reflection was caused by an abrupt bonding change of the sludge, since it is hard to guarantee the simulant to have uniform contact with the pipe when it was transferred into the pipe. The reflection coefficient amplitude spectra of the reflection 1 and the reflection 2 is shown in Fig 5.15b.

For the transmission measurement, an excitation signal of 150 kHz with 2 cycles was employed and the measurement was made at a local point in the blocked pipe region about 0.1m away from where the sludge starts (the transmission measurement point in Fig. 5.14). The reassigned spectrogram analysis is shown in Fig. 5.16. Instead of revealing a regular dispersion change as in the last case, the spectrum of the transmitted signal shows a complex dispersion change of the signal. As shown in the FE model, this can be caused by the non-symmetric circumferential profile of the sludge which causes different modes to be generated in the blocked part of the pipe, with different propagation velocities. Also we noticed that the signal attenuated quickly as the receiver point was moved further away from the entry point

of the sludge and became too low to be measured after 0.3 m. Thus, the significant attenuation of the torsional modes may also be an additional indicator of the sludge, since the modes propagating in the clean metal pipe have little attenuation over long distances.

5.3.2 Realistic experiment

To test the applicability of the measurement ideas in practice, a realistic experiment was performed on a nominal 3 inch (88.9mm OD and 2.5mm wall thickness) steel pipe using a commercial WaveMaker Pipe Screening system from Guided Ultrasonics Ltd [93]. The 3-m long pipe was in good condition (no cracks or defects) and had no welds or flanges. The sludge material was made by mixing Magnesium Hydroxide, Magnesium Oxide and water in the proportions 54:9:37. The material was then transferred into the 3 inch pipe to build up the sludge layer which extended up to 1m in length from one end of the pipe. The speculated axial profile is shown in Fig. 5.17a. Due to the method of manufacturing, the pipe is fully blocked at the beginning of the sludge for a very short length. The sludge forms a layer with an estimated average thickness of 15mm for about 0.4m and gradually decreases its thickness to about 5mm towards the end of the pipe. The pipe was then sealed at both ends to minimise contact with air and was stored for 14 days to dry before the tests started. Both reflection measurement and transmission measurements were carried out at two different times. The first one was conducted immediately after 14 days when sludge was still fairly wet. The second measurements was made one month after the first one during which the inside of the pipe was open to the air. This made the sludge become completely dry and solid by the time of the second measurement.

The setup of the reflection measurement is illustrated in Fig. 5.18a and photographed in Fig. 5.17c. A Guided Ultrasonics Ltd. transducer ring placed at the outside surface of the pipe was used to send the T(0,1) mode in both the forward and backward directions and to receive the reflected signals from any feature in the pipe. Fig. 5.19a shows a typical reflected signal (25 kHz central frequency with 8 cycles) from the first measurements when the transducer was placed 1.4m away from the start of the blocked part of the pipe. The arrival time of the signal was converted to

distance by measuring the propagation velocity T(0,1) in the clean pipe. The figure thus shows the amplitude (vertical axis) and the source location (horizontal axis) of the reflections that can be received by the transducer ring in Fig. 5.18a . The backward end reflection occurs at -0.6 m, and in the forward direction, there is a mirroring of the backward end reflection signal at the exact same distance from the ring. This mirror is known to occur in cases when the reflections in both directions occur in the near field of the transducer (± 1 meter from the ring), because it is not possible to control the direction of the transmitted and received waves adequately. In practice, with longer pipes, this problem of mirror signals is avoidable. The reflection occurring at 1.6m comes from the sludge, but not from the entry point of the sludge. This may be due to the poor bonding condition at the beginning of the sludge. Also note that there is little forward end reflection received because of the large material damping of the sludge.

To calculate the reflection coefficient spectrum, the amplitude of the reflected signal from the sludge was divided by that of the backward end reflection signal which can be used to approximate the incident signal. The measured reflection coefficient obtained from the first experiment is shown in Fig. 5.19b and exhibits a decreasing trend as the testing frequency increases. A maximum reflection around 17% was measured at 25 kHz.

The same measurement was repeated one month after the first when the sludge had become completely dry and solid. The measured reflection coefficient shows very different frequency dependence from the first measurement as shown in Fig. 5.19b. A maximum reflection of about 21% can be achieved at 32 kHz. We speculate that the discrepancy between the two measurements is largely due to the change of properties of the sludge during the period between the two measurements. As the sludge becomes more solid, its bonding to the pipe wall improves. This can result in strong reflections at higher frequencies. Also the material properties may change as the sludge dries out, which changes its sound velocity. This implies for practical tests that the frequency range to obtain a strong reflection from sludge may change significantly as the condition of the sludge changes.

The setup of the transmission measurement is illustrated in Fig. 5.18b and photographed in Fig. 5.17d. The transmission measurement uses two transducer rings

working in pitch catch mode: one transducer ring sends the signal which is received by another one. The excitation employs an excitation signal of 40 kHz central frequency with 3 cycles which covers the frequency band from 20 kHz to 60 kHz. The guided modes experienced significant attenuation at the time of the first measurements when the sludge was wet. The attenuation caused by the sludge was measured between 35-40 dB/m which is much stronger than the attenuation caused by any other feature. A typical site weld is a -14dB [13] reflector and the attenuation caused by bitumen coating is between 3-10 dB/m [13].

The attenuation of the transmitted signals is much lower at the time of the second measurements, when the sludge become dry and solid. Both transducer rings were first placed in the clean pipe region with 1m separation distance. The signal received by the receiver transducer ring was analyzed by the reassigned spectrogram showing the non-dispersive T(0,1) mode (Fig. 5.20a). Then the transmitter transducer was placed in the blocked region keeping the same distance (1 meter) from the receiver transducer as for the clean pipe (Fig. 5.18b). Its reassigned spectrogram shows the sludge-induced dispersion of the transmitted signal as some frequencies are delayed in their arrival time (Fig. 5.20b).

The noise may affect the signal so that the spectrogram may not reveal a strict non-dispersive signal in the clean pipe as revealed in (Fig. 5.20a). The capability to identify the sludge-induced dispersion will depend on the noise level. To calibrate the influence of the noise, it is important to quantify the extent of dispersion of the signal from the spectrogram. One method to assess dispersion is to calculate the standard deviation of the arrival time (SDT) of all the frequencies in the received signal. Figs. 5.21 shows SDT of the signals in Figs. 5.20 a and b respectively, when different values of threshold are set to extract the dispersion curve from the spectrogram. The SDT of the signal in the clean pipe (SDT_{Clean}) is due to the noise and ideally it should be zero; the SDT of the signal in the blocked pipe ($SDT_{Blocked}$) contains the information about the sludge-induced dispersion. To calibrate sludge-induced dispersion from the influence of the noise, a ratio of SDT (SDTR) can be defined as

$$SDTR(dB) = 20 \log_{10}(\frac{SDT_{Blocked}}{SDT_{Clean}}).\qquad (5.1)$$

It can be seen from Figs. 5.21 that the SDTR is always larger than 6dB. In practice, it will be very useful to identify a threshold of the SDTR from which the sludge induced dispersion can be reliably detected. This should be achieved through extensive practical tests to obtain empirical data.

5.4 Discussion

Here we address some issues that will affect the proposed measurements for sludge and blockage detection in practice.

Firstly, in many circumstances pipes will contain fluid. The proposed measurements will not be affected by the presence of fluids inside the pipes if they are inviscid such as water; however, if the fluid is viscous, the torsional mode will have attenuation which is controlled by the viscosity of the fluid and the operating frequency. This requires the inspection to use low frequencies to maintain a large testing range.

Secondly, we have shown that it is still possible to detect the sludge if the bonding is imperfect to a certain extent. However, if the sludge makes a slip contact or is almost disbonded, then the torsional mode will fail to detect the blockage, since there is no coupling of guided wave energy between the sludge and the pipe.

Lastly, as we see, the material damping of the sludge or blockage affects the measurements. If the sludge is a highly attenuative material, it may considerably attenuate the magnitude of both the reflected and transmitted signals. On the other hand, the large attenuation of the transmitted signal may also be an additional indicator of presence of the sludge, if the pipe is free from any other attenuative media either inside or outside.

5.5   Conclusions

In this chapter we have studied the feasibility of sludge and blockage detection and characterization using guided torsional waves. Two guided wave techniques developed from earlier work were advanced by taking into account practical issues about the sludge, including irregular axial and circumferential profiles of the sludge layer, imperfect bonding state between the sludge and the pipe and the material damping of the sludge. The study has investigated the effects of each of these factors on the two techniques. An overall assessment of the feasibility of sludge detection and characterisation using guided wave can be summarized as follows.

The reflections of guided ultrasonic waves from sludge can be measured to effectively locate the sludge in the pipe. The reflection can be caused by any abrupt change of the properties of the sludge along its axial or circumferential profiles including bonding state, thickness or material properties. The more abrupt these changes are, the stronger the reflections will be. The strength of the reflection also enhances with increasing circumferential extent of the sludge layer. On the other hand, the material damping of the sludge weakens the strength of the reflection.

The strength of the reflection is frequency dependent. The frequency to obtain the strongest reflection is determined by the thickness, material properties and the bonding state. So a practical implementation should sweep the testing frequency or employ broadband frequency excitation in order to guarantee a strong reflection from the sludge.

The transmission of guided ultrasonic waves propagating past the blocked pipe region can be measured to detect the presence of the sludge or blockage, however this method cannot locate them. The measurement employing a broad band excitation reveals the sludge-induced dispersion change of the guided waves. The revealed dispersion may be complex or regular depending on the asymmetry of the sludge in its circumferential and axial profiles. The transmitted signal may suffer from large attenuation caused by material damping of the sludge. This may also be an additional indicator of the presence of the sludge, if the pipe is free from any other attenuative media either inside or outside.

For reliable sludge and blockage detection, both the reflection and transmission measurements should be used since they are two complementary measurements. For example, when the reflection is weak, most energy of guided wave is transmitted through the blocked region leading to more sensitive transmission measurements.

Quantification of the extent and material properties of the sludge is difficult because of their arbitrary shapes and properties. An effective characterisation of the geometrical and material properties of sludge is only possible when the sludge has a uniform shape and its bonding condition is known.
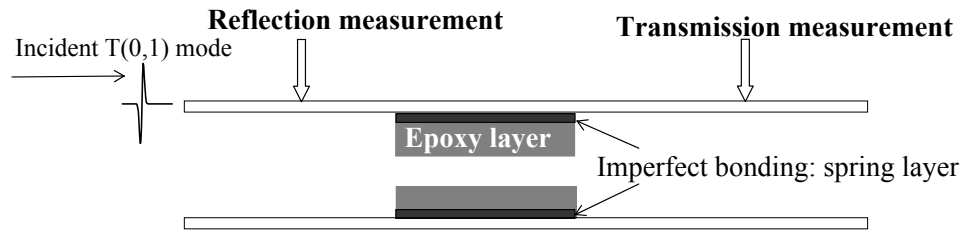
Figure 5.1: Schematic of the model in which the pipe is locally coated with 6-mm thickness epoxy with an imperfect bonding state.
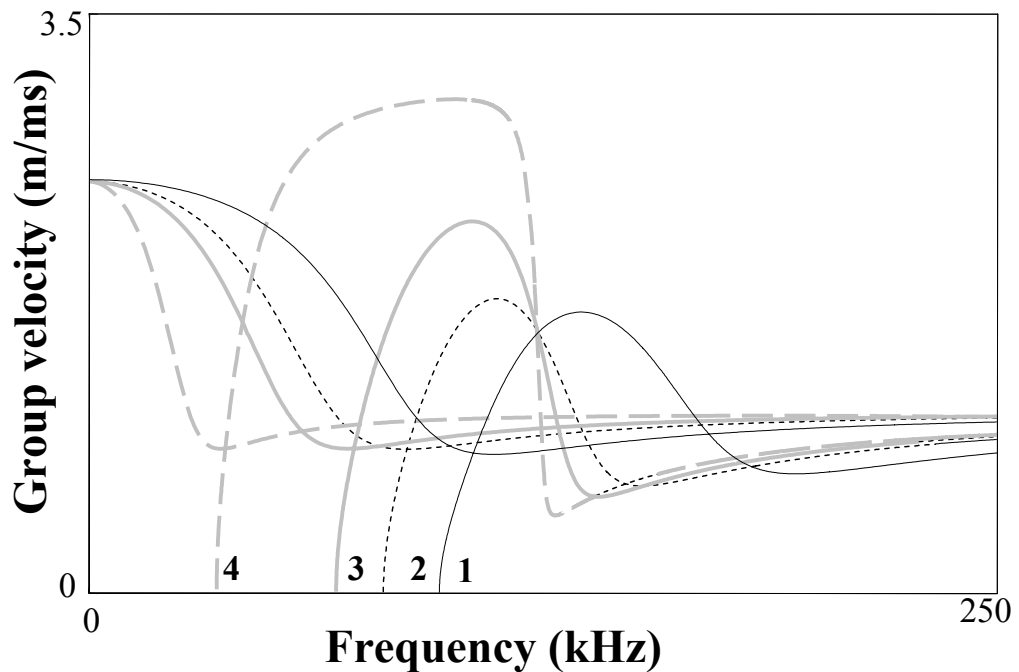
Figure 5.2: Dispersion curves of the first two torsional modes in the pipe coated with 6-mm thickness epoxy layer for different bonding states. Case 1: perfect bonding, shear stiffness $K_T \in \infty$; Case 2: $K_T = 0.71 GPa/mm$; Case 3: $K_T = 0.355 GPa/mm$; Case 4: $K_T = 0.071 GPa/mm$.
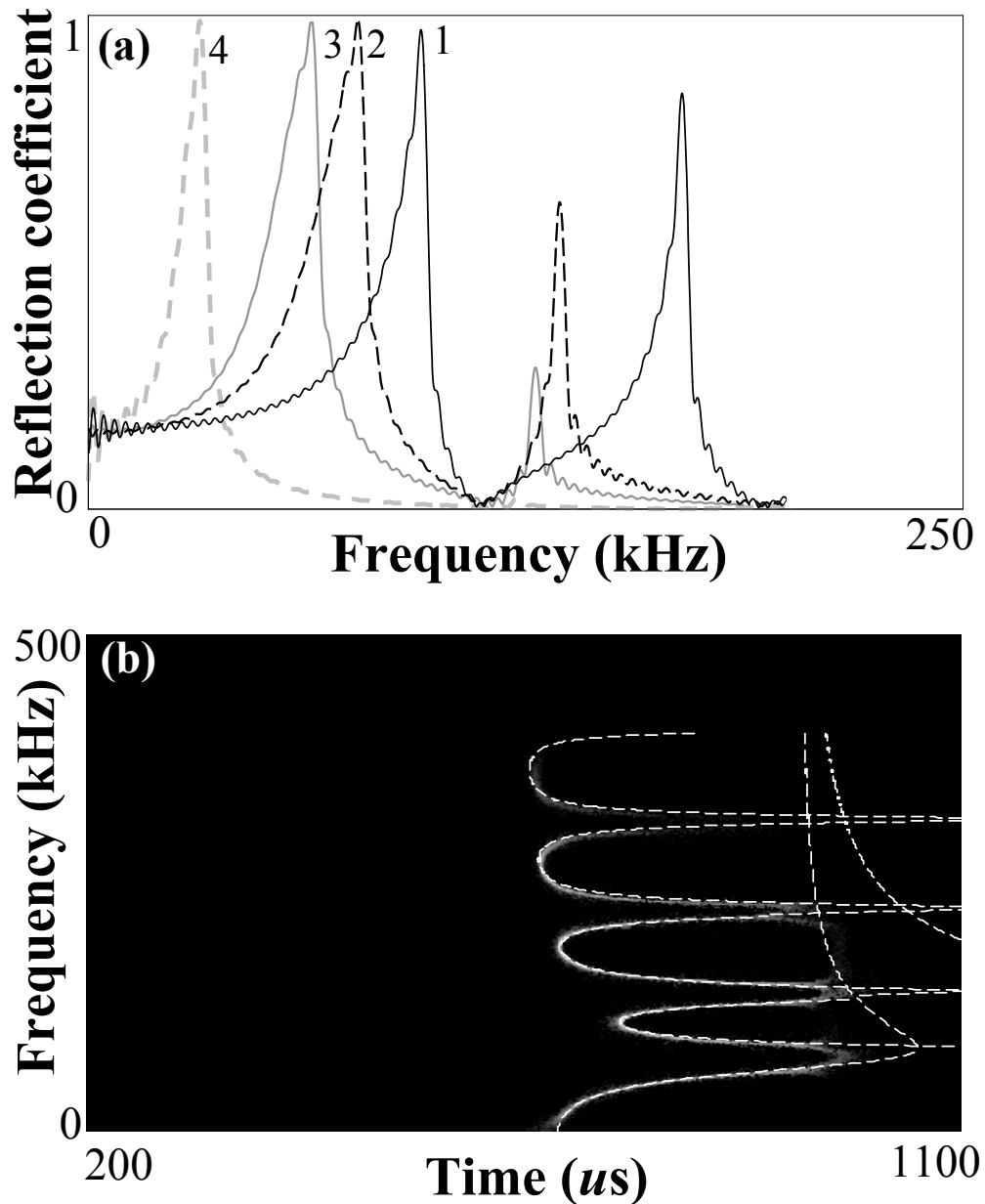
Figure 5.3: (a) Reflection coefficient spectrum obtained from FE simulations for the T(0,1) mode when incident at the region where the pipe is locally coated with 6-mm thickness epoxy layer, for different bonding states. Case 1: perfect bonding, shear stiffness $K_T \in \infty$; Case 2: $K_T = 0.71GPa/mm$; Case 3: $K_T = 0.355GPa/mm$; Case 4: $K_T = 0.071GPa/mm$; (b)Reassigned Spectrogram analysis of the transmitted signal in the pipe locally coated with 6-mm thickness epoxy layer with imperfect bonding state (case 2) and the corresponding numerical calculation with DISPERSE (white dashed curves).
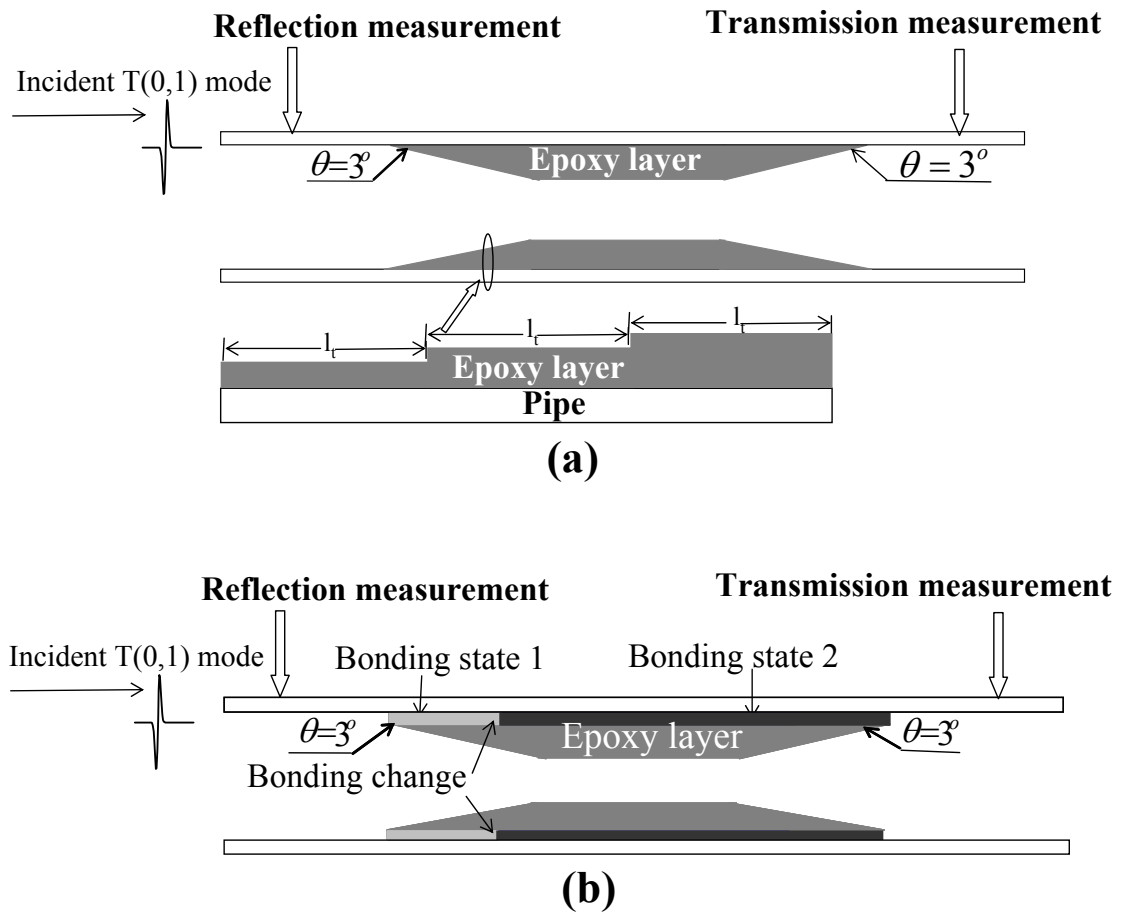
Figure 5.4: (a) Schematic of the model in which the pipe is locally coated by an epoxy layer that has varying thickness. The tapered region of the bilayered pipe can be thought of as a succession of local uniform bilayered pipes; (b) Schematic of the model in which the pipe is locally coated by an epoxy layer that has varying thickness and varying bonding state.
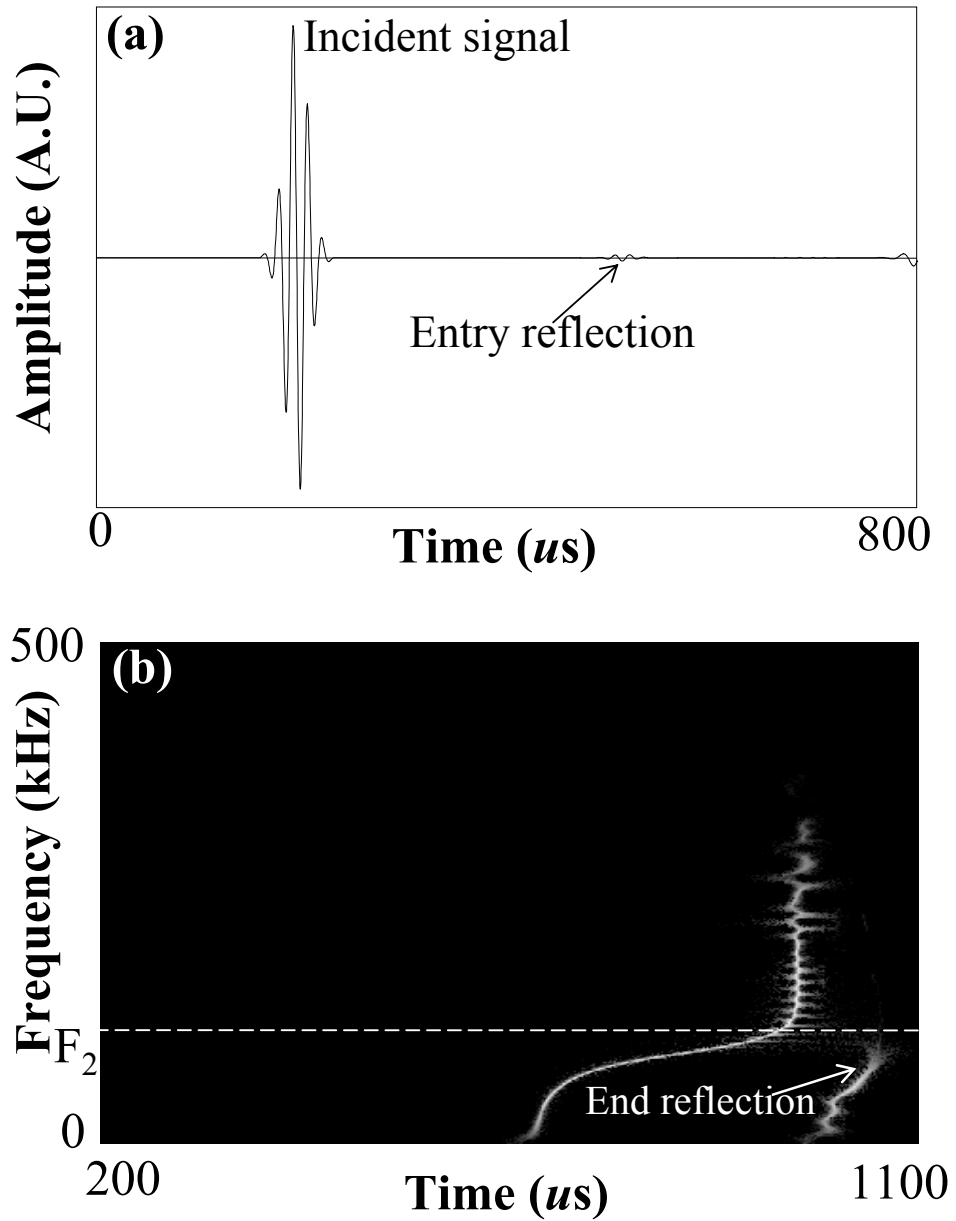
Figure 5.5: (a) Time trace of the incident and the reflected signals monitored at the reflection measurement point in Fig. 5.4a; (b) Reassigned Spectrogram analysis of the transmitted signal monitored at the transmission measurement point in Fig. 5.4a.
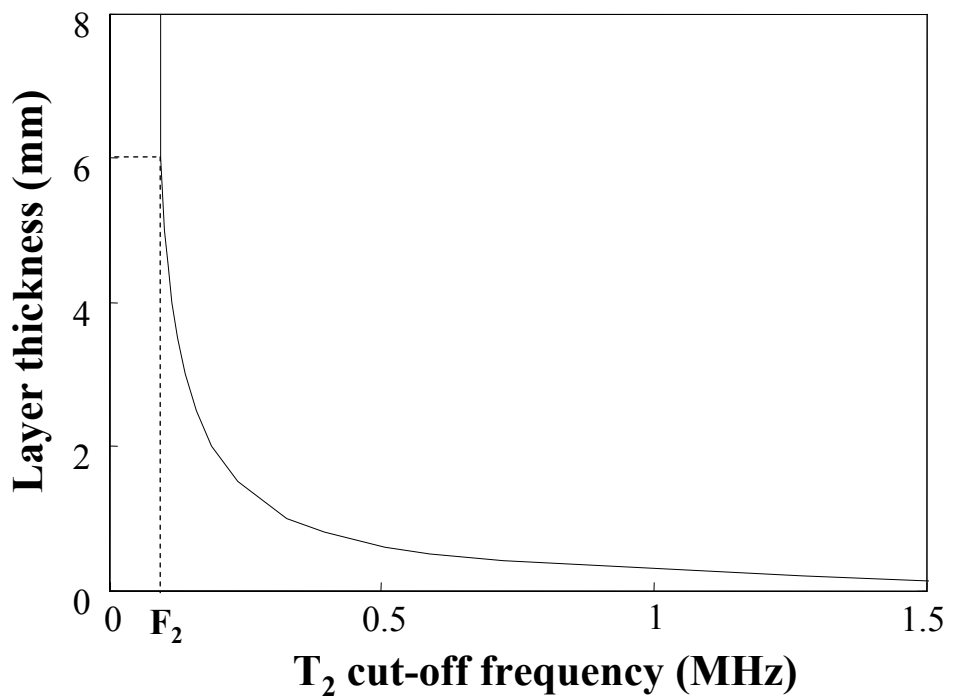
Figure 5.6: Cutoff frequency of the second torsional modes in the pipe coated with epoxy layer as a function of the thickness of the layer.
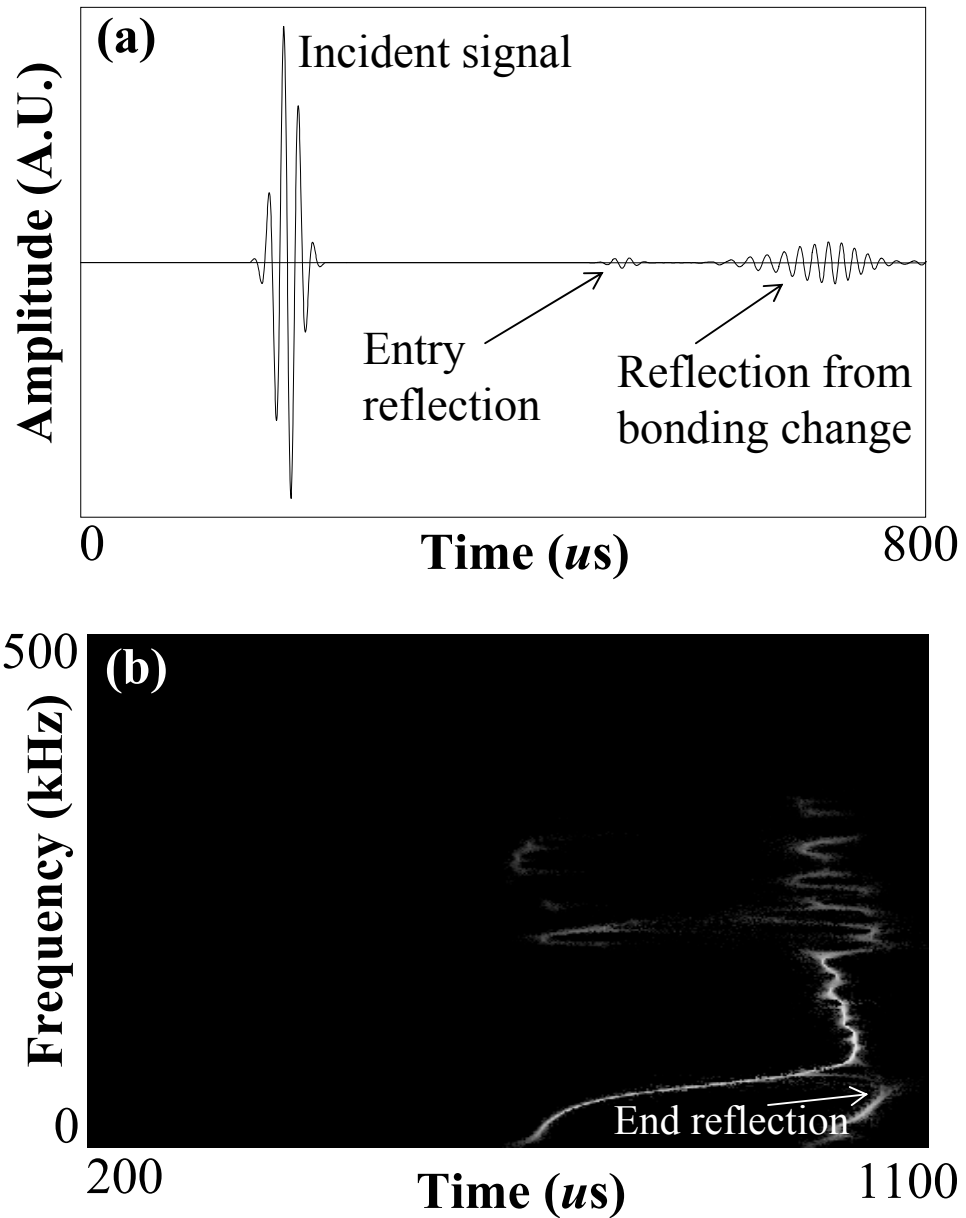
Figure 5.7: (a) Time trace of the incident and the reflection signals monitored at the reflection measurement point in Fig. 5.4b; (b) Reassigned Spectrogram analysis of the transmitted signal monitored at the transmission measurement point in Fig. 5.4b.
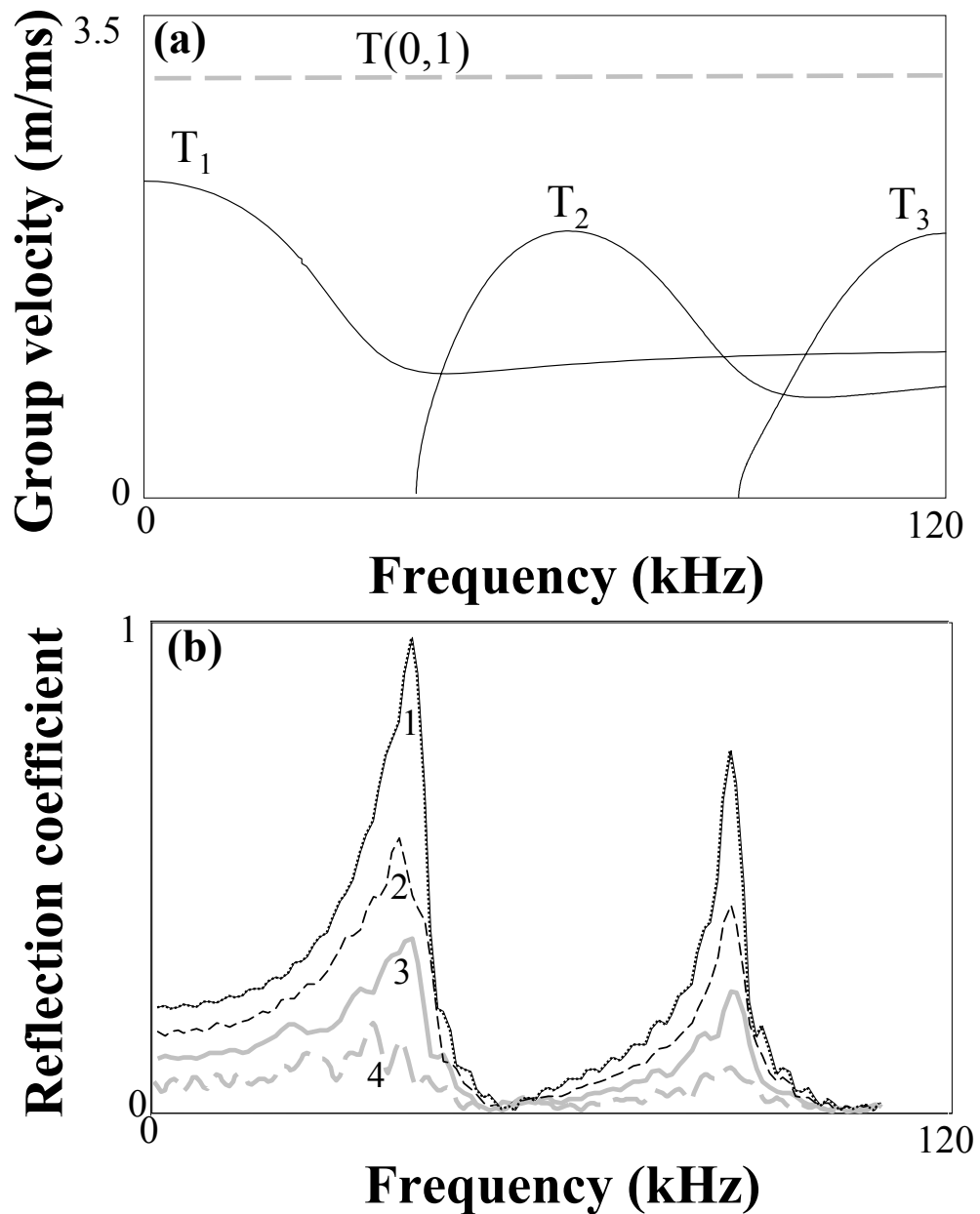
Figure 5.8: (a) Dispersion curves of the torsional modes in a 3 inch aluminium pipe coated with 10-mm thickness epoxy layer (black curves) and the T(0,1) mode in the clean 3 inch pipe (gray dashed line); (b) Reflection coefficient amplitude spectrum of the T(0,1) mode in the 3 inch aluminium pipe coated with 10-mm thickness sludge layer for different circumferential extents. Case 1: 100% (solid line: 3D model, dotted line: 2D model), Case 2: 75%, Case 3: 50%, Case 4: 25%.
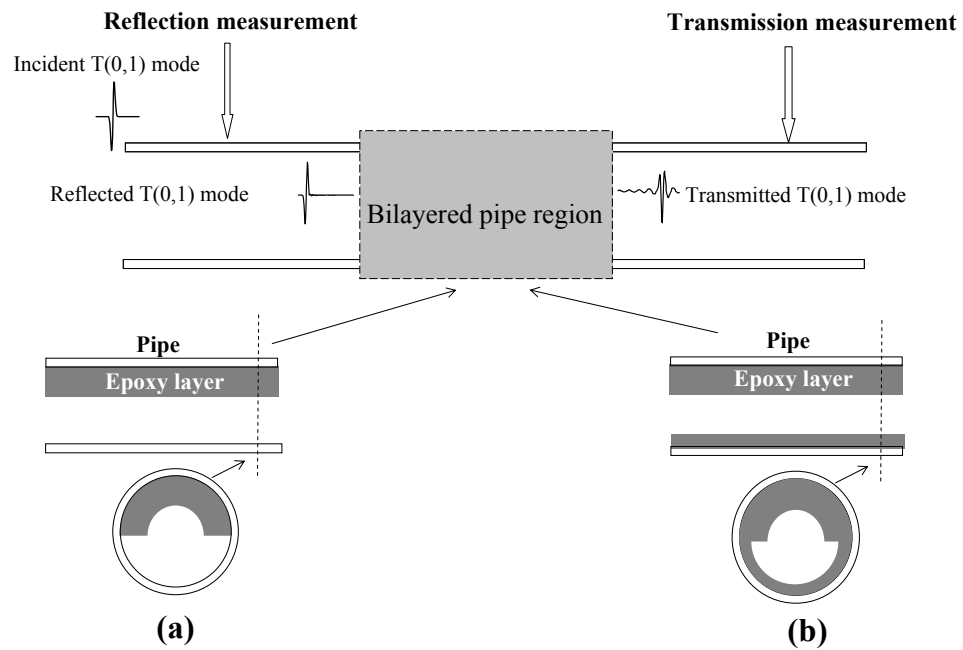
Figure 5.9: (a) Schematic of the model in which the pipe is partially coated with an epoxy layer that has 50% circumferential extent; (b) Schematic of the model in which the pipe is coated with an epoxy layer that has 10-mm thickness and 5-mm thickness, each for 50% circumferential extent.
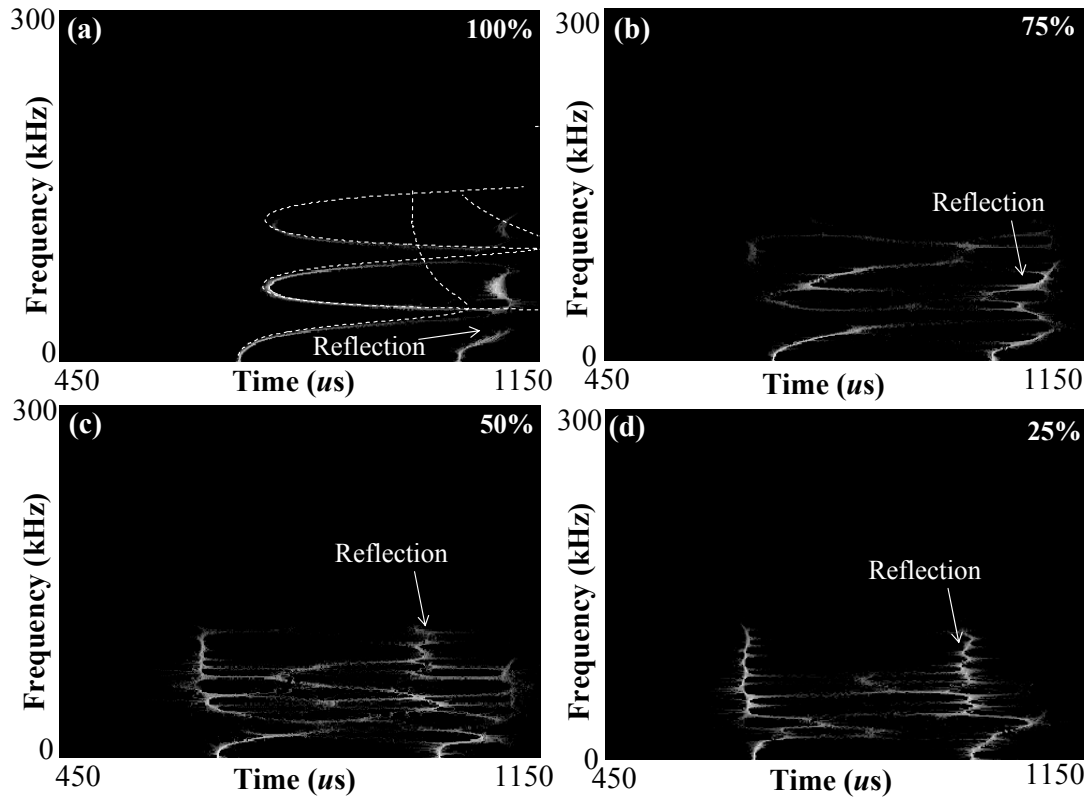
Figure 5.10: (a) Reassigned Spectrogram analysis of the transmitted T(0,1) mode in the 3 inch pipe partially coated with 10-mm thickness epoxy layer that has 100% circumferential extent and the corresponding numerical calculation with DISPERSE (white dashed curves); (b) 75% circumferential extent;(c) 50% circumferential extent ; (d) 25% circumferential extent.
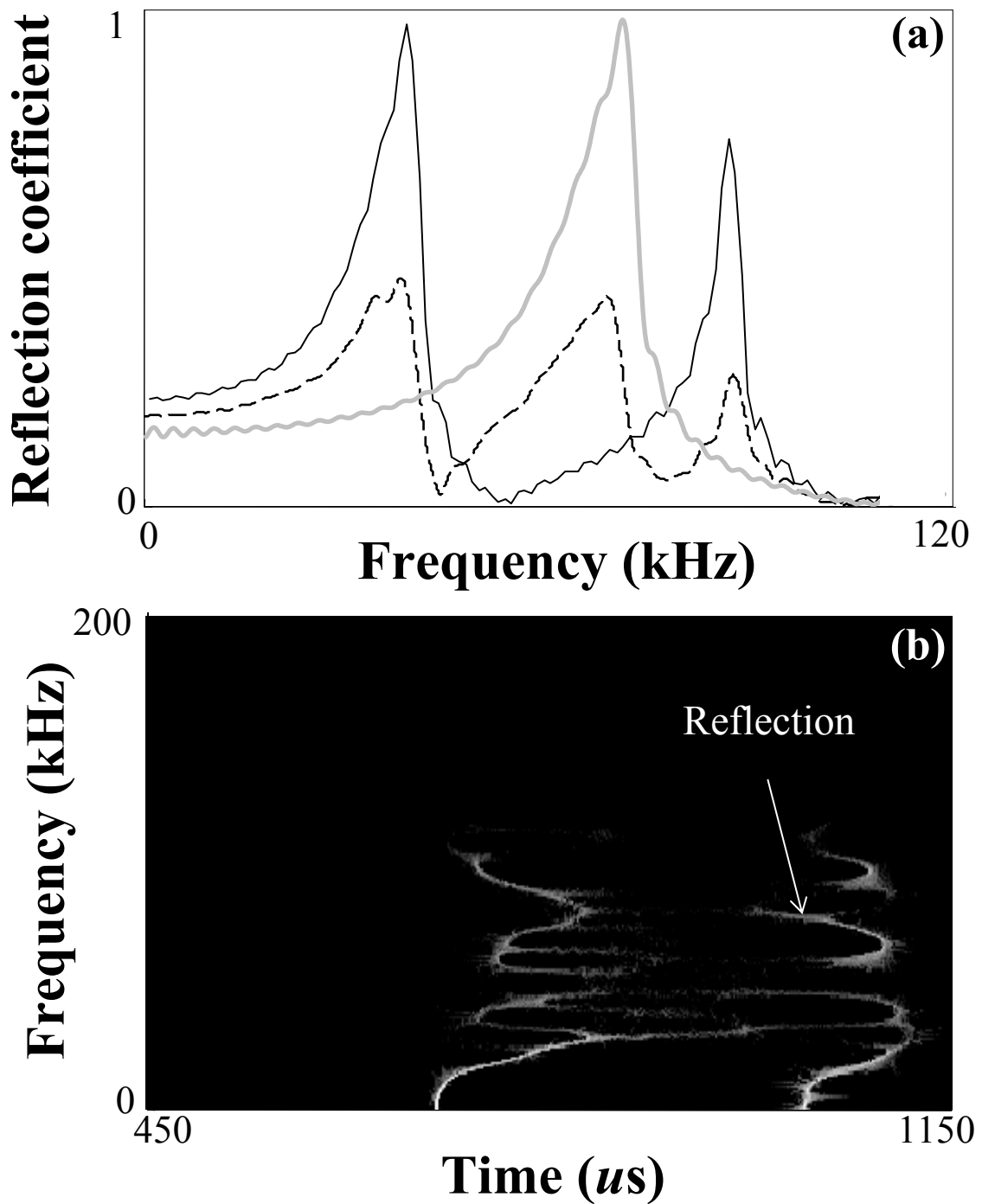
Figure 5.11: (a) Reflection coefficient amplitude spectrum of the T(0,1) mode calculated from the signals monitored at the reflection measurement point in Fig. 5.9. For comparison, reflection coefficient spectra are also calculated from two cases in which the layer respectively has 10-mm thickness for 100% circumferential extent (black solid curves) and 5-mm thickness for 100% circumferential extent (gray solid curves); (b) Reassigned Spectrogram analysis of the signals monitored at the transmission measurement point in Fig. 5.9.
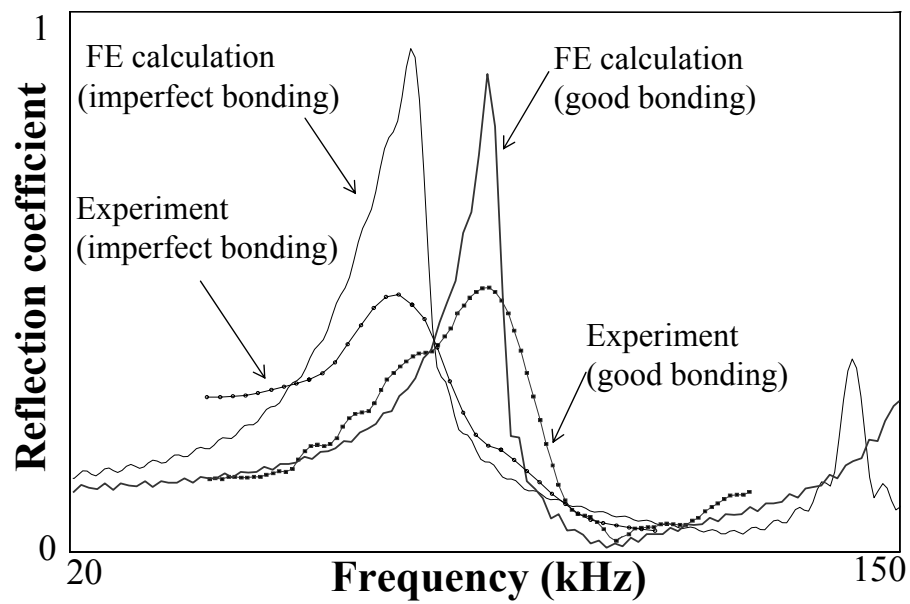
Figure 5.12: Reflection coefficient amplitude of the T(0,1) mode reflected by a 6-mm thickness epoxy layer inside an aluminium pipe. Experimental results with perfect bonding case (line with black squares) and imperfect bonding (line with circles) case. The reflection coefficient spectra amplitude from FE models for both cases are also provided for comparison (solid lines).
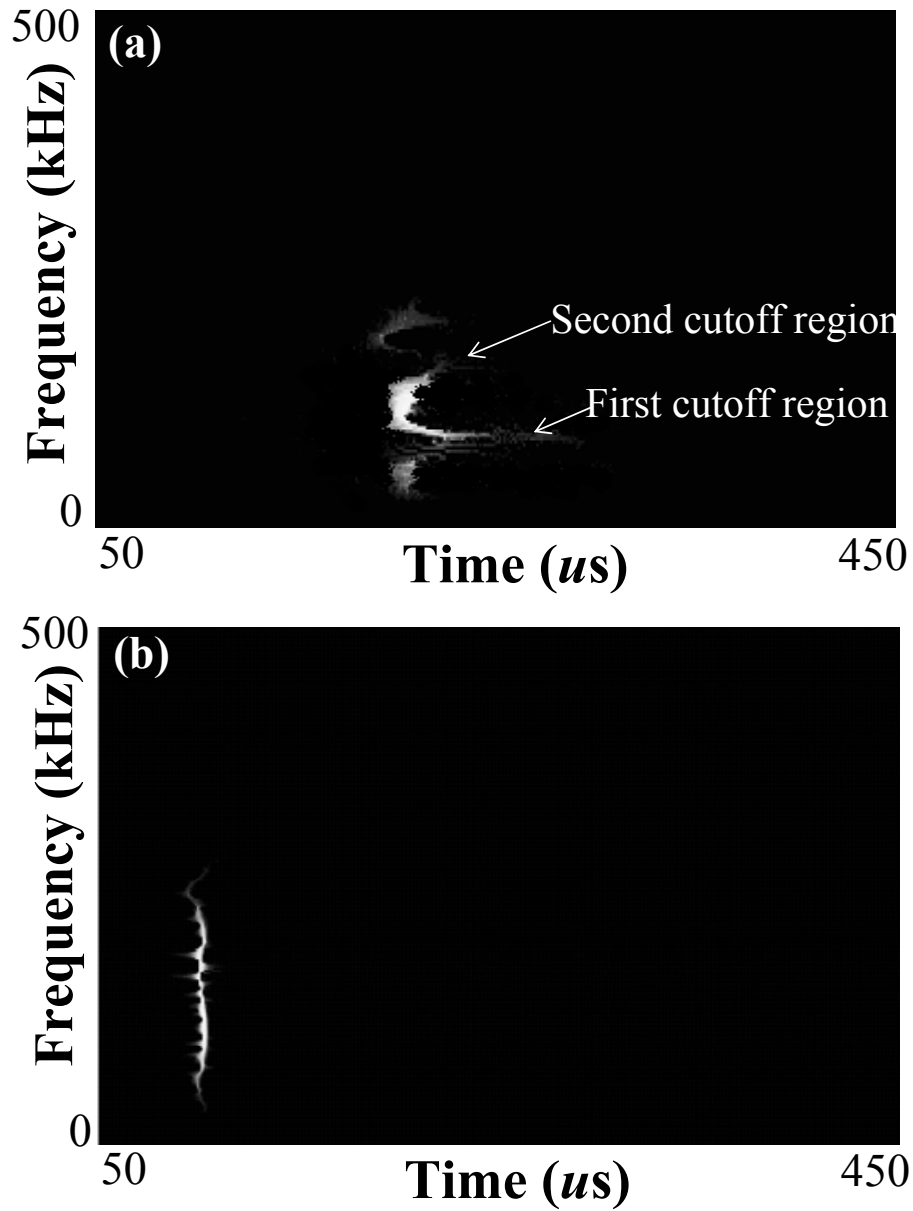
Figure 5.13: (a) Reassigned Spectrogram of the transmitted signal measured in the blocked pipe region; (b) Reassigned Spectrogram of the incident signal before the blocked pipe region.
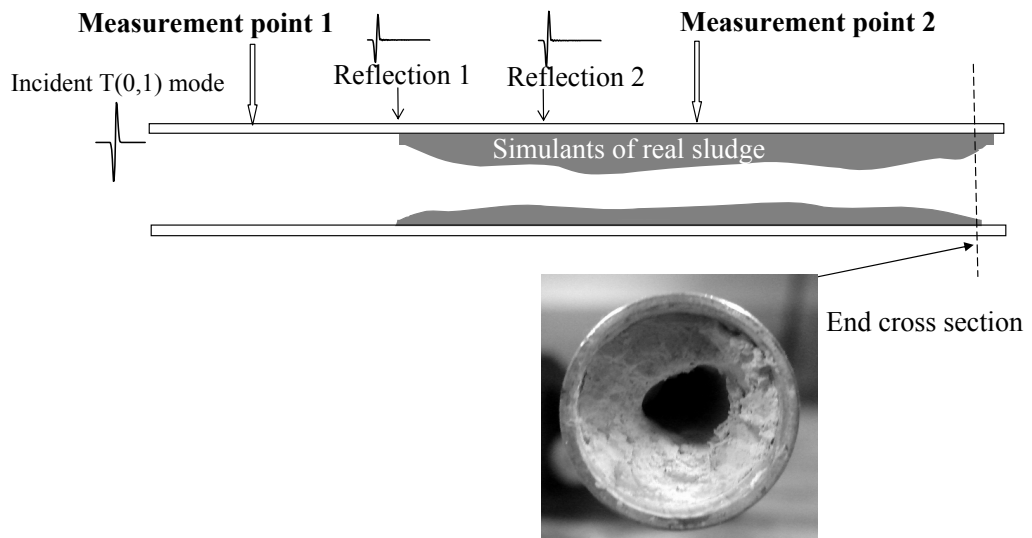
Figure 5.14: Schematic of the measurements conducted on the pipe with randomly shaped sludge layer made of simulant representing a real sludge material.
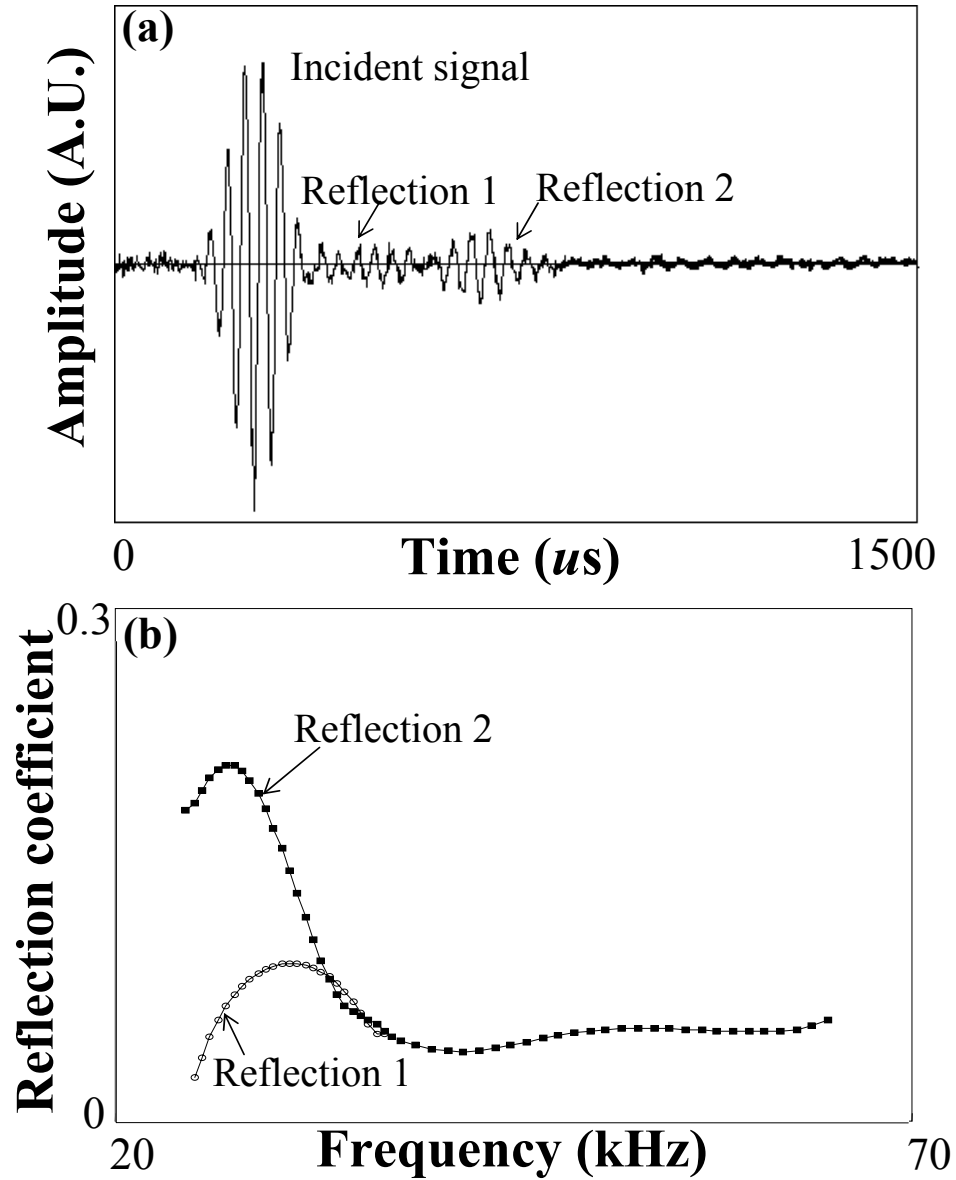
Figure 5.15: (a) Time trace showing the incident signal and the reflected signals measured at reflection measurement point in Fig. 5.14; (b) Reflection coefficient spectra magnitude of reflection 1 and reflection 2 in Fig. 5.15a.
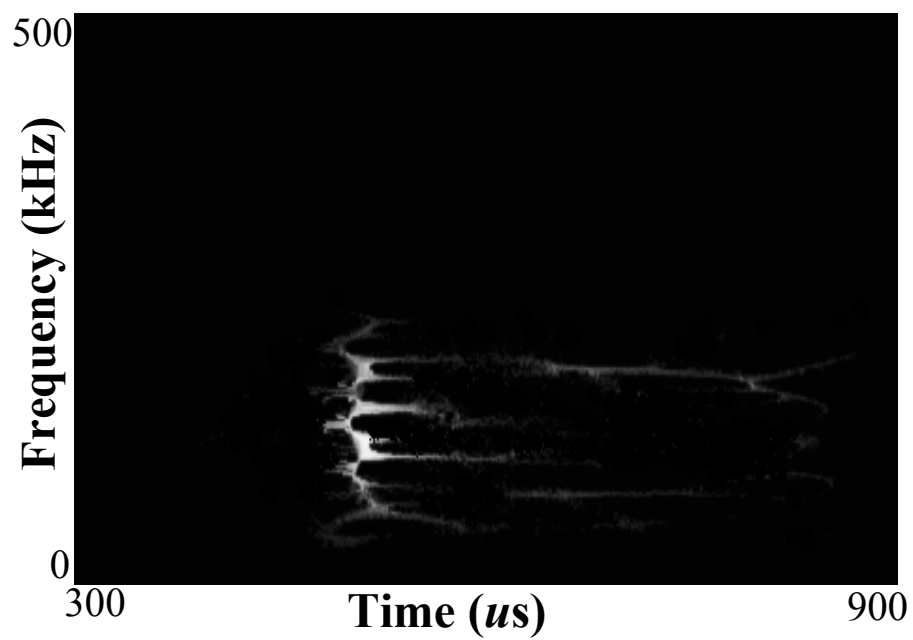
Figure 5.16: Reassigned spectrogram analysis of the local signal measured at transmission measurement point in Fig. 5.14
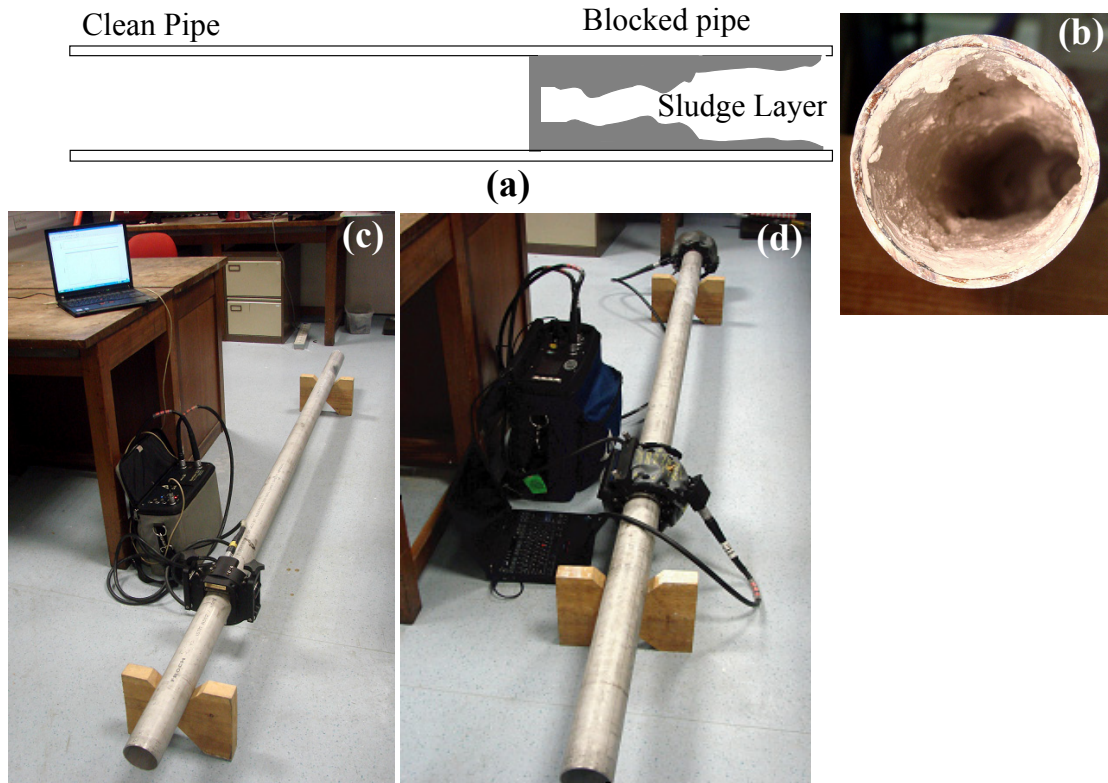
Figure 5.17: (a) Speculated axial profile of the sludge made up by the simulant of real sludge in the 3 inch steel pipe; (b) End view photography the blocked pipe with the sludge layer; (c) The setup of the reflection measurement using commercial WaveMaker Pipe Screening system to detect the sludge inside the 3.5 inch pipe; (d) The setup of the transmission measurement.

Incident signal   Incident signal

End reflection   Reflection from sludge   **Sludge Layer**   End reflection

Transducer ring

(a)

Transmission signal

Sludge Layer

Transducer ring (Receiver)   **Transducer ring (Transmitter)**

(b)
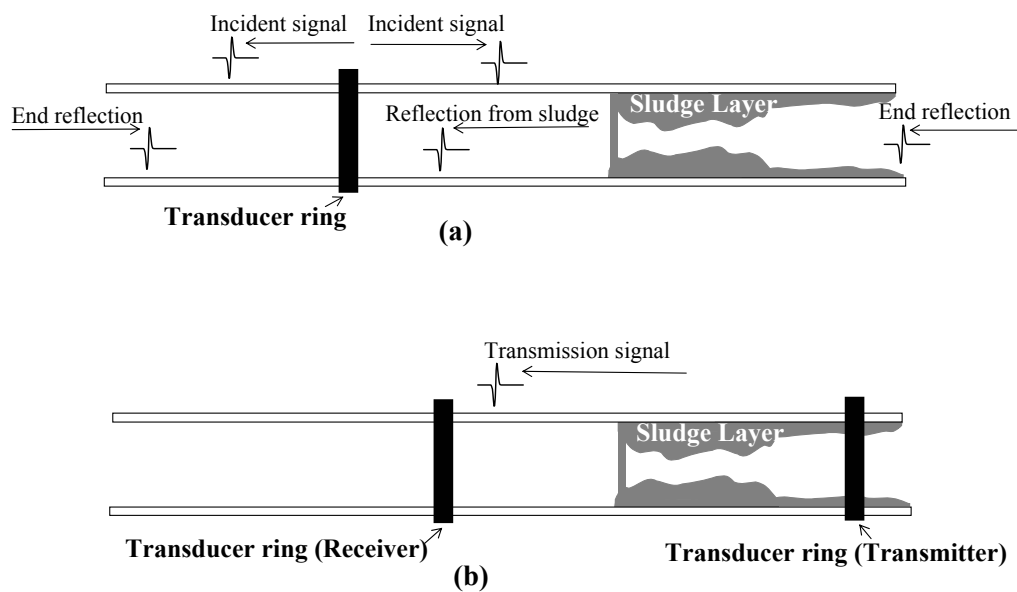
Figure 5.18: (a) Schematic of the reflection measurements conducted on a 3 inch pipe with a sludge layer made of simulant of real sludge material, using commercially available guided wave transducer rings; (b) Schematic of the transmission measurements using a pair of transducer rings.
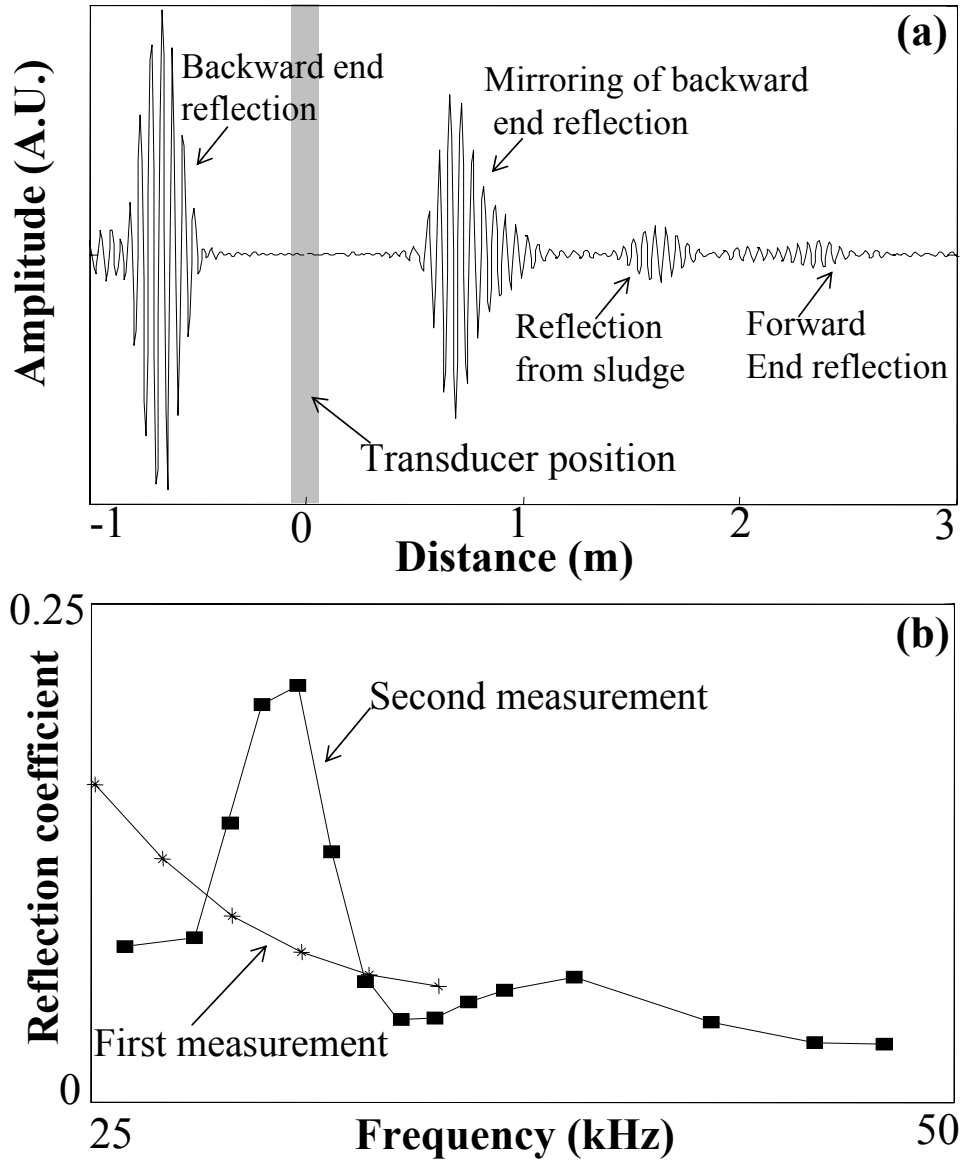
Figure 5.19: (a) Testing result of the reflection measurement conducted on the 3 inch pipe with sludge using a single commercially available guided wave transducer ring as shown in Fig. 5.18; (b) Reflection coefficient of the measured reflected T(0,1) mode from the sludge at two different times (line with stars): first measurement; (line with black squares): second measurement.
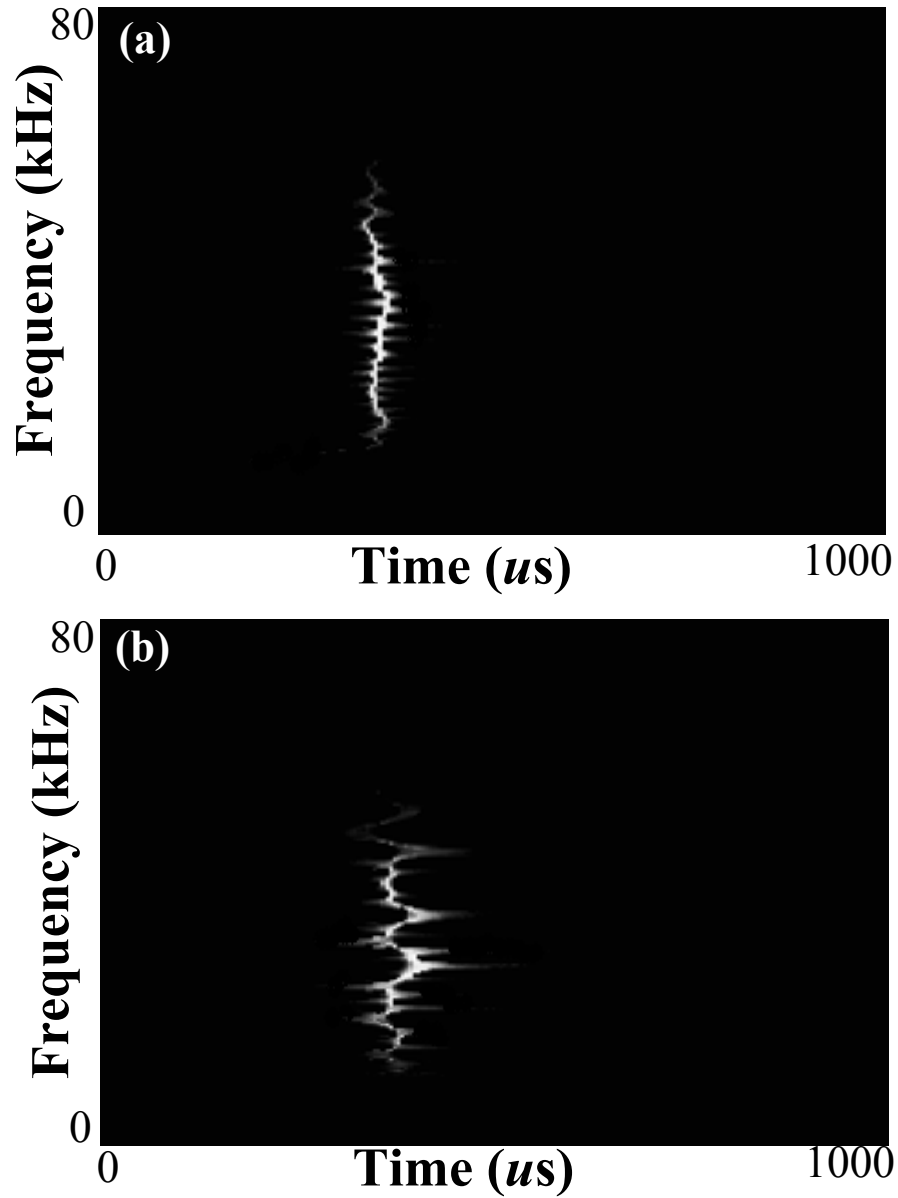
Figure 5.20: (a) Reassigned spectrogram analysis of the transmitted signal conducted on the clean part of the 3 inch pipe with sludge layer using two guided wave transducer rings; (b) as in (a) but the measurement were conducted on the blocked part of the pipe.
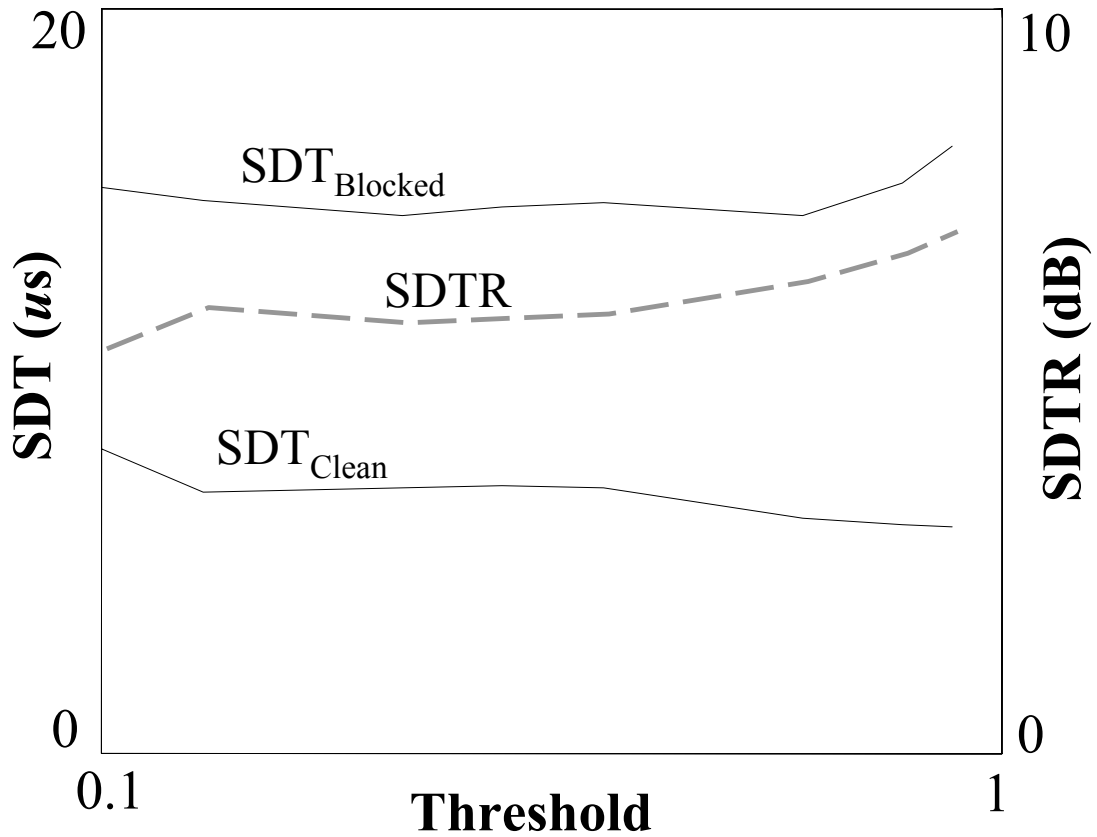
Figure 5.21: Standard deviations of arrival time (SDT) of the signals in Figs. 5.20a and b (black curves), when different values of threshold are used to extract the dispersion curves from the reassigned spectrogram. The corresponding ratio (SDTR) is also given (gray dashed curve).

Chapter 6

Feasibility of Sludge and Blockage Detection inside Pipes using Guided Longitudinal Waves

6.1 Background

Chapters 4 and 5 presented two techniques using guided torsional waves to detect and in some cases characterise sludge and blockages inside pipes. This chapter investigates the feasibility of these two approaches when using the guided longitudinal waves.

The use of longitudinal modes can be more complicated than torsional waves. Unlike the T(0,1) which is non-dispersive, the longitudinal modes can be highly or little dispersive depending on the frequency ranges and the dimension of the pipe. Therefore, the reflection and the transmission measurements can only be carried out at limited frequencies where the selected modes exhibit little dispersion. For example, Fig. 6.1a shows the group velocity dispersion curves of the longitudinal modes (labelled as L(0,1) and L(0,2)) in a clean aluminum pipe (16-mm ID, and 1-mm thickness). For such a pipe, the L(0,1) mode at low frequencies and the L(0,2) mode at high frequencies have little dispersion and therefore can be used for the measurements (indicated in Fig. 6.1a). Also, the longitudinal modes can actively interact

with the fluid inside the pipe as shown in Chapters 2 and 3. Thus the measurement using longitudinal modes can be expected to be highly complicated when fluid is present inside the pipe.

On the other hand, longitudinal waves couple through a slip interface and therefore can be more sensitive than torsional waves when the shear coupling is low.

The purpose of the study in this chapter is to assess the feasibility of an approach based on longitudinal guided waves and to compare it with the torsional wave techniques discussed in Chapters 4 and 5.

The investigation starts with the same idealised model used in Chapter 4 in which the layer is simplified in terms of geometry, material and bonding state. The dispersive characteristics of guided longitudinal modes propagating in such a bilayered pipe are presented in Sec. 6.2, followed by an analysis of the reflection and transmission techniques based on FE simulations in Sec. 6.3. The effects of irregular properties of the layer on the measurements are studied in Sec. 6.4. In Sec. 6.5, the study is expanded to discuss the case when a fluid is present inside the pipe. Experimental results are presented in Sec. 6.6. Finally, the advantages and disadvantages of the guided longitudinal wave approach versus the torsional one are discussed in Sec. 6.7.

6.2   Longitudinal Modes in the Bilayered Pipe

Let us consider an aluminium pipe (Inner diameter 16mm and thickness 1.4mm) coated with an axisymmetric epoxy layer that has uniform 5-mm thickness. Fig. 6.1a shows the group velocity dispersion curves of the longitudinal modes in such a bilayered pipe (labelled as L_1, L_2.... L_6) as well as the modes in the clean pipe (labelled as L(0,1) and L(0,2)). The material the pipe and the coating layer are summarized in Table 6.1.

Fig. 6.1a shows that the presence of the layer increases the number of the modes of the clean pipe and causes strong dispersion. For example, at low frequencies, the L_1 mode is much more dispersive than the L(0,1) mode. At high frequencies the the modes of the bilayered pipe are very complex and dispersive, unlike the L(0,2)

Table 6.1: Material properties used for DISPERSE calculations and FE simulations.

	Longitudinal velocity(m/s)	Shear velocity(m/s)	Density(kg/m^3)
Aluminium	6320	3130	2700
Epoxy	2610	1100	1170
Water	1500		1000

mode of the free pipe which has little dispersion.

The longitudinal modes in the bilayered pipe originate from the interaction between the modes of the clean pipe and those of the equivalent layer if it were rigidly clamped at the bilayer interface [52]. Therefore, the dispersion characteristics of the modes in the bilayered pipe are greatly determined by the longitudinal bulk velocity, the shear bulk velocity and the thickness of the coating layer. However, it is interesting to find that at low frequencies, the L_1 mode is little affected by the longitudinal bulk velocity of the layer, while it is only determined by the shear bulk velocity and the thickness of the layer. This is shown in Fig. 6.1b.

6.3 Scattering of the Longitudinal Modes: Idealised Model

The scattering of the longitudinal modes by the idealised layer is studied as in the case of torsional waves (shown in Fig. 4.1). Instead of using the T(0,1) mode, a longitudinal mode is incident from the free end of the pipe. At the discontinuity, the incident mode is partly reflected back into the free pipe (reflected signal), and also partly transmitted into the longitudinal modes in the bilayered pipe and then further converted back into the modes of the clean pipe after the bilayered region (transmitted signal). A 2D FE model is used to model the scattered signals of the longitudinal modes in such a structure, using the FE software ABAQUS [92]. Its details are summarized in Appendix B.1.

6.3.1 Reflection measurement

The reflection measurement uses both the L(0,1) mode and the L(0,2) mode at plateau regions on their dispersion curves. The incident and the reflected longitudinal modes from the FE simulation are monitored in the reflection measurement point in Fig. 4.1 to calculate the reflection coefficient spectrum amplitude. This is shown in case 1 of Fig. 6.2a when the L(0,1) mode is incident and Fig. 6.2b when the L(0,2) mode is incident. The behavior of the reflection coefficient spectrum amplitude can be explained by examining the energy flow distribution of guided longitudinal waves in the bilayered pipe. The parameter of energy flow ratio (EFR) is similarly defined as the ratio of the energy flow in the pipe to that in the layer and is plotted in Fig. 6.3 as a function of frequency.

When the the L(0,1) mode is incident at low frequencies, only L_1 is present in the bilayered pipe. Thus the magnitude of the reflected L(0,1) mode uniquely depends on the EFR of the L_1 mode which shows a decreasing trend until a minimum as frequency increases (Fig. 6.3). This correspondingly increases the mismatch of the energy flow mode shapes between the L(0,1) mode and the L_1 mode and therefore results in an increasing reflection. As the EFR of the L_1 mode at low frequencies is only determined by the shear bulk velocity and the thickness of the layer, the reflection coefficient spectrum amplitude also only depends on these two parameters while it is independent of the longitudinal bulk velocity of the layer. Once the reflection coefficient spectrum is experimentally measured, it is possible to obtain the thickness of the layer by a best-fitting procedure, provided that the shear bulk velocity is known, and vice versa.

The situation becomes more complex when the L(0,2) mode is incident at high frequencies where there are multiple longitudinal modes present in the bilayered pipe. The magnitude of the reflection depends on the energy flow mode shapes of all the modes present in the bilayered pipe weighed by their transmittability from the incident L(0,2) mode. The peak of the reflection coefficient spectrum amplitude in Fig. 6.2b approximately occurs at the frequency where the EFR of all the present modes in the bilayered pipe reaches a local minimum such as the one indicated as f_0 in Fig. 6.3. This frequency is now determined by the longitudinal bulk and shear velocities and the thickness of the layer.

Besides the reflected L(0,2) mode, there is also a reflected L(0,1) mode that is mode-converted from the incident L(0,2) mode at the discontinuity. However, the reflected L(0,1) mode is much weaker than the reflected L(0,2) mode. The approach to separate the L(0,1) mode with the L(0,2) mode in FE simulation is described in Appendix B.1.

6.3.2 Transmission measurement

The transmission measurement reconstructs the layer-induced dispersion from the transmitted longitudinal modes. A broadband longitudinal excitation (100 kHz central frequency with 2 cycles) is applied at one end of the clean pipe in its axial-direction. At low frequencies, L(0,1) is the only mode to be generated and at higher frequencies, the L(0,2) mode is dominantly excited compared to the L(0,1) mode due to the match of its mode shape displacement with the excitation. This can be seen in Fig. 6.4a, the reassigned spectrogram of the FE simulated signals monitored at the transmission measurement point in Fig. 4.1 for the clean pipe.

The transmitted longitudinal modes propagating past the bilayered pipe is monitored at the transmission measurement point in Fig. 4.1 and its reassigned spectrogram analysis is shown in Fig. 6.4b. The numerical calculation is obtained with DISPERSE showing excellent agreement. The presence of the layer changes the dispersion of the transmitted longitudinal modes. The most dramatic dispersion change occurs for the L(0,2) mode, which has little dispersion after its cutoff region in the clean pipe as shown in Fig. 6.4a. The change of dispersion depends on the four parameters of the layer: the longitudinal and shear bulk velocities, the thickness and the length; however, for the transmitted L(0,1) mode, the longitudinal bulk velocity does not effect the dispersion. It should be noted that there is a spike on the dispersion curves calculated by DISPERSE. This is due to the intersection of two neighboring modes and their velocities reach a local minima at a very narrow frequency range. However, the reassigned spectrogram cannot represent this frequency range due to the resolution limit.

6.4 Irregular Properties of the Layer

The effects of irregular properties of the layer on the reflection and transmission measurements are also studied. A 2D model was used with the FE software ABAQUS to study the case in which the layer has an irregular axial profile, but an axisymmetric circumferential profile. The details of the models are outlined in Appendix B. The dimensions and the material properties of the pipe and the layer used in the model are the same as those used in the idealised model and are listed in Table 6.1.

6.4.1 Imperfect bonding state

The effect of the bonding state is also simulated by inserting a spring layer between the pipe and the layer consisting of one spring perpendicular to the bilayer interface with compressional stiffness K_N and another along the interface in the axial direction with shear stiffness K_T. The decreasing of bonding is simulated by reducing both stiffnesses. More details of the model can be found in Appendix B.2.

The effects of the imperfect bonding on the reflection coefficient spectrum amplitude (calculated from the FE simulated signals monitored at the reflection measurement point in Fig. 5.1) are respectively shown in Fig. 6.2a for the cases of the L(0,1) mode incident and Fig. 6.2b for the case of the L(0,2) mode incident. At low frequencies when the L(0,1) mode is incident, the imperfect bonding just shifts the peak positions of the reflection coefficient amplitude spectrum towards lower frequencies. The similar effect is observed when L(0,2) is incident. It is also clear that the poor bonding state significantly reduces the magnitude of the reflection at high frequencies.

The reassigned spectrogram analysis of the FE simulated transmitted signals from an imperfectly bonded bilayered pipe (case 2: $K_T = 0.71 GPa/mm$) is shown in Fig. 6.5, as well as the numerical calculation by DISPERSE (dashed curves). Compared to Fig. 6.4b (perfect bonding case), it shows that the the bonding also changes the dispersion of the transmitted longitudinal modes.

An extreme condition of the imperfect bonding, commonly referred to as 'slip bond-

ing' [94], is also considered here. For such a bonding, the compressional stiffness of the spring layer K_N approaches infinity and the shear stiffness K_T approaches zero. So the energy coupling between the pipe and the layer is mainly through the radial displacement of a guided wave mode. In this case, torsional modes would be insensitive to the presence of the layer.

The dispersion curves of the longitudinal modes in the bilayered pipe with a slip bonding are shown in Fig. 6.6a (calculated with DISPERSE). The modes in the clean pipe are also given for comparison.

Fig. 6.7a shows a time-trace signal of the reflection measurement, when the L(0,1) mode is incident at low frequencies (50 kHz central frequency with 5 cycles). The slip bonding is assumed between the pipe and the layer. It shows that there is little signal reflected by the layer. This is due to the fact that at low frequencies, the L_1 mode has dominant axial displacement compared to the radial displacement. This is shown in Fig. 6.6b. The energy of the mode is coupled into the layer only thorough its radial displacement. Therefore, the energy flow mode shape of the L_1 mode is predominantly in the pipe wall matching well the incident L(0,1) mode and no strong reflection can occur.

The reassigned spectrogram analysis of the transmitted longitudinal modes from the bilayered pipe with the slip bonding is shown in Fig. 6.6b. The transmission measurement is still capable to reveal the layer-induced dispersion on the transmitted signals for the slip bonding. The comparison with numerical calculations by DISPERSE (dashed curves) shows a very good agreement.

6.4.2 Varying thickness and bonding state

The effects of varying thickness and bonding state are also studied. The details of this model can be found in Appendix B.3.

Fig. 6.8 shows FE simulated time-trace signals of the reflection measurement when the L(0,1) mode is incident at low frequencies (50 kHz central frequency with 5 cycles). In the case of Fig. 6.8a, the layer has a gentle change of thickness and consistent perfect bonding (shown in Fig. 5.4a); while in the case of Fig. 6.8b, the

layer has the same change of thickness but an abrupt change of bonding in the middle of the tapered bilayered pipe region (shown in Fig. 5.4b). The smooth change of thickness of the layer considerably reduces the strength of the reflection by the layer, but the abrupt change of bonding state can still result in large reflections.

Correspondingly, the FE simulated transmitted signals monitored at the transmission measurement points in the two models are processed by the reassigned spectrogram. Fig. 6.9a shows that the very gentle change of thickness of the layer delays the frequencies which are above the first cutoff frequency of the longitudinal mode in the uniform part of the bilayered pipe. The layer-induced dispersion therefore can be revealed from the transmitted L(0,1) mode when comparing the reconstructed spectrum with dispersion of the L(0,1) mode when the layer is not present (white dashed curve calculated with DISPERSE). The interpretation of such phenomena can follow the one given in Chapter 5 for the case of the torsional modes. When the layer has varying thickness and inconsistent bonding, the transmitted longitudinal modes show complex dispersion as shown in Fig. 6.9b.

6.5   Presence of Fluid inside the Pipe

It has been discussed in Chapter 5 that the presence of inviscid fluid inside the pipe has no influence on the proposed two measurements when using the guided torsional waves. However, such fluids can significantly complicate the same measurements when using the longitudinal waves. It has been shown in Chapters 2 and 3 that the longitudinal modes can actively interact with the fluid and behave differently from the modes in the clean pipe.

The model used to study the effect of fluid is illustrated in Fig. 6.10. The pipe and the layer are modelled to be the same as those in Sec 6.3; additionally, the pipe is filled with water. The region of pipe filled with fluid is denoted as 'water-filled pipe' and the region when the layer is present is termed as 'water-layer pipe'. The group velocity dispersion curves of the longitudinal modes in the water-filled pipe (labeled as L_1^w, L_2^w, L_3^w and L_4^w) and modes in the water-layer pipe (labeled as L_1^{w-l}, L_2^{w-l}....L_6^{w-l}) are shown in Fig 6.11. The material properties of the pipe, water and

the layer are summarized in Table 6.1.

The dispersion curves of the longitudinal modes in the water-filled pipe exhibit plateau regions and branching regions as observed in Chapters 2 and 3. Due to these dispersion characteristics, the reflection measurement can only be carried out at the plateau regions of each mode, where the mode exhibits little dispersion. For example, Fig. 6.12 shows time-trace signals monitored at the reflection measurement point in Fig. 6.10, when the plateau regions of the L_1^w mode and the L_4^w mode are individually chosen as the incident mode (see dashed loops in Fig 6.11). The magnitude of the reflection by the layer depends on the extent of the mismatch of the energy flow mode shapes between the incident water-filled pipe modes (at plateau region, the mode shape is dominant in the pipe wall) and the modes in the water-layer pipe.

The transmission measurement uses a broadband excitation (100 kHz central frequency with 2 cycles) to generate the modes in the water-filled pipe, and the transmitted signal is monitored at the transmission measurement point in Fig. 6.10.

Assuming that at each frequency, one mode in the water-filled pipe is dominantly present, the transmitted signals in Fig. 6.10 can be expressed as

$$U(\omega) = U_0(\omega)e^{ik_w(L-l)} \sum_{J=1}^{N(\omega)} T_J^{wl}(\omega)T_J^{lw}(\omega)e^{ik_{J(w-l)}l}, \tag{6.1}$$

where, U_0 is the amplitude of the excitation signal, ω is the angular frequency and $N(\omega)$ is the number of longitudinal modes in the water-layer pipe at the frequency ω. $k_w = \frac{\omega}{C_w(\omega)}$, $k_{J(w-l)} = \frac{\omega}{C_{J(w-l)}(\omega)}$. $C_w(\omega)$, $C_{J(w-l)}(\omega)$ are the phase velocity of the modes propagating in the water-filled pipe, and in the water-layer pipe respectively. $T_J^{wl}(\omega)$ is the transmission coefficient from the incident water-filled pipe mode into the Jth water-layer pipe mode, whereas $T_J^{lw}(\omega)$ is the transmission coefficient from the Jth water-layer pipe mode to the transmitted water-filled pipe mode. L denotes the total length between the transmitter and the receiver and l is the length of the water-layer pipe region.

As the modes in both the water-filled pipe and the water-layer pipe are dispersive,

the dispersion of the transmitted signal depends on the factor $e^{ik_{J(w-l)}l}$ in the water-layer pipe and the factor $e^{ik_w(L-l)}$ in the water-filled pipe. To identify the dispersion change induced by the layer, a ratio $\frac{L-l}{l}$, the length of the unblocked region between the transmitter and receiver to that of the blocked region plays an important role. When the ratio is small, the change of dispersion due to the layer can be clearly identified from the transmitted signal. This is shown in Fig. 6.13a, which is the reassigned spectrogram analysis of the transmitted signal when the length of the water-filled region is 3 times that of the water-layer region. The numerical calculation is provided by DISPERSE showing excellent agreement.

However, when $\frac{L-l}{l}$ is large, the dispersion change due to the layer is too subtle to be appreciated from the transmitted signal. This is shown in Fig. 6.13b, the reassigned spectrogram of the transmitted signal monitored in Fig. 6.10 when the length of the water-filled region is 10 times that of the water-layer region. The represented dispersion curves of the transmitted signal are very close to those of the water-filled modes. This implies that the capability of remote detection by the transmission measurement is impaired by the presence of the water when using the guided longitudinal waves.

6.6   Experiments

Experiments have also been carried out to demonstrate the use of the longitudinal modes. The experimental setup is illustrated in Fig. 6.14 and is similar to the one used for the torsional mode experiment; however, different excitation and receiving methods are used. In order to generate longitudinal modes, a commercial longitudinal transducer (Panametrics, 200 kHz central frequency) is fixed at one end of the pipe by a transducer holder to generate longitudinal vibration in the axial direction of the pipe. The axial displacements of the modes propagating in the pipe is received by focusing the two beams at 30° with respect to the radial direction and by orienting the beams in the plane parallel to the axis of the pipe. Waveforms were sampled at eight equally spaced points around the circumference of the pipe at the same axial location. By adding the eight sampled waveforms, the flexural modes can be cancelled by circumferential averaging.

The sample of pipe consists of a 1.6-m long aluminum pipe (14-mm inner diameter and 1-mm wall thickness), 0.25m of which contains an epoxy circular tube of 14-mm external diameter starting from one end of the pipe. The epoxy tube is manufactured to be axisymmetric, but has a varying thickness along the pipe axis. It is tapered at both ends for 0.075 m, but keeps a uniform thickness in the middle part (5-mm thickness) for 0.1 m. The tube was press-fitted inside the pipe, so its bonding with the pipe wall is imperfect. The epoxy resin employed is the Araldite 2020, whose acoustic properties were listed in Table 4.2.

The reflection measurement has been carried out at the clean pipe region 0.68m away from the start of the epoxy tube. Both L(0,1) mode and L(0,2) mode are used as the incident mode. Fig. 6.15a shows the the measured reflection coefficient amplitude spectrum from the sample when the L(0,1) mode at low frequencies is incident. The strong reflection from a layer with tapered interface is anomalous. However by closely examining the arrival time of the reflected signal, it was found that the reflected signal actually occurs at a position 0.1m away from the start of the epoxy tube which is in the uniform part of the layer. This implies that the contact between the layer and the pipe is inconsistent along the layer.

Fig. 6.15b shows a time-trace signal monitored at the same position when the L(0,2) mode (180 kHz central with 10 cycles) is incident. Little reflection from the the epoxy layer can be measured. This confirms the FE predictions that the the imperfect bonding significantly reduces the magnitude of the reflections at high frequencies.

The principle of the transmission measurement is demonstrated by a local measurement. A broadband longitudinal excitation is used (250 kHz central frequency with 2 cycles) and the local signal is measured on the layered part of the pipe, 0.12m away from where the layer starts in the pipe. The reassigned spectrogram analysis of the measured local signal is shown in Fig. 6.16a. The reassigned spectrogram analysis of the incident longitudinal modes measured in the clean part of the pipe is also given in Fig. 6.16b. The dispersion changes on both the L(0,1) mode and the L(0,2) mode induced by the layer can be clearly identified.

6.7 Conclusions

This Chapter has investigated the feasibility of using guided longitudinal waves to detect and characterise sludge and blockages inside pipes. It is a generalization of the two techniques developed in Chapters 4 and 5 which used guided torsional waves.

It has been shown through the FE simulations and experiments that both reflection and the transmission measurements can employ guided longitudinal waves to detect presence of the sludge and blockages inside pipes, although characterisation is difficult. Both measurements need to be carried out at suitable frequency ranges on the dispersion curves of the chosen longitudinal modes, where they exhibit little dispersion.

An advantage of using guided longitudinal waves is that they can interact with the layer through both the normal and the shear stiffnesses of the interface. Therefore, techniques using longitudinal modes are more likely to lead to a successful detection when the bonding interface has small shear stiffness, such as in the case of slip bonding.

On the other hand, compared to the measurements based on torsional waves, the longitudinal waves can only be used in limited frequency ranges where the modes have little dispersion. This reduces the possibility of detection. However, this problem is less severe for larger pipes in which the L(0,2) mode has little dispersion in the most commonly used frequency range (20 kHz to 70 kHz) for practical tests.

The presence of fluid inside the pipe severely affects the measurement using the longitudinal modes. For example, the test frequency range for the reflection measurement is further limited and the remote detection capability of the transmission measurement is significantly impaired. Therefore, for such situation, torsional waves should be used instead of longitudinal waves.
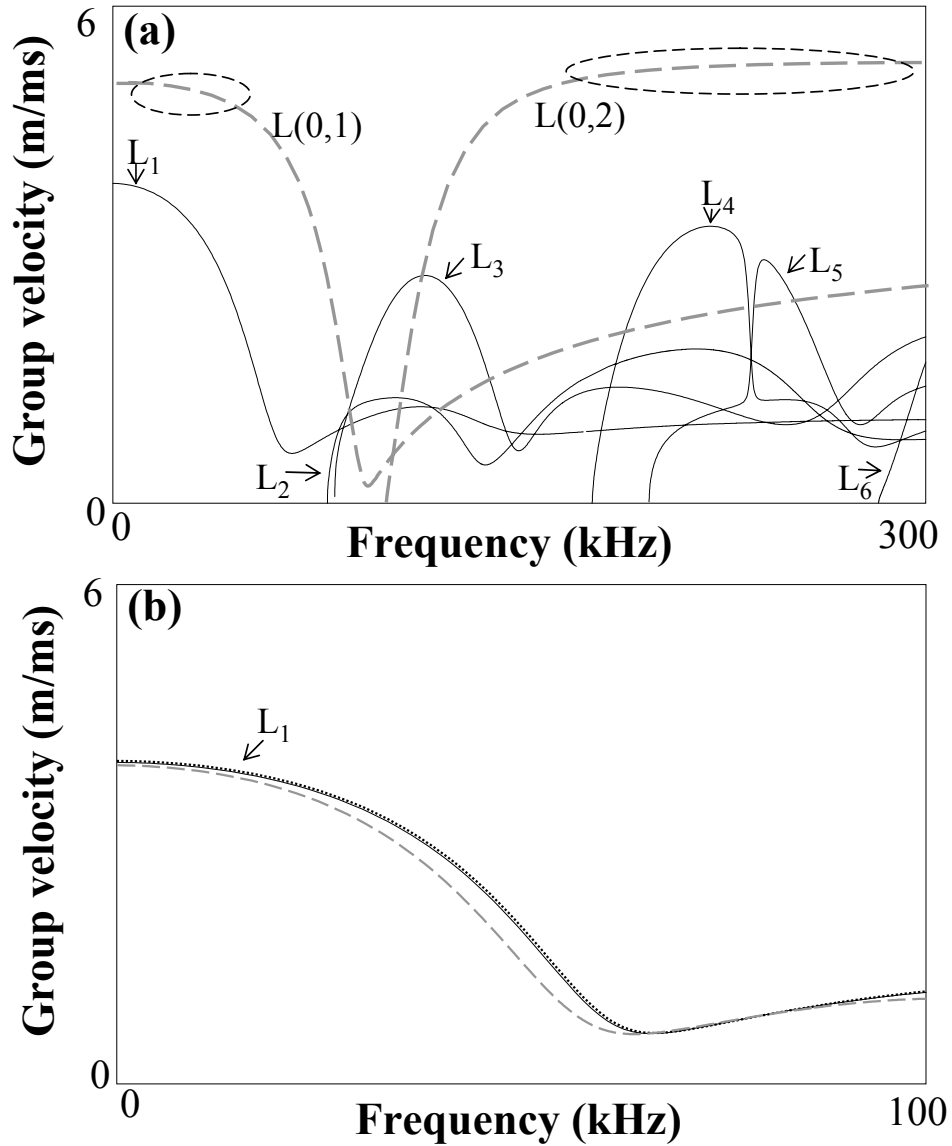
Figure 6.1: (a) Group velocity dispersion curves of the longitudinal modes in an aluminum pipe (Inner diameter 16mm and thickness 1.4mm) coated with a 5-mm thickness epoxy layer inside (black solid curves). For comparison, the longitudinal modes in a pipe without coating are also shown (dashed curves). Material properties are given in Table 6.1. (b) Dispersion curves of the L_1 mode for different bulk velocities. Bulk longitudinal velocity $C_l = 2610m/s$ and bulk shear velocity $C_s = 1100m/s$ (black solid curve); $C_l = 2610m/s$ and $C_s = 1000m/s$ (gray dashed curve); $C_l = 4000m/s$ and $C_s = 1100m/s$ (black dotted curve).
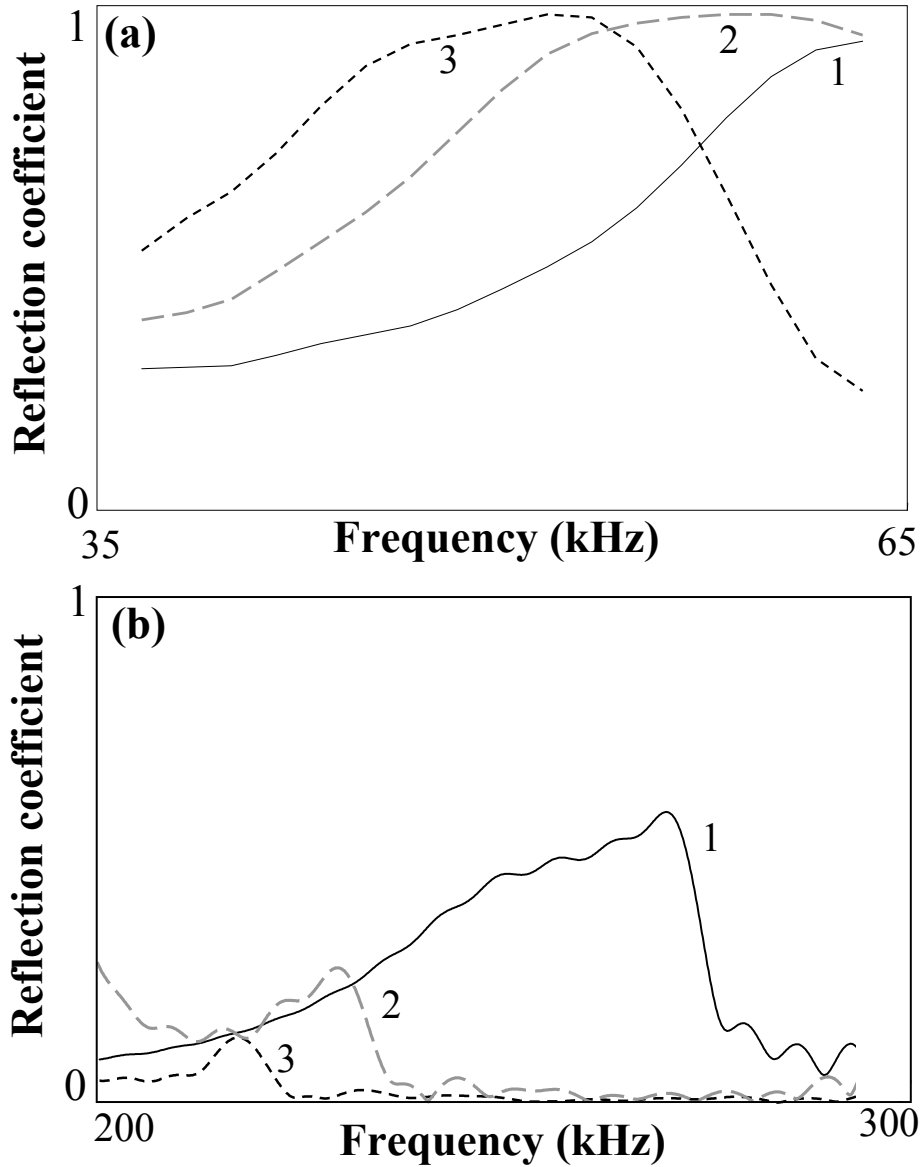
Figure 6.2: (a) Reflection coefficient spectrum obtained from FE simulations, when the L(0,1) mode is incident at the region where the pipe is locally coated with 5-mm thickness epoxy layer, for different bonding states. Case 1: Perfect bonding ; Case 2: $K_N = 5 GPa/mm$, $K_T = 1.4 GPa/mm$; Case 3: $K_N = 2.5 GPa/mm$, $K_T = 0.7 GPa/mm$. (b) As a, but for the case when the L(0,2) mode is incident.
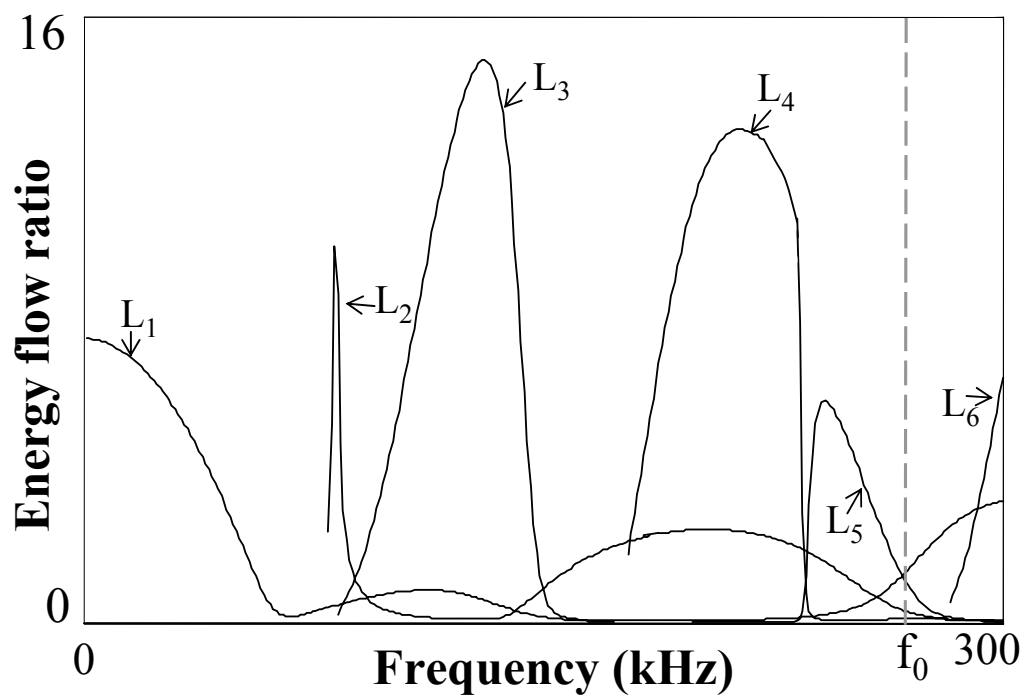
Figure 6.3: (a) Energy flow ratio (FER) of the longitudinal modes in Fig. 6.1a.
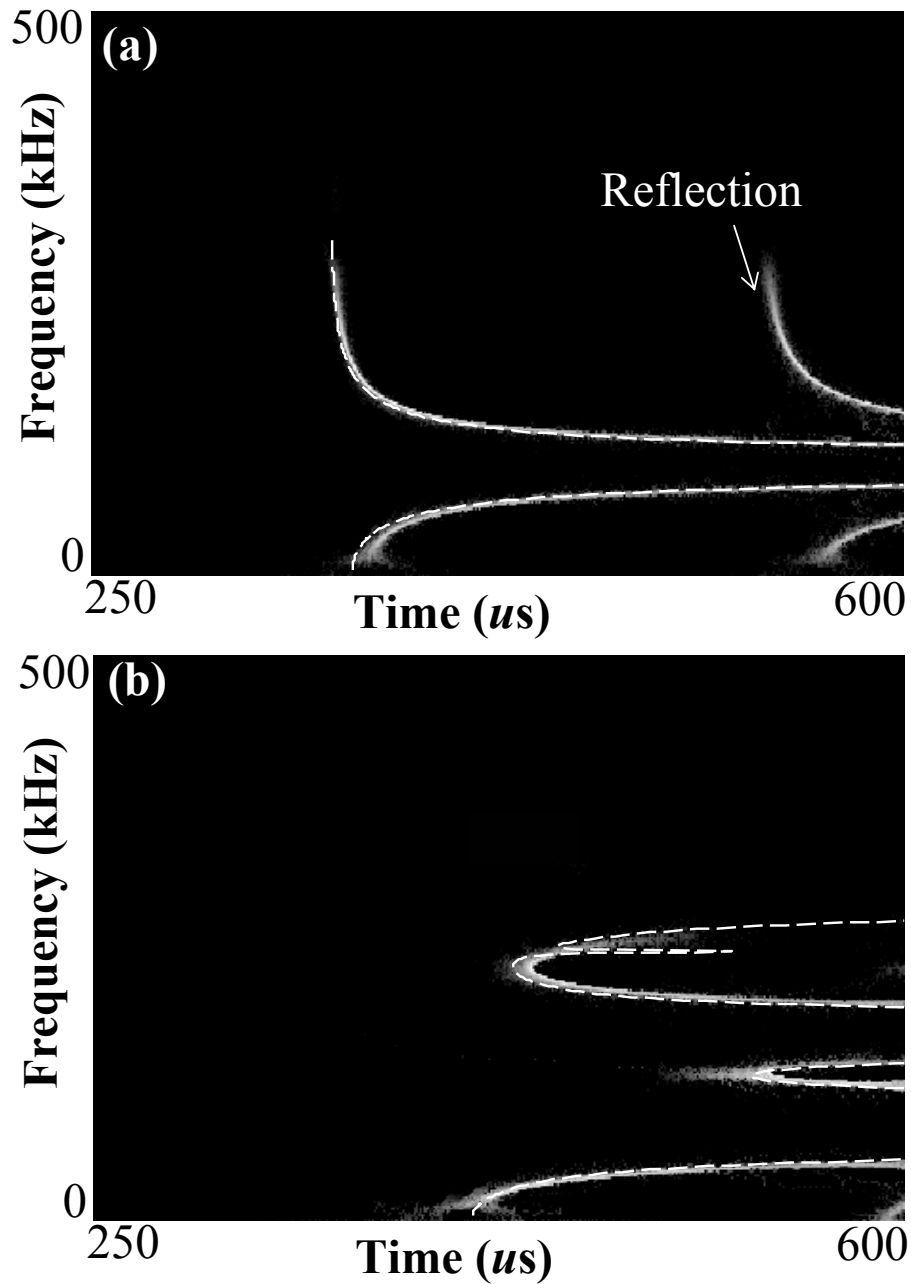
Figure 6.4: (a) Reassigned spectrogram analysis of the FE simulated transmitted signals monitored at the transmission measurement point in Fig. 4.1, assuming the layer is not present. (b) Reassigned spectrogram analysis of the FE simulated transmitted signals monitored at the transmission measurement point in Fig. 4.1. The comparisons with numerical calculations (white dashed curves) is provided by DISPERSE.
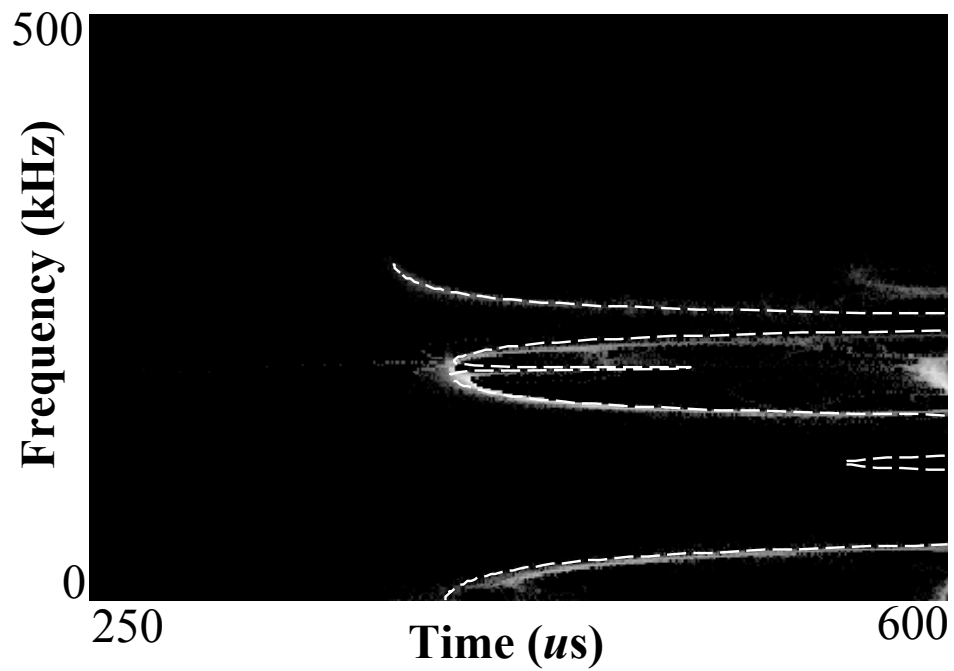
Figure 6.5: Reassigned spectrogram analysis of the FE simulated transmitted signals of longitudinal modes monitored at the transmission measurement point in Fig. 5.1 ($K_N = 5GPa/mm$, $K_T = 1.4GPa/mm$) and the corresponding numerical calculation with DISPERSE (white dashed curves).
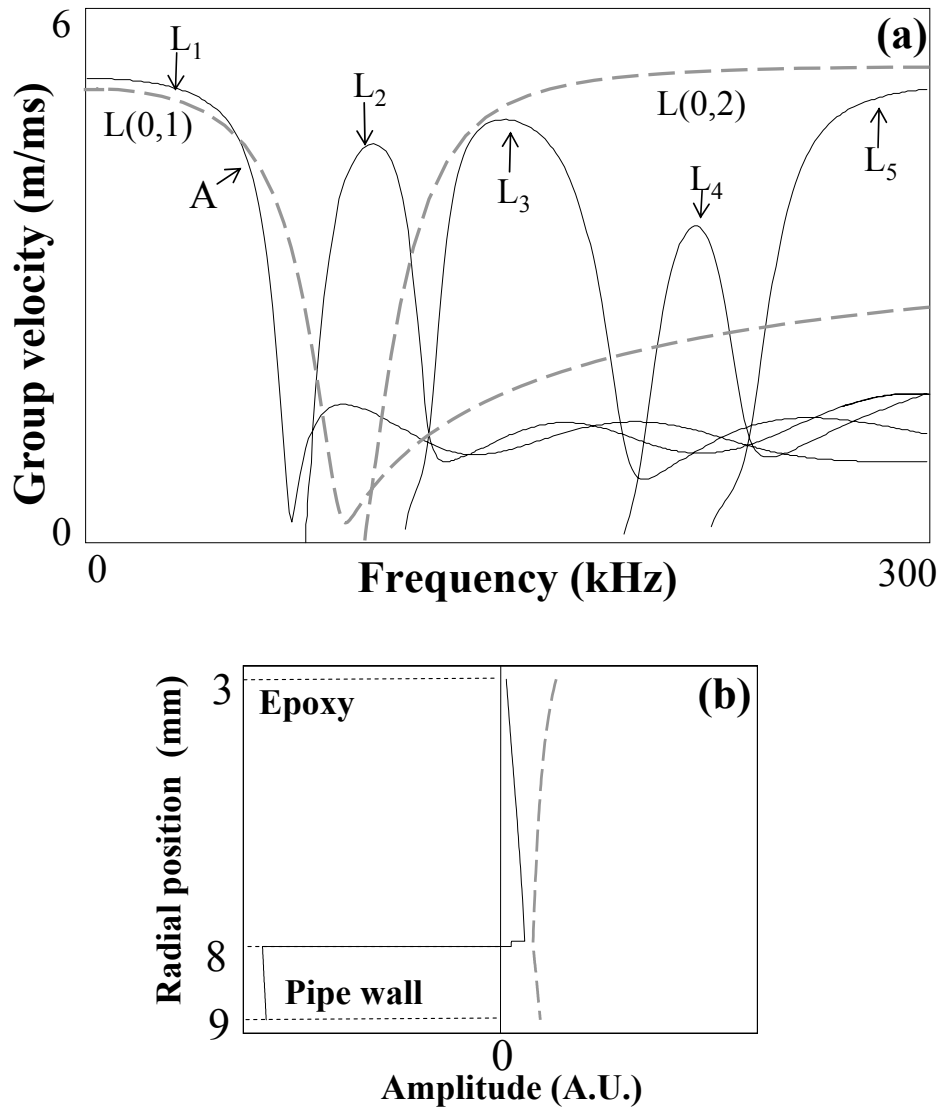
Figure 6.6: (a) Group velocity dispersion curves of the longitudinal modes (black solid curves) in an aluminum pipe coated with a 5-mm thickness epoxy layer inside. A slip bonding is assumed at the bilayer interface. The modes in the corresponding free pipe are also given (gray dashed curves); (b) Displacement mode shape at point A (solid line) axial displacement; (dashed line) radial displacement.
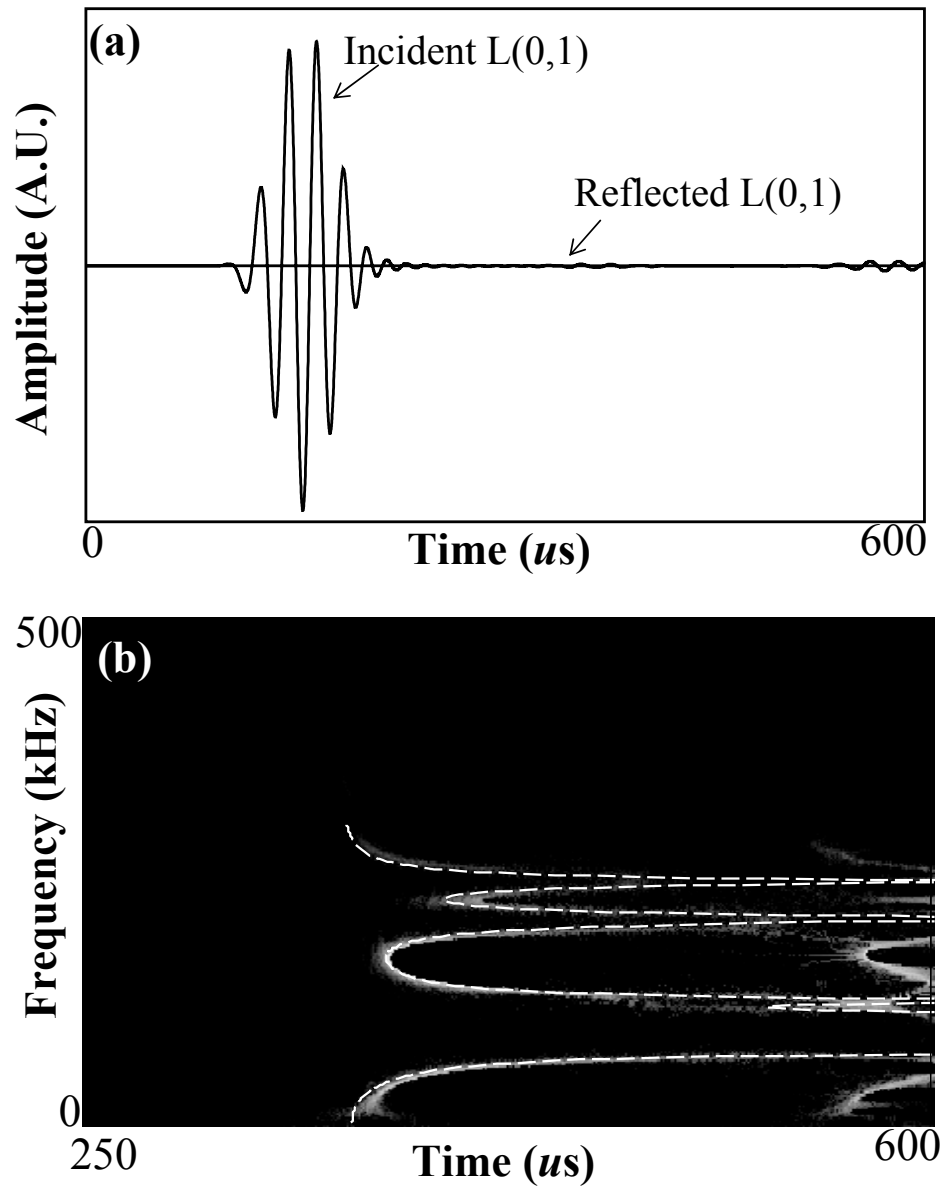
Figure 6.7: (a) Time-trace signals of the incident and the reflected signals monitored at the reflection measurement point in Fig. 5.1, when the slip bonding is assumed. The L(0,1) mode is selected as the incident mode; (b) Reassigned Spectrogram analysis of the transmitted signal monitored at the transmission measurement point in Fig. 5.1.
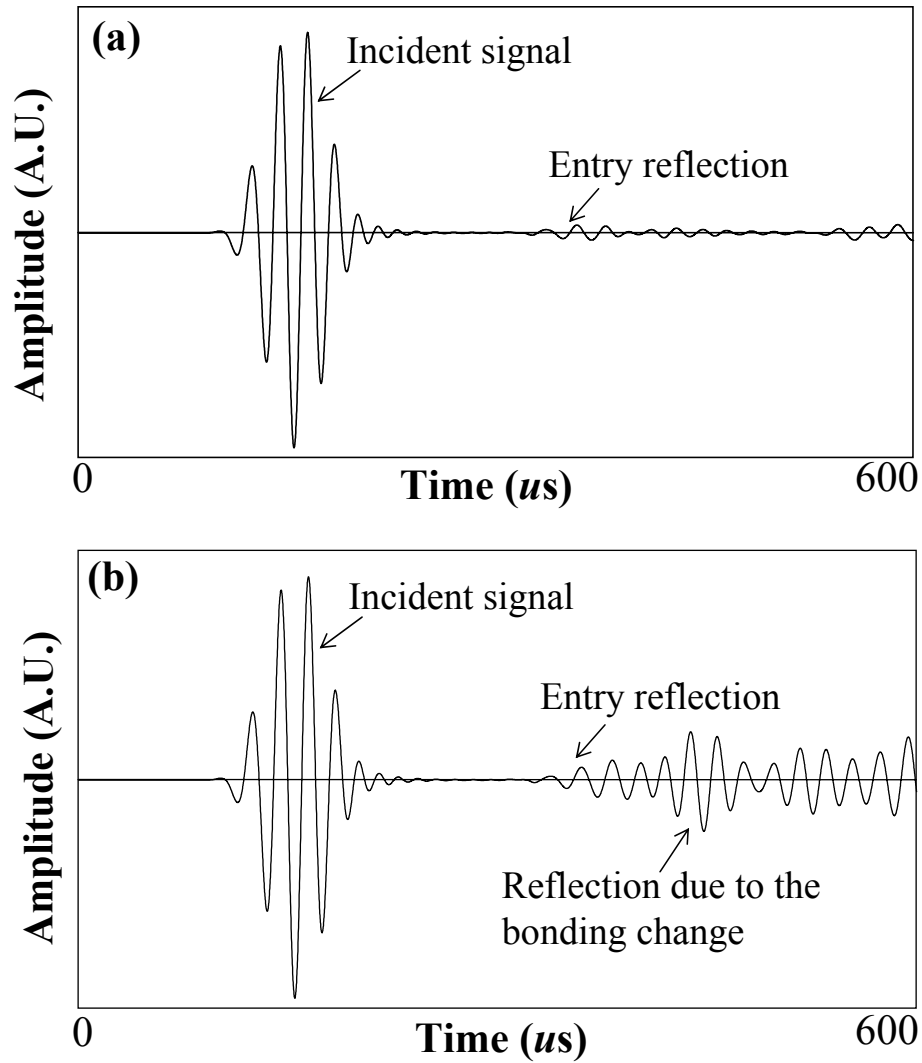
Figure 6.8: (a) Time-trace signals of the incident and the reflected signals monitored at the reflection measurement point in Fig. 5.4a, when the L(0,1) mode is incident; (b) Time trace of the incident and the reflected signals monitored at the reflection measurement point in Fig. 5.4b, when the L(0,1) mode is incident.
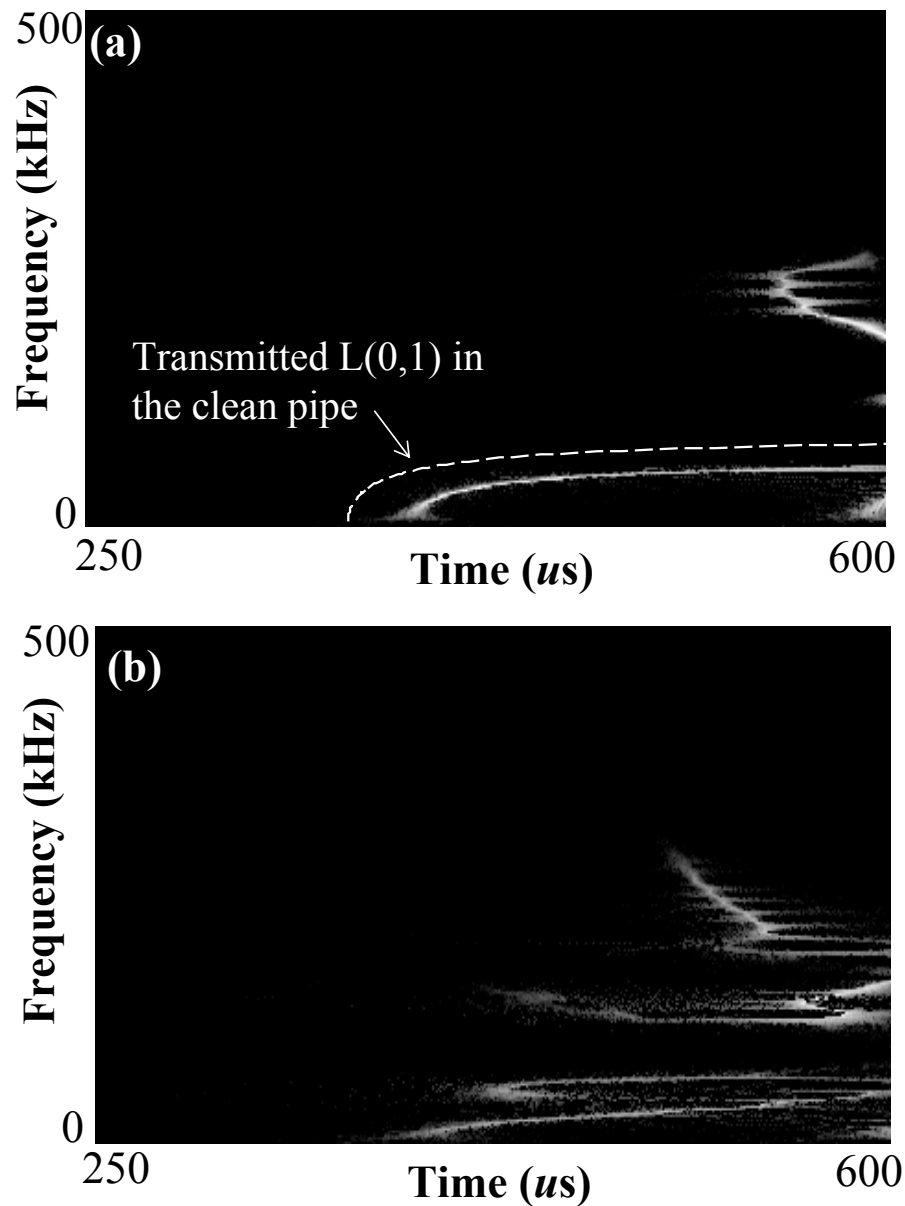
Figure 6.9: (a) Reassigned Spectrogram analysis of the transmitted signal monitored at the transmission measurement point in Fig. 5.4a, using the longitudinal modes for incidence. The numerical calculation of the dispersion curve of the L(0,1) mode in the clean pipe is also provided by DISPERSE (white dashed curve);(b) Reassigned Spectrogram analysis of the transmitted signal monitored at the transmission measurement point in Fig. 5.4b, using the longitudinal modes for incidence.
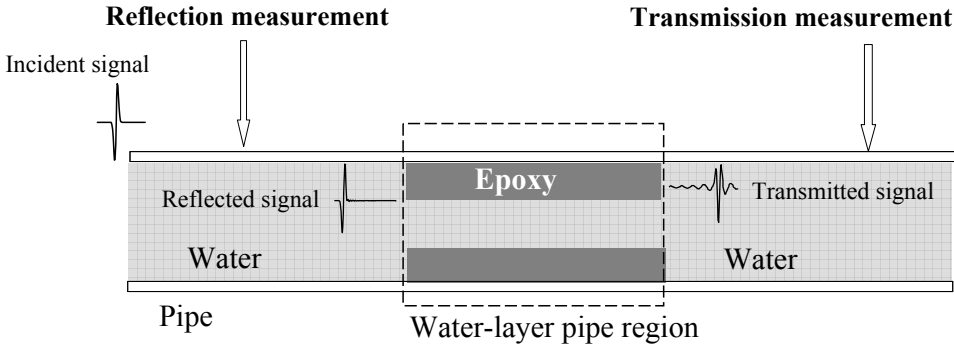
Figure 6.10: Schematic of the model in which an aluminum pipe (Inner diameter 16mm and thickness 1.4mm) is filled with water and also is locally coated by a 5-mm thickness epoxy layer.
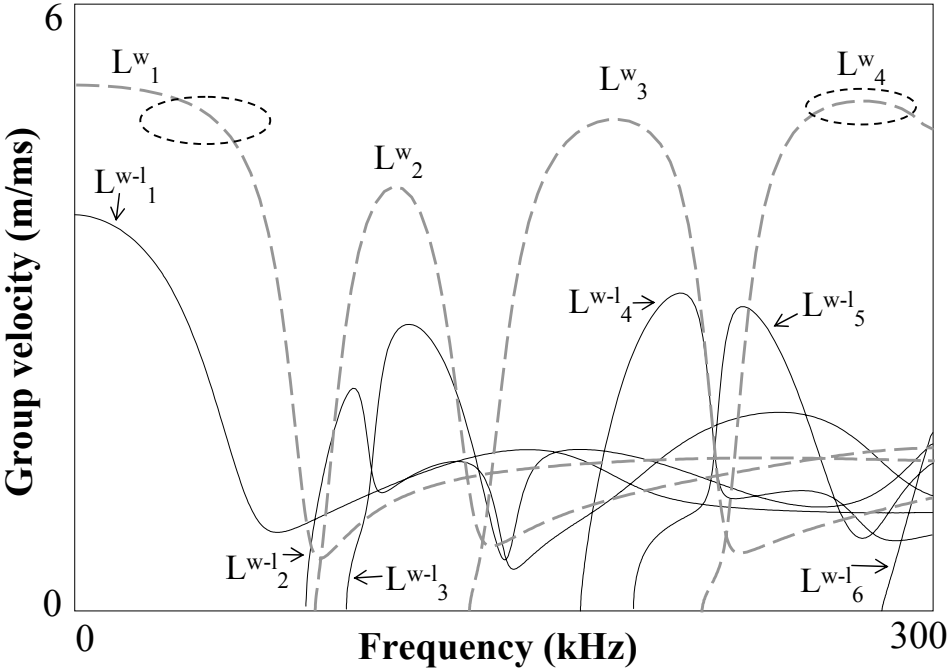
Figure 6.11: Dispersion curves of the longitudinal modes in the water-filled pipe (gray dashed curves) and the longitudinal modes in the water-layer pipe (black solid curves).
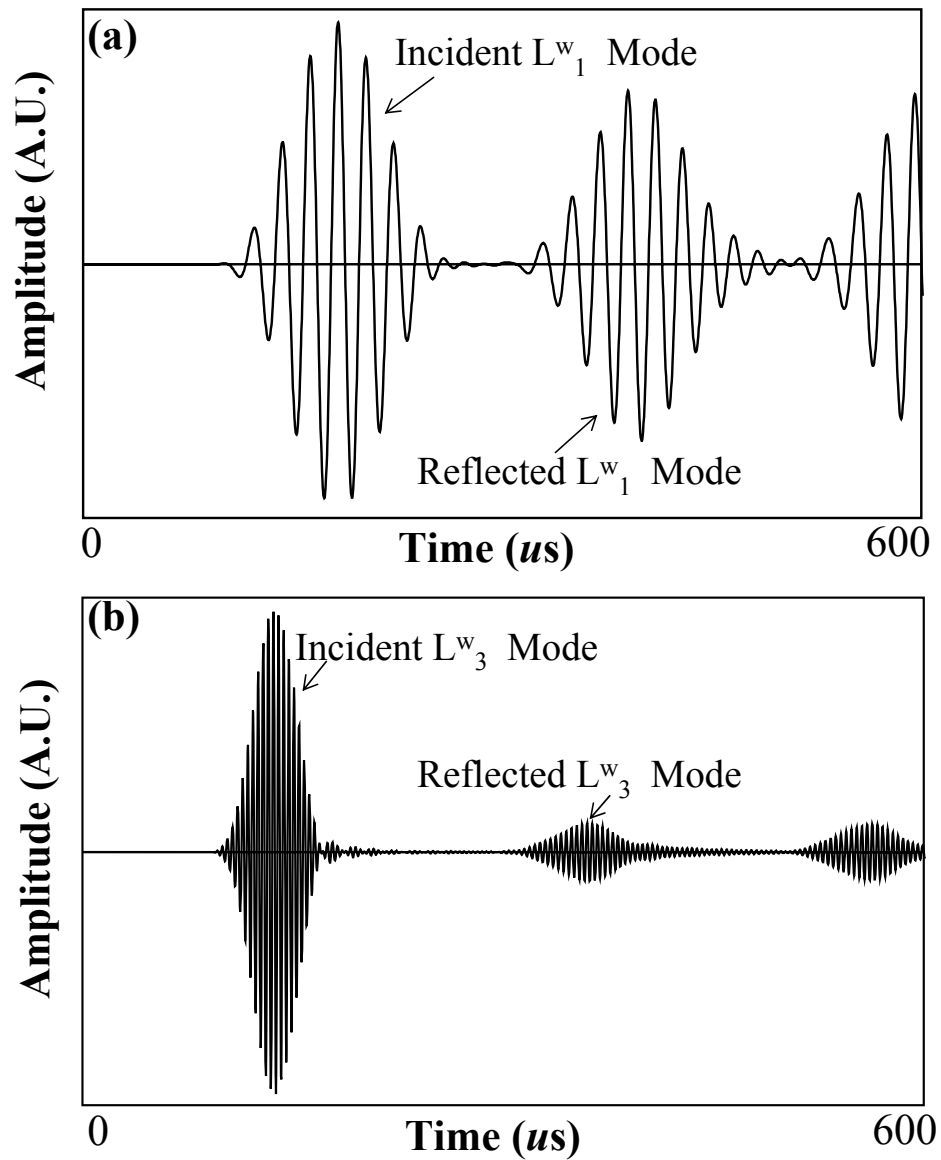
Figure 6.12: (a) Time-trace signals of the incident and the reflected signals monitored at the reflection measurement point in Fig. 6.10, when the L_1^w mode at its plateau region is used for incidence; (b) For the case when the L_4^w mode at its plateau region is used for incidence.
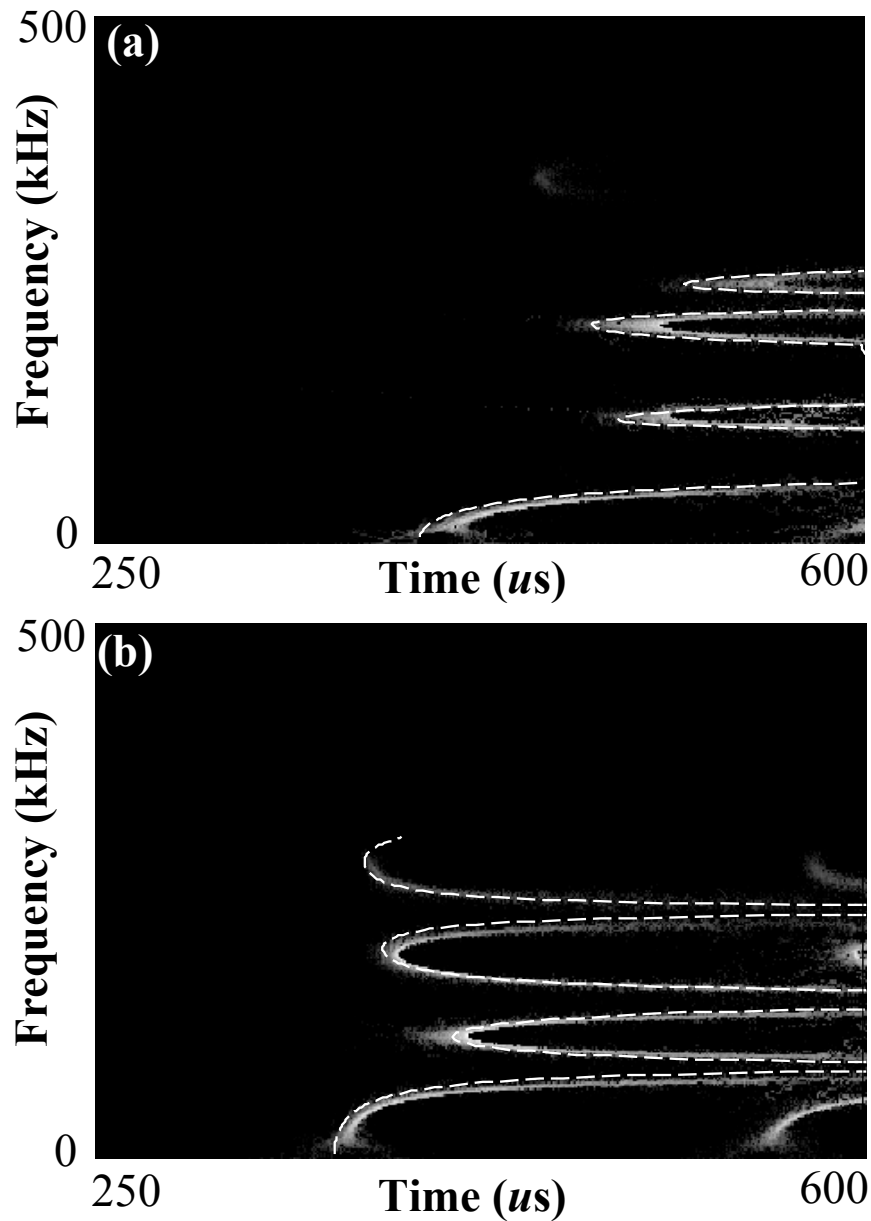
Figure 6.13: (a) Reassigned Spectrogram analysis of the transmitted signal monitored at the transmission measurement point in Fig. 6.10, when the length of the water-filled region is 3 times that of the water-layer region. The numerical calculation is also provided by DISPERSE (white dashed curve);(b) as (a), for the case, when the length of the water-filled region is 10 times that of the water-layer region.
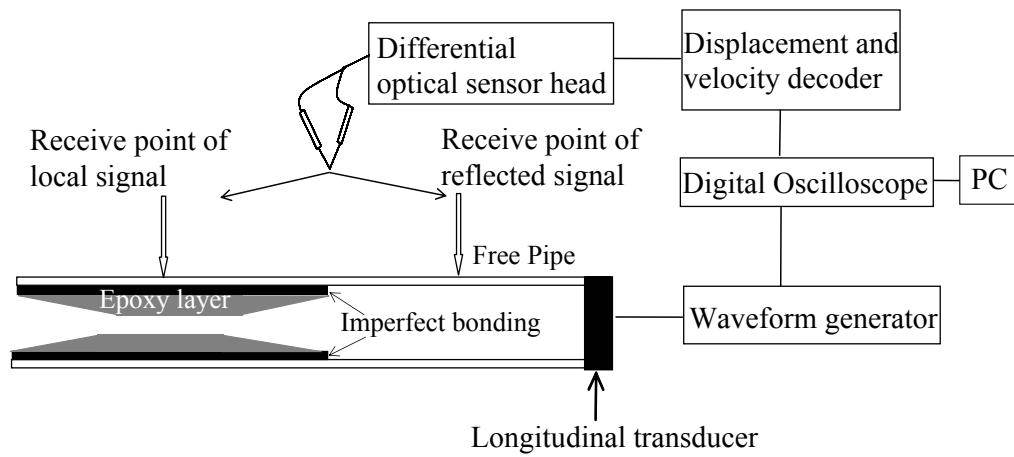
Figure 6.14: Schematic of the experiment measurements conducted on a pipe locally containing an epoxy tube that has varying thickness and imperfect bonding state.
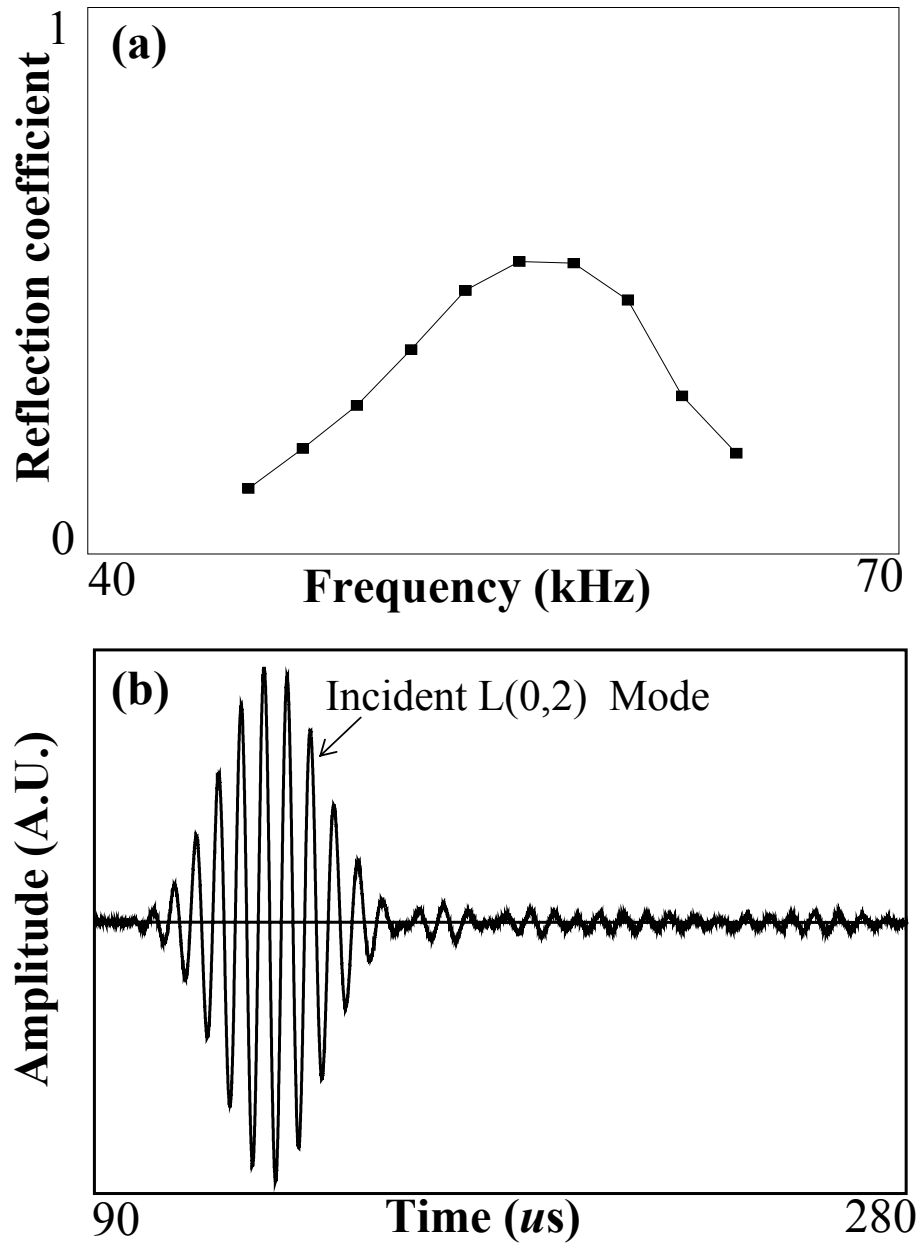
Figure 6.15: (a) Reflection coefficient spectrum amplitude measured from the sample shown in Fig. 6.14, when the L(0,1) mode is incident; (b) Time-trace signals of the reflection measurement conducted on the sample shown in Fig. 6.14, when the L(0,2) mode is incident.
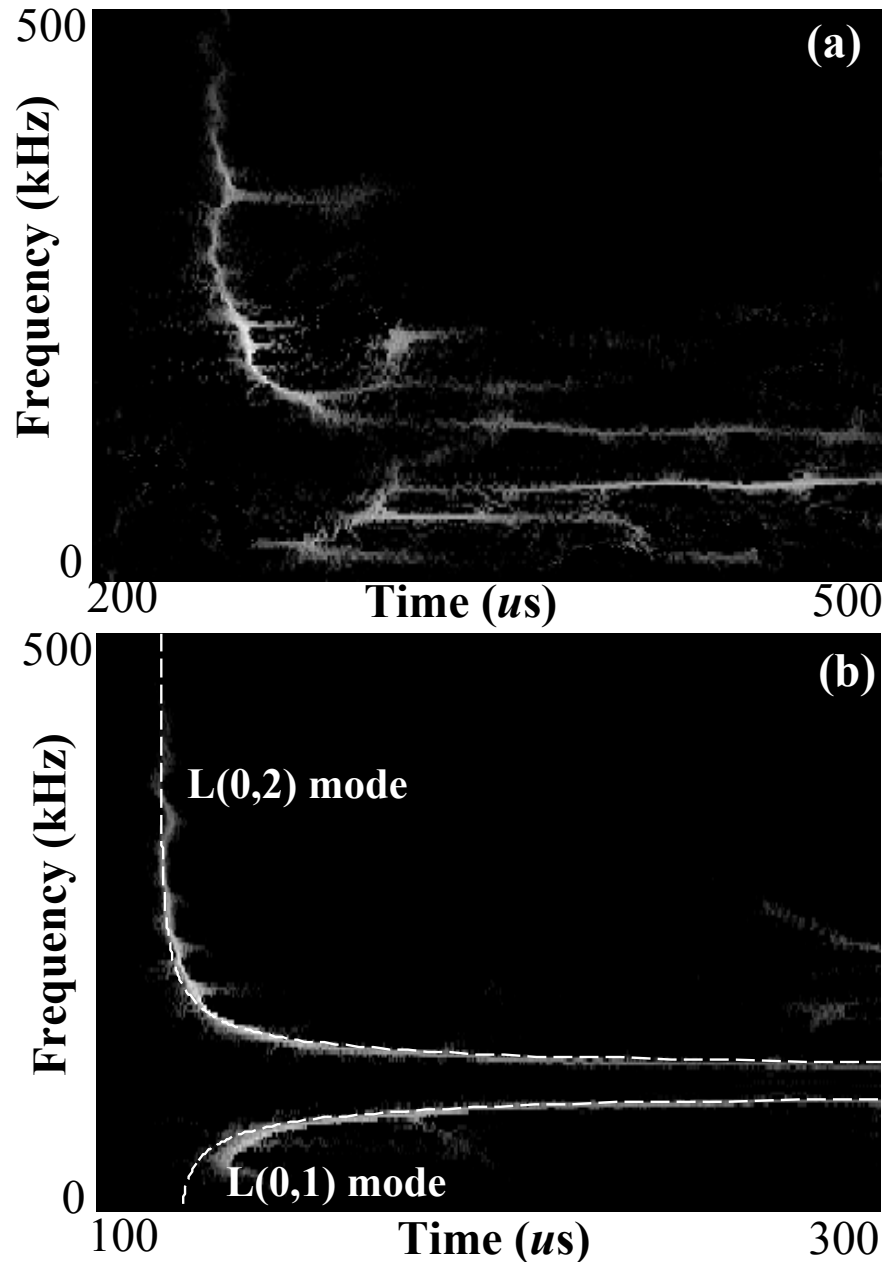
Figure 6.16: (a) Reassigned Spectrogram analysis of the local signal measured from the sample shown in Fig. 6.14; (b) Reassigned Spectrogram analysis of the incident signals measured from the sample shown in Fig. 6.14 at the receiver point of the reflected signal. The numerical calculation is provided by DISPERSE (white dashed curve).

Chapter 7

Conclusions

7.1 Review of Thesis

There are many circumstances in the process, power and oil industries, where it is necessary to determine information about the material inside a pipeline and it would be a great benefit if on-line measurements could be conducted without taking samples from the pipeline. In this thesis the use of guided ultrasonic waves for on-line measurements of contents inside pipes was investigated. Guided wave measurements are completely non-intrusive to the pipeline and promise to overcome the limitations associated with current measurement techniques (background and motivation are given in Chapter 1). The work in the thesis has been conducted mainly for two specific applications: (a) characterisation of fluids inside pipes (Chapters 2 and 3) and (b) sludge and blockages detection inside pipes (Chapters 4, 5 and 6).

In Chapter 2, the fundamental theory of bulk ultrasonic waves and guided ultrasonic waves were reviewed. For the particular purpose of fluid characterisation, the model of guided longitudinal waves propagating in pipes filled with fluids was examined. New properties of the guided wave modes due to the presence of the filling fluid were identified.

Chapter 3 presented a new guided wave technique to measure the longitudinal bulk velocity and shear viscosity of a fluid inside a pipe by using the principles identified in Chapter 2. It was demonstrated that this new technique is capable of non-intrusively

characterising both low-viscosity and highly viscous fluids inside the pipe. In the same chapter, existing ultrasound techniques for fluid characterisation inside pipes were also reviewed.

Chapter 4 studied the scattering of the fundamental guided torsional mode T(0,1) by an axisymmetrical elastic layer inside a pipe. The model was considered as a simplified representation of sludge inside pipes and revealed the underpinning physics of more complex scenarios. Two techniques exploiting the reflected and transmitted T(0,1) mode were developed to detect and characterise the geometry or acoustic properties of the layer.

Chapter 5 proceeded the work in Chapter 4 by taking into account more realistic characteristics of sludge and blockages, such as their irregular profiles, strength of the bonding to the pipe and damping within the sludge material. The influence of these factors on the reflection and transmission techniques was investigated and the practical feasibility of the proposed techniques was also demonstrated.

The two blockage detection techniques based on torsional modes were then extended to longitudinal modes in Chapter 6. The techniques using these two families of modes were compared to evaluate their relative advantages and disadvantages so as to facilitate the optimal mode choice for sludge detection in practice.

7.2 Summary of Findings

The findings of this thesis are summarized here according to the application to which they refer to.

7.2.1 Characterisation of fluid properties inside pipes

The models of guided longitudinal modes propagating in fluid-filled pipes have been examined in Chapter 2, which revealed that the presence of the fluid changes the velocity dispersion of the longitudinal modes in a clean pipe. It was shown that such a change results from an interaction between two families of asymptotic modes

which are the modes of the clean pipe, and the modes of the fluid column with a rigid boundary condition at the internal pipe wall. For a low-viscosity fluid, each longitudinal mode in the fluid-filled pipe jumps from one asymptotic family to the other. However, as the viscosity increases the interaction becomes weak and most of the energy is confined in either the pipe or in the filling fluid, and modes no longer jump.

The parametric study in Chapter 2 showed that for a low-viscosity fluid in a given pipe, the dispersion curves of the longitudinal modes and the corresponding branching frequencies (where group dispersion curves reach a local minimum) are uniquely determined by the bulk longitudinal velocity of the fluid. For highly viscous fluid, the velocity dispersion of the modes are influenced simultaneously by the bulk velocity and shear viscosity of the fluid; however, the branching frequencies remain determined by the bulk velocity only. At the same time, the shear viscosity of the fluid causes attenuation of the longitudinal modes whose sensitivity to the viscosity varies as frequency changes.

A new technique was developed in Chapter 3 to measure the bulk longitudinal velocity and shear viscosity of fluids inside pipes. The velocity measurement used a broadband excitation to generate multiple longitudinal modes in the pipe filled with fluid. These modes were measured from a single signal which was analyzed by two signal processing methods. The amplitude spectrum analysis of the signal showed periodic dips which were found to occur right at the branching frequencies; the time-frequency analysis, reassigned spectrogram, reconstructed the whole dispersion curves of the longitudinal modes. The measured dispersion curves and branching frequencies were back fitted to a forward model to extract the longitudinal velocity of the fluid. On the other hand, the viscosity of the fluid was determined from the attenuation of the modes measured at the suitable frequency ranges which were identified from the measured dispersion curves.

The technique were demonstrated by measuring both low-viscosity and highly viscous fluids inside a pipe. The measured properties of a low-viscosity fluid (glycerol) agreed well with conventional methods and literature data for both the longitudinal bulk velocity (within 0.8%) and the viscosity (within 4%). For highly viscous fluid (mineral oil) the accuracy of the velocity measurement was found to be reduced

slightly (within 1%) while the viscosity measurement became more accurate (within 1%).

The technique can be employed both when the pipe is completely filled or when the filling is local. In the latter case, the technique can be exploited as a pipe "dipstick" sensor dipped into the fluid to be measured. The sensor has the advantages that the velocity measurement requires a single pulse echo measurement without the need for knowing the depth of immersion of the pipe, and it can be carried out at a remote position away from the fluid free surface.

7.2.2 Sludge and blockages detection and characterisation inside pipes

Principle study

The work was conducted in two stages. The first stage (Chapter 4) investigated the fundamental effects of the presence of sludge on the guided wave characteristics. This made use of a model system consisting of a uniform axially symmetric layer of a polymer material bonded to the inside wall of the pipe (referred to as bilayered pipe). Although such a system falls far short of the complexities of real sludge, it was a vital step to understand the fundamental physical phenomena.

The propagation characteristics of the guided torsional modes in the clean pipe and the bilayered pipe were examined. It was found that the presence of the layer inside the pipe increases the number of torsional modes that can propagate in a clean pipe (T(0,1) mode) which accordingly brings more cutoff frequencies. These new modes show strong dispersion, while the T(0,1) mode in the clean pipe is non-dispersive. The dispersion curves and the cutoff frequencies of the modes in the bilayered pipe are determined by the bulk shear velocity and the thickness of the layer.

When the T(0,1) mode is incident at the bilayered part of the pipe, due to the mismatch of its mode shape with that of the modes in the bilayered pipe, the T(0,1) mode is scattered: part of its energy is reflected back and the other is transmitted into the multiple torsional modes in the bilayered pipe. The modes traveling in

the bilayered region are converted back into the T(0,1) mode after they leave the bilayered region. The characteristics of both the reflected and transmitted signals were studied.

The strength of the reflected T(0,1) mode shows strong frequency dependence. This was shown by the reflection coefficient spectrum amplitude which exhibits periodic peaks occurring at the cutoff frequencies of the modes in the bilayered pipe. This phenomenon is due to the fact that at the cutoff frequencies, the energy of torsional modes in the bilayered pipe tends to flow in the coating primarily, while little remains in the pipe wall. This causes a large mismatch of the wave fields between the clean pipe and the bilayered pipe, so resulting in a strong reflection.

On the other hand, the transmitted signals propagating in the bilayered pipe region or past it show strong dispersion characteristics, which are due to the dispersive torsional modes propagating in the bilayered part of the pipe. The extent of the dispersion of the transmitted signal depends on the thickness and bulk shear velocity of the layer.

Two techniques were developed to characterise the geometry or acoustic properties of the layer, which respectively made use of the reflected and transmitted signals. The first technique determined the cutoff frequencies of the torsional modes in the bilayered pipe by measuring the peak positions on the reflection coefficient spectrum. The measured cutoff frequencies can be used to extract the thickness of the layer through a forward model, provided the bulk shear velocity in the layer is known, and vice versa.

The second technique measured the transmitted signal and quantitatively reconstructed the dispersion curves of modes in the bilayered pipe from the signal by the reassigned spectrogram. The thickness of the layer may be extracted by best fitting the reconstructed dispersion curves to the model prediction, provided that the shear bulk velocity of the layer is known, and vice versa.

Both techniques allow the characterisation of the layer to be carried out remotely i.e. without the need to access the bilayered region. The second technique only requires to measure a single time-domain signal.

Practical considerations

The second stage further exploited the feasibility of the two techniques for sludge and blockages detection and characterisation by considering more realistic properties of the sludge and blockages. The potential of the techniques was investigated using both the torsional (Chapter 5) and longitudinal (Chapter 6) modes and the following findings are applicable to both cases.

Using the first technique, measurable reflections were observed when there is any abrupt change of the properties of the sludge along its axial or circumferential profiles including bonding state, thickness or material properties. The strength of the reflection shows strong frequency dependence which is determined by the thickness, bulk velocity and the bonding state of the sludge layer. The peaks on the reflection coefficient spectrum shift to low frequencies as the bulk velocity and the bonding state of the layer decrease or as the thickness of the layer increases. Also, the strength of the reflection enhances with increasing circumferential extent of the sludge layer. On the other hand, the material damping of the sludge reduces the strength of the reflection.

The reflection technique can effectively locate the sludge in the pipe and it requires a single transducer working in pulse echo mode. The strong frequency dependence of the reflection implies that a practical implementation should sweep the testing frequency or employ broadband frequency excitation in order to guarantee a good sensitivity to the sludge.

The second technique detected the sludge or blockages by revealing the dispersion and attenuation changes to the transmitted modes propagating in the blocked region or past it. The extent of the dispersion change of the transmitted signal is determined by the geometry, bonding and the material properties of the sludge. The irregular axial and circumferential profiles of the sludge increase the complexity of the dispersion. Besides dispersion, the material damping of the sludge or blockages can cause significant attenuation to the transmitted signals. This can be an additional indicator of the presence of the sludge, provided the pipe is free from other attenuative media.

The transmission technique requires two transducers working in pitch catch mode and can detect the presence of the sludge and blockages; however, it cannot accurately identify the location of the sludge between the two transducers.

Although both torsional and longitudinal modes can be used for sludge detection, the two families of modes prove different performance and can complement each other. It was found that the transmission technique using longitudinal modes is more likely to lead to a successful detection when the bonding interface has small shear stiffness, such as slip bonding, compared to the use of torsional modes. On the other hand, the use of longitudinal modes is not viable when fluid is present inside the pipe due to the excitation of water-born modes which mask the desired signals, whereas the presence of fluid has no influence on the torsional modes. Therefore, the decision regarding the mode choice for sludge and blockages detection should be made in accordance to the types and properties of the sludge and the conditions of the pipeline encountered in practice.

The study also suggested that both the reflection and transmission techniques should be used for reliable sludge and blockage detection, since they are two complementary measurements. For example, when the reflection is weak, most of the energy of the guided wave is transmitted through the blocked region leading to more sensitive transmission measurements.

Characterising the geometry or acoustic properties of realistic sludge or blockages was found to be difficult because of their arbitrary shapes and properties, but it may be achievable if there are specific applications in which the sludge has simple geometry and uniform properties.

7.3   Future Work

In future, the presented technique to characterise homogeneous Newtonian fluids inside pipes may be extended to complex fluids such as particle mixtures or supercritical fluids.

Particle mixtures are produced by many industries ranging from food and beverages

to petro chemical products and paints. It is important to measure the properties of these fluids inside the pipeline so as to help the monitoring and control of processes. These fluids can be treated as homogeneous because the particle sizes are much smaller than the wavelengths of the guided waves. However the particles have significant effects on the bulk velocity and attenuation of the host fluids, which accordingly will affect the propagation of guided waves in pipes filled with such fluids. A model to predict the propagation of guided waves in pipes filled with complex fluids needs to be developed. The applicability of the proposed technique to the complex fluids needs to be examined.

Besides, proper apparatus to excite and receive guided waves should be developed for specific on-line applications. For example, a magnetostrictive transduction system is being developed by a research partner (Nottingham University) to apply the technique to track the phase behavior of supercritical fluids under high temperature condition.

Finally it is important to further investigate the practical applicability of the two techniques developed for sludge and blockage detection. This will require a series of experimental investigations carried out on pipelines with sludge and blockages of different properties and geometries under real plant conditions. The range of sludge or blockages that can be detected needs to be identified in terms of their material, geometry and bonding. The influences from other features on the real pipelines such as bends and supports need to be investigated. Moreover, the feasibility of conducting the test when the pipelines are in-service needs to examined, which can be highly valuable in industry.

Appendix A

Finite Element Models of Guided Torsional Modes Propagating in a Pipe Locally Coated inside with an Elastic Layer

A.1 2D Finite Element Models

A.1.1 Idealised model

The 2D finite element (FE) modelling was carried out using the software FINEL, developed at Imperial College [85]. FINEL performs efficient modelling of elastic wave propagation using a time-marching procedure, and so produces simulations of the signals which would be seen experimentally. The 2D model was axially symmetric, representing a radial-axial section through the pipe and thus enabling two-dimensional axially symmetric elements to be used. The aluminium pipe with 16-mm inner diameter and 1-mm wall thickness was 2.5 m long, 0.5 m of which was coated with 6-mm uniform thickness epoxy layer (Fig. 4.1). The layer started at 1 m away from the end where the torsional wave is excited. The elements were defined to be perfectly square in shape with the size of 0.2 mm. Thus, there were 5 elements through the thickness of the pipe and 30 elements through the thickness of the epoxy layer. A 1-cycle pulse excitation of 90 kHz central frequency was applied at the free

end of the pipe. Because the excitation has no significant energy above the cutoff frequency of T(0,2), the only propagating mode excited by this configuration was the T(0,1) mode. The results of the models were obtained by monitoring tangential displacements at the outside surface of the pipe. Two monitoring points are set for measuring the reflected signals and transmitted signal respectively: the monitoring point of the remote measurement was set at the half way point between the free end of the pipe and the entry point of the epoxy layer, so that both the incident and the reflected signals could be measured; the monitoring point of the transmission measurement was set 0.5 m away after the layer ends in the pipe.

A.1.2   Imperfect bonding

The dimension, material properties and mesh of the pipe and the epoxy layer in the model were the same as in the idealised model. Additionally, a thin spring layer (0.1 mm thickness) was placed between the layer and the pipe to simulate the imperfect bonding. The size of the square elements used to mesh the spring layer was chosen to be 0.05 mm. Thus, there were 2 elements through the thickness of the spring layer. The ways of excitation and the monitoring were the same as used in the idealised model.

A.1.3   Varying thickness

The dimension, material properties and mesh size of the pipe in this model were the same as in the idealised model. The layer was divided into tapered layer parts at both its ends and a uniform part in the middle(Fig. 5.4). The tapered part at each end was 0.18 m long and the uniform part was 0.14 m long. The total length of the layer was 0.5 m as in the idealised model. The elements size used for both tapered part and uniform part of the layer was 0.2 mm. To model the tapered part of the layer, we equally divided the tapered layer into 30 local uniform layers with the same length of $l_t = 6mm$ (30 elements). Each local uniform layer had 0.2mm (1 element) increment on its thickness before or after its previous layer, depending on the positive or negative slope of thickness variation. The ways of excitation and the monitoring were the same as used in the idealised model.

A.1.4   Varying thickness and varying bonding

The dimension, material properties and mesh of the pipe and the layer in this model were the same as in the model of varying thickness. Additionally, a thin spring layer (0.1 mm thickness) was placed between the layer and the pipe to simulate the imperfect bonding. The size of the square elements used to mesh the spring layer was chosen to be 0.05 mm. Thus, there were 2 elements through the thickness of the spring layer. The material properties of the spring layer was not consistent along its length. The first 0.1 m of the spring layer was assigned a material whose shear stiffness was half of that of the material assigned to the remaining part of the spring layer. This was to simulate a bonding change at 0.1 m from where the layer starts in the pipe. The ways of excitation and the monitoring were the same as used in the idealised model.

A.2   3D Finite Element Model

The 3D model was studied using the finite element software ABAQUS 6.5 [92]. A 3.5 inch aluminium pipe (89 mm OD and 2.5 mm thickness) coated with a 10-mm thickness epoxy layer was modelled. The pipe was 2.5 m in length, 0.5 m of which was coated with a layer inside. The layer started at 1 m away from the end where the torsional wave was excited. The layer was modelled to have a consistent axial profile (perfect bonding and uniform thickness), but a non-symmetric circumferential profile. 8-node solid 'brick' elements were used to mesh both the pipe and the layer. For the pipe there were 2 elements through its thickness, 268 elements around the circumference and 2500 elements in the length. For the layer, there are 8 elements in its thickness, 500 elements along the length and a varying number of elements around its circumference depending on the circumferential extent of the layer.

A 2-cycle pulse excitation of 70 kHz central frequency was applied at the outside surface of the free end of the pipe. The excitation was placed at the full circumference of the outside surface with a circumferential displacement. The results of the models are obtained by monitoring circumferential displacements at 18 equally spaced points around the circumference of the pipe, but at the same axial location.

By adding the 18 sampled waveforms, we can obtain both the signals only containing a single T(0,1) mode, since the flexural modes which have a sinusoidal displacement distributed around the pipe circumference are canceled by circumferential averaging. Two monitoring points were set for measuring the reflected signal and transmitted signal respectively: the monitoring point of the remote measurement was set at the half way point between the free end of the pipe and the entry point of the epoxy layer, so that both the incident and the reflected signals could be measured; the monitoring point of the transmission measurement was set 0.5 m away after the end of the layer.

Appendix B

Finite Element Models of Guided Longitudinal Modes Propagating in a Pipe Locally Coated inside with an Elastic Layer

B.1 Idealised Model

The finite element (FE) modelling was carried out with the software Abaqus [92] using its time marching *Explicit* solver. The idealised model is 2-dimensional which represents a radial-axial section through the pipe. This enables two-dimensional axially symmetric elements to be used. The aluminium pipe with 16-mm inner diameter and 1-mm wall thickness was 2.5 m long, 0.5 m of which was coated with 5-mm uniform thickness epoxy layer (Fig. 4.1). The layer started at 1 m away from the end where the torsional wave is excited. The elements were defined to be perfectly square in shape with the size of 0.2 mm. Thus, there were 5 elements through the thickness of the pipe and 25 elements through the thickness of the epoxy layer.

An axial-direction force was applied on the nodes at the free end of the pipe to generate the longitudinal modes. For reflection measurement, two different excitation signals were used: a 5-cycle toneburst signal of 50 kHz central frequency was used

to generate the L(0,1) mode in the frequency range of 35-65 kHz; while a 8-cycle toneburst signal of 250 kHz central frequency was used to generate the L(0,2) mode in the the frequency range of 200-300 kHz. For the transmission measurement, a 2-cycle toneburst signal of 100 kHz central frequency was used which generated both L(0,1) and L(0,2) modes in the frequency range of 30-300 kHz. At low frequencies, L(0,1) is the only mode to be generated and at higher frequencies, the L(0,2) mode is dominantly excited compared to the L(0,1) mode due to the match of its mode shape displacement with the excitation.

The results of the models were obtained by monitoring axial-direction displacements at a single point right in the middle of the pipe wall. The position was chosen such that no L(0,1) mode was monitored when the L(0,2) mode was incident at high frequencies (note that the L(0,1) mode was also be weakly generated). This made use of the discrepancy of their displacements as illustrated in Fig. 2.3: at high frequencies, the L(0,1) mode has little axial displacement in the central of the pipe wall while the L(0,2) mode still has significant displacement at this point. Thus, by monitoring exactly at the central of the pipe wall, the L(0,1) mode will not be present. Two monitoring points were set for measuring the reflected signals and transmitted signal respectively: the monitoring point of the remote measurement was set at the half way point between the free end of the pipe and the entry point of the epoxy layer, so that both the incident and the reflected signals could be measured; the monitoring point of the transmission measurement was set 0.5 m away after the layer ends in the pipe.

B.2   Imperfect Bonding

The dimension, material properties and mesh of the pipe and the epoxy layer in the model were the same as in the idealised model. Additionally, a thin spring layer (0.1 mm thickness) was placed between the layer and the pipe to simulate the imperfect bonding. The size of the square elements used to mesh the spring layer was chosen to be 0.05 mm. Thus, there were 2 elements through the thickness of the spring layer. The ways of excitation and the monitoring were the same as used in the idealised model.

B.3   Varying Thickness

The dimension, material properties and mesh of the pipe in this model were the same as in the idealised model. The layer was divided into tapered layer parts at both its ends and a uniform part in the middle. The tapered part at each end was 0.15 m long and the uniform part was 0.2 m long. Triangular elements with the size of 0.2 mm were used to mesh the epoxy layer as they provided finer mesh for tapered structures than the squire elements. The mesh of the pipe still consisted of square element with the size of 0.2 mm. The ways of excitation and the monitoring were the same as used in the idealised model.

B.4   Varying Thickness and Varying Bonding

The dimension, material properties and mesh of the pipe and the layer in this model were the same as in the model of varying thickness. Additionally, a thin spring layer (0.1 mm thickness) was placed between the layer and the pipe to simulate the imperfect bonding. The size of the square elements used to mesh the spring layer was chosen to be 0.05 mm. Thus, there were 2 elements through the thickness of the spring layer. The material properties of the spring layer was not consistent along its length. The first 0.1 m of the spring layer ($K_N = 0.5GPa/mm$, $K_T = 0.14GPa/mm$) was assigned a material whose stiffness was one tenth of that of the material assigned to the remaining part of the spring layer($K_N = 5GPa/mm$, $K_T = 1.4GPa/mm$). This was to simulate a bonding change at 0.1 m from where the layer starts in the pipe. The ways of excitation and the monitoring were the same as used in the idealised model.

B.5   Presence of Fluid inside the Pipe

The dimension, material properties and mesh of the pipe and the epoxy layer in the model were the same as in the idealised model, additionally, the pipe was modelled to be filled with water (Fig. 6.10). The mesh of the water consisted of square-shaped

acoustic elements with size of 0.2 mm. For reflection measurement, the excitation signals were concentrated on the frequency ranges where the modes in the water-filled pipe have little dispersion. For example, a 8-cycle toneburst signal of 50 kHz central frequency was used to generate the L_1^w mode in its little-dispersive frequency range; a 20-cycle toneburst signal of 265 kHz central frequency was used to generate the L_4^w mode in its little-dispersive frequency range (shown in Fig 6.11). For the transmission measurement, a 2-cycle toneburst signal of 100 kHz central frequency was used which generated all the modes in the fluid-filled pipe in the frequency range of 30-300 kHz. The way of monitoring was the same as used in the idealised model.

References

[1] M. R. Giles, J. N. Hay, and S. M. Howdle, "Copolymerisation of methyl and ethyl methacrylate in Supercritical CO2," Macromolecular Rapid Communications **21**, 1019 – 1023 (2000).

[2] S. M. Howdle, M. Watson, M. Whitaker, K. M. Shakesheff, M. C. Davies, F. S. Mandel, J. D. Wang, and V. K. Popov, "Supercritical Fluid Mixing: Preparation of Polymer Composites Containing Bioactive Materials," Chemical Communications 109 – 110 (2001).

[3] M. J. Whitaker, R. A. Quirk, S. M. Howdle, and K. M. Shakesheff, "Growth Factor Release from Tissue Engineering Scaffolds," Journal of Pharmacy and Pharmacology **53**, 1427 – 1437 (2001).

[4] R. E. Challis, G. P. Wilkinson, and R. J. Freemantle, "Errors and uncertainties in the ultrasonic pulse-echo reflectometry method for measuring acoustic impedance," Measurement Science Technology **9**, 692–700 (1998).

[5] D. J. Hibberd, A. K. Holmes, M. Garrood, A. Fillery-Travis, M. M. Robins, and R. E. Challis, "Ultrasonic monitoring of oil-in-water emulsions during depletion flocculation," Journal of Pharmacy and Pharmacology **193**, 77–87 (1997).

[6] J. S. Tebbutt, T. Marshall, and R. E. Challis, "The monitoring of copper (II) sulfate pentahydrate crystallization using ultrasound," Langmuir **15**, 3356–3364 (1999).

[7] R. C. Sarmento, G. S. Ribbe, and L. A. Azevedo, "Wax blockage removal by inductive heating of subsee pipelines," Heat Transfer Engineering **25**, 2–12 (2004).

[8] P. J. Rathbone, "Sludge Characterisation for Ultrasonic Wave Guide Blockage Testing," Tech. Rep., BNFL Nexia Solutions. (2005).

[9] T. P. Bott, *Fouling of heat exchangers* (New York: Elsevier, 1995).

[10] C. Kuchpil, M. Gonalves, and L. Marquez, "Blockage Location and Remediation in Subsea Pipelines," (Deep Offshore Technology Conference, New Orleans,Louisiana., 2002).

[11] M. F. De Salis and D. J. Oldham, "Determination of the blockage area function of a finite duct from a single pressure response measurement," Journal of Sound and Vibration **221**, 180–186 (1999).

[12] M. F. De Salis and D. J. Oldham, "The development of a rapid single spectrum method for determining the blockage characteristics of a finite length duct," Journal of Sound and Vibration **243**, 625–640 (2001).

[13] D. N. Alleyne, B. Pavlakovic, M. J. S. Lowe, and P. Cawley, "Rapid, Long Range Inspection of Chemical Plant Pipework Using Guided Waves," Insight **43**, 93–96,101 (2001).

[14] D. N. Alleyne and P. Cawley, "Long Range Propagation of Lamb waves in chemical plant pipework," Materials Evaluation **55**, 504–508 (1997).

[15] J. L. Rose, J. J. Ditri, A. Pilarski, K. Rajana, and F. Carr, "A guided wave inspection technique for nuclear steam generator tubing," NDT & E Int. **27**, 307–310 (1994).

[16] W. Bottger, H. Schneider, and W. Weingarten, "Prototype EMAT system for tube inspection with guided ultrasonic waves," Nuclear Eng. Design **102**, 356–376 (1987).

[17] D. N. Alleyne, M. J. S. Lowe, and P. Cawley, "The reflection of guided waves from circumferential notches in pipes," Journal of Applied Mechanics **65**, 635–641 (1998).

[18] M. J. S. Lowe, D. N. Alleyne, and P. Cawley, "The mode conversion of a guided wave by a part-circumferential notch in a pipe," Journal of Applied Mechanics **65**, 649–656 (1998).

[19] K. Lohr and J. Rose, "Ultrasonic guided wave and acoustic impact methods for pipe fouling detection," Journal of Food Engineering **56**, 315–324 (2003).

[20] R. Hay, T and J. Rose, "Fouling detection in the food industry using ultrasonic guided waves," Food Control **14**, 481–488 (2003).

[21] P. Withers, "Ultrasonic, acoustic and optical techniques for the non-invasive detection of fouling in food processing equipment," Trends in Food Science and Technology **7**, 293298 (1996).

[22] B. A. Auld, *Acoustic Fields and Waves in Solids*, vol. 1 (Krieger Publishing Company, Malabar, Florida, 1990).

[23] J. L. Rose, *Ultrasonic Waves in Solid Media* (Cambridge University Press, Cambridge, UK, 1999).

[24] K. F. Graff, *Wave motion in elastic solids* (Clarendon Press, Oxford, 1975).

[25] P. M. Morse and H. Feshbach, *Methods of theoretical physics* (McGraw-Hill Book Company, New York, London, 1953).

[26] W. Fluegge, *Viscoelasticity* (Springer-Verlag, second edition, 1975).

[27] R. M. Christensen, *Theory of viscoelasticity: an introduction* (Academic Press, New York, London, 1971).

[28] Y. M. Haddad, *Viscoelasticity of engineering materials* (Chapman and Hall, New York, London, 1995).

[29] D. C. Gazis, "Three dimensional investigation of the propagation of waves in hollow circular cylinders," J. Acoust. Soc. Am. **31**, 568–578 (1959).

[30] Y. H. Pao and R. D. Mindlin, "Dispersion of flexural symmetric waves in elastic circular cylinder," Journal of Applied Mechanics **27**, 513–520 (1960).

[31] M. Onoe, H. D. McNiven, and R. D. Mindlin, "Dispersion of Axially Symmetric Waves in Elastic Rods," Journal of Applied Mechanics **29**, 729–734 (1962).

[32] M. G. Silk and K. F. Bainton, "The propagation in metal tubing of ultrasonic wave modes equivalent to Lamb waves," Ultrasonics **17**, 11–19 (1979).

[33] M. J. S. Lowe, "Matrix techniques for modelling ultrasonic waves in multi-layered media," IEEE Trans. Ultrason. Ferroelectr. Freq. Control **42**, 525–542 (1995).

[34] B. N. Pavlakovic, M. J. S. Lowe, D. N. Alleyne, and P. Cawley, "DISPERSE: A general purpose program for creating dispersion curves," in D. O. Thompson and D. E. Chimenti, editors, *Review of Progress in Quantitative NDE* (Plenum Press, New York, 1997), vol. 16, 185–192.

[35] B. N. Pavlakovic and M. J. S. Lowe, "A general purpose approach to calculating the longitudinal and flexural modes of multi-layered, embedded, transversely isotropic cylinders," in D. Thompson and D. Chimenti, editors, *Review of Progress in Quantitative NDE* (Plenum Press, New York, 1999), vol. 18, 239–246.

[36] L. Knopoff, "A matrix method for elastic wave problems." Bull. Seism. Soc. Am. **54**, 431–438 (1964).

[37] H. Schmidt and F. B. Jensen, "Efficient numerical solution technique for wave propagation in horizontally stratified environments." Comput. Math. Appl. **11**, 699–715 (1985).

[38] L. Rayleigh, *The theory of sound*, vol. 1 (Dover, New York, 1945).

[39] A. Bernard, M. J. S. Lowe, and M. Deschamps, "Guided waves energy velocity in absorbing and non-absorbing plates," J. Acoust. Soc. Am. **110**, 186–196 (2001).

[40] T. C. Lin and G. W. Morgan, "Wave propagation through fluid contained in a cylindrical elastic shell," J. Acoust. Soc. Am. **28**, 1165–1176 (1956).

[41] C. R. Fuller and F. J. Fahy, "Characteristics of wave propagation and energy distribution in culindrical elastic shell filled with fluid," Journal of Sound and Vibration **81**, 501–518 (1982).

[42] Y. P. Guo, "Approximate solution of the dispersion equation for fluid-loaded cylindrical shells," J. Acoust. Soc. Am. **95**, 1435–1440 (1994).

[43] Y. P. Guo, "Attenuation of helical wave radiation from cylindrical shells by viscoelastic layer," J. Acoust. Soc. Am. **97**, 298–308 (1995).

[44] B. K. Sinha, T. J. Plona, S. Kostek, and S.-K. Chang, "Axisymmetric wave propagation in fluid-loaded cylindrical shells. I: Theory," J. Acoust. Soc. Am. **92**, 1132–1143 (1992).

[45] T. J. Plona, B. K. Sinha, S. Kostek, and S.-K. Chang, "Axisymmetric wave propagation in fluid-loaded cylindrical shells. II: Theory versus experiments," J. Acoust. Soc. Am. **92**, 1144–1155 (1992).

[46] L. D. Lafleur and F. D. Shields, "Low-frequency propagation modes in a liquid-filled elastic tube waveguide," J. Acoust. Soc. Am. **97**, 1435–1445 (1995).

[47] L. Elvira-Segura, "Acoustic wave dispersion in a cylindrical elastic tube filled with a viscous liquid," Ultrasonics. **37**, 537–547 (2000).

[48] R. S. Long, P. Cawley, and M. J. S. Lowe, "Acoustic wave propagation in buried iron water pipes," Proc. Royal Society **459**, 2749–2770 (2003).

[49] J. Vollmann and J. Dual, "High-resolution analysis of the complex wave spectrum in a cylindrical shell containing a viscoelastic medium. I: Theory and numerical results," J. Acoust. Soc. Am. **102**, 896–908 (1997).

[50] M. Redwood, *Mechanical Waveguides: The Propagation of Acoustic and Ultrasonic Waves in Fluids and Solids with Boundaries* (Pergamon, New York, 1960).

[51] F. Simonetti and P. Cawley, "On the nature of shear horizontal wave propagation in elastic plates coated with viscoelastic materials," Proc. Royal Society **460**, 2197–2221 (2004).

[52] F. Simonetti, "Lamb wave propagation in elastic plates coated with viscoelastic materials," J. Acoust. Soc. Am. **115**, 2041–2053 (2004).

[53] B. N. Pavlakovic, "Leaky guided ultrasonic waves in NDT," Ph.D. thesis, University of London (1998).

[54] B. A. Auld, *Acoustic Fields and Waves in Solids*, vol. 2 (2nd edition, Krieger Publishing Company, Malabar, Florida, 1990).

[55] A. H. Nayfeh and P. B. Nagy, "Excess attenuation of leaky Lamb waves due to viscous fluid loading," J. Acoust. Soc. Am. **101**, 2649–2658 (1997).

[56] H. Kwun, K. Bartels, and C. Dynes, "Dispersion of longitudinal waves propagating in liquid-filled cylindrical shells," J. Acoust. Soc. Am. **105**, 2601–2611 (1999).

[57] C. Aristegui, M. J. Lowe, and P. Cawley, "Guided waves in fluid-filled pipes surrounded by different fluids," Ultrasonics. **39**, 367–375 (2001).

[58] J. Vollmann, R. Breu, and J. Dual, "High-resolution analysis of the complex wave spectrum in a cylindrical shell containing a viscoelastic medium. II: Experimental results versus theory," J. Acoust. Soc. Am. **102**, 909–920 (1997).

[59] M. Castaings and B. Hosten, "Guided waves propagating in sandwich structures made of anisotropic, viscoelastic, composite materials," J. Acoust. Soc. Am. **113**, 2622–2634 (2003).

[60] F. Simonetti and P. Cawley, "A guided wave technique for the characterisation of highly attenuative viscoelastic materials," J. Acoust. Soc. Am. **114**, 158–165 (2003).

[61] J. A. Bamberger and M. S. Greenwood, "Measuring fluid and slurry density and solids concentration non-invasively," Ultrasonics. **42**, 563–567 (2004).

[62] P. Hauptmann, N. Hoppe, and A. Püttmer, "Application of ultrasonic sensors in the process industry," Measurement Science and Technology. **13**, 73–83 (2002).

[63] B. S. Hoyle, "Process tomography using ultrasonic sensors," Measurement Science and Technology. **7**, 272–280 (1996).

[64] M. Yang, H. I. Schlaberg, B. S. Hoyle, M. S. Beck, and C. Lenn, "Real-time ultrasound process tomography for two-phase flow imaging using a reduced number of transducers," IEEE Transactions on Sonics and Ultrasonics **46**, 492–501 (1999).

[65] M. S. Greenwood, J. R. Skorpik, J. A. Bamberger, and R. V. Harris, "On-line ultrasonic density sensor for process control of liquids and slurries," Ultrasonics. **37**, 159–171 (1997).

[66] M. S. Greenwood, J. R. Skorpik, J. A. Bamberger, and R. V. Harris, "Ultrasonic sensor to measure the density of a liquid or slurry during pipeline transport," Ultrasonics. **40**, 413–417 (2002).

[67] X. Li, J. N. Cheeke, Z. Wang, C. K. Jen, M. Viens, G. Yi, and S. M., "Ultrasonic thin-walled tube wave devices for sensor applications," Appl. Phys. Lett. **67**, 37–39 (1995).

[68] D. N. Alleyne and P. Cawley, "The Excitation of Lamb Waves in Pipes Using Dry-coupled piezoelectric transducers," J NDE **15**, 11–20 (1996).

[69] M. Niethammer, L. J. Jacobs, J. Qu, and J. Jarzynski, "Time-frequency representations of Lamb waves," J. Acoust. Soc. Am. **109**, 1841–1847 (2001).

[70] F. Auger and P. Flandrin, "Improving the readability of time-frequency and time-scale representations by the reassignment method," IEEE Trans. Signal Processing **43**, 1068–1089 (1995).

[71] K. Kodera, R. Gendrin, and C. de Villedary, "Analysis of time-varying signals with small BT values," IEEE Trans. Acoust., Speech, and Signal Processing. **26**, 64–76 (1978).

[72] K. Kodera, C. de Villedary, and R. Gendrin, "A new method for the numerical analysis of time-varying signals with small BT values," Phys.Earth Planet. Interiors. **12**, 142–150 (1976).

[73] M. Niethammer, L. J. Jacobs, J. Qu, and J. Jarzynski, "Time-frequency representation of Lamb waves using the reassigned spectrogram," J. Acoust. Soc. Am. **107**, L19–L24 (2000).

[74] R. Benz, M. Niethammer, S. Hurlebaus, and L. J. Jacobs, "Localization of notches with Lamb waves," J. Acoust. Soc. Am. **114**, 677–685 (2003).

[75] A. N. Kalashnikov and R. E. Challis, "Errors in the measurement of ultrasonic absorption for material evaluation," in D. O. Thompson and D. E. Chimenti, editors, *Review of Progress in Quantitative NDE* (2002), vol. 21, 1997–2004.

[76] M. J. W. Povey, *Ultrasonic Techniques for fluids Characteriztion* (Academic, New York, 1997).

[77] G. W. C. Kaye and T. H. Laby, *Tables of Physical and Chemical Constants* (Longman, Essex, England, 1995).

[78] D. R. Lide, *Handbook of Chemistry and Physics*, vol. 70th (CRC, Boca Raton, 1989).

[79] T. Vogt, M. J. S. Lowe, and P. Cawley, "Measurement of the material properties of viscous liquids using ultrasonic guided waves," IEEE Trans. Ultrason. Ferroelect. Freq. Contr. **51**, 737–747 (2004).

[80] F. B. Cegla, P. Cawley, and M. J. S. Lowe, "Material property measurement using the quasi-Scholte mode-A waveguide sensor," J. Acoust. Soc. Am. **117**, 1098–1107 (2005).

[81] J. Ma, F. Simonetti, and M. J. S. Lowe, "Scattering of the fundamental torsional mode by an axisymmetric layer inside a pipe," J. Acoust. Soc. Am. **120**, 1871–1880 (2006).

[82] Z. Zhu and J. Wu, "The propagation of Lamb waves in a plate bordered with a viscous liquid," J. Acoust. Soc. Am. **98**, 1057–1064 (1995).

[83] J. Laperre and W. Thys, "Experimental and theoretical study of Lamb wave dispersion in aluminium / polymer bilayers," J. Acoust. Soc. Am. **94**, 268–278 (1993).

[84] C. L. Yapura and V. K. Kinra, "Guided waves in a fluid-solid bilayer," Wave motion **21**, 35–46 (1995).

[85] D. Hitchings, "FE77 User Manual," Tech. Rep., Imperial College (1994).

[86] A. S. Birks, R. E. Green, and P. Mclntire, *Nondestructive testing handbook*, vol. 7 (second edition, Amercian Society of Nondestructive Testing, The United States of American, 1991).

[87] R. J. Freemantle and R. E. Challis, "Combined compression and shear wave ultrasonic measurements on curing adhesive," Measurement Science and Technology **9**, 1291–1302 (1998).

[88] M. Castaings and C. Bacon, "Finite element modelling of torsional wave modes along pipes with absorbing materials," J. Acoust. Soc. Am. **119**, 3741–3751 (2006).

[89] B. Hosten and M. Castaings, "Finite elements methods for modeling the guided waves propagation in structures with weak interfaces," J. Acoust. Soc. Am. **117**, 1108–1113 (2005).

[90] F. Lanza di Scalea and P. Rizzo, "Propagation of ultrasonic guided waves in lap-shear adhesive joints: Case of incident a_0 Lamb wave," J. Acoust. Soc. Am. **115**, 146–156 (2004).

[91] A. Cheng, T. W. Murray, and J. D. Achenbach, "Simulation of laser-generated ultrasonic waves in layered plates," J. Acoust. Soc. Am. **110**, 848–855 (2001).

[92] ABAQUS., *ABAQUS Analysis User Manual*, vol. Version 6.5 (2004).

[93] *http://www.guided-ultrasonics.com*.

[94] P. B. Nagy, "Ultrasonic classification of imperfect interfaces," Journal of Non-destructive Evaluation. **11**, 127–139 (1992).

List of Publications

J. Ma, F. Simonetti and M. J. S. Lowe. Sludge and blockage characterization inside pipes using guided ultrasonic waves. in D. Thompson and D. Chimenti, editors, *Review of Progress in Quantitative NDE,* 25: 1656-1663, 2005.

J. Ma, F. Simonetti and M. J. S. Lowe. Scattering of the fundamental torsional mode by an axisymmetric layer inside a pipe. *Journal of the Acoustic Society of America,* 120:1871-1880, 2006.

J. Ma, M. J. S. Lowe and F. Simonetti. Measurement of the properties of fluids inside pipes using guided longitudinal waves. *IEEE Transactions on Ultrasonics, Ferroelectrics and Frequency Control,* 54: 647-658, 2007.

J. Ma, F. Simonetti and M. J. S. Lowe. Practical considerations of sludge and blockage detection inside pipes using guided ultrasonic waves. in D. Thompson and D. Chimenti, editors, *Review of Progress in Quantitative Nondestructive Evaluation,* 26:136-143, 2007.

J. Ma, M. J. S. Lowe and F. Simonetti. Measurement of the properties of fluids inside pipes using guided longitudinal waves. in D. Thompson and D. Chimenti, editors, *Review of Progress in Quantitative Nondestructive Evaluation,* 26:1624-1631, 2007.

J. Ma, M. J. S. Lowe and F. Simonetti. Feasibility study of sludge and blockage detection inside pipes using guided torsional waves. *Measurement Science and Technology,* 18: 2629-2641, 2007.